NASA TECHNICAL
MEMORANDUM

NASA TM X-62,296

NASA TM X-62,296

(NASA-TM-X-62296) WIND TUNNEL INVESTIGATION OF A LARGE-SCALE UPPER SURFACE BLOWN-FLAP TRANSPORT MODEL HAVING TWO ENGINES (NASA) 69 p HC $5.50 CSCL 01C G3/02

N73-32973

Unclas
19797

WIND TUNNEL INVESTIGATION OF A LARGE-SCALE UPPER SURFACE BLOWN-FLAP TRANSPORT MODEL HAVING TWO ENGINES

Kiyoshi Aoyagi, Michael D. Falarski and David G. Koenig

Ames Research Center

and

U.S. Army Air Mobility Research and Development Laboratory
Moffett Field, Calif. 94035

August 1973

SYMBOLS

b wing span, m (ft)

c wing chord measured parallel to the plane of symmetry, m (ft)

C_p pressure coefficient, $P_\ell - P_s/q_\infty$

c_t horizontal tail chord measured parallel to the plane of symmetry, m (ft)

$\bar{c}$ mean aerodynamic chord of wing, $2/S\int_0^{b/2} c^2 dy$, m (ft)

C_D drag coefficient, drag/$q_\infty S$

$C_{D_{ram}}$ ram drag coefficient, $Wv/gq_\infty S$

C_J jet momentum coefficient, $Fg/q_\infty S$

C_L lift coefficient, lift/$q_\infty S$

C_ℓ rolling-moment coefficient about stability axis, rolling moment/$q_\infty Sb$

C_m pitching-moment coefficient about 0.40 $\bar{c}$, pitching moment/$q_\infty S\bar{c}$

C_n yawing-moment coefficient about stability axis, yawing moment/$q_\infty Sb$

C_y side-force coefficient about stability axis, sideforce/$q_\infty S$

F_A static (wind off) incremental axial force due to flap deflection with power on, N (lb)

F_g gross thrust with engine alone, N (lb) (obtained statically)

F_N static (wind off) incremental normal force due to flap deflection with power on, N (lb)

F_R resultant force $\sqrt{F_A^2 + F_N^2}$, N (lb)

g acceleration of gravity, 9.81 m/sec^2(32.2 ft/sec^2)

i_t horizontal tail incidence, deg

P_ℓ local static pressure, N/m^2 (lb/sq ft)

P_s free-stream static pressure, N/m^2 (lb/sq ft)

P_∞ free-stream total pressure, N/m^2 (lb/sq ft)

q_∞ free-stream dynamic pressure, N/m^2 (lb/sq ft)

S	wing area, m^2 (sq ft)
V	free-stream air velocity, m/sec (ft/sec)
W	engine inlet weight rate of flow, kg/sec (lb/sec)
WCP	wing chord plane
y	spanwise distance perpendicular to the plane of symmetry, m (ft)
α	angle of attack of fuselage, deg
δ_a	aileron deflection, deg
δ_e	horizontal tail elevator deflection, deg
δ_f	deflection of Coanda plate trailing edge measured parallel to the plane of symmetry, deg (see fig. 2(d))
δ_{f_2}	trailing-edge second flap deflection measured parallel to the plane of symmetry, deg (see fig. 2(d))
δ_j	jet exhaust deflection angle wind off, $\tan^{-1} F_N/F_A$, deg (average value)
δ_s	slat deflection, measured parallel to the plane of symmetry, deg
δ_{sp}	spoiler deflection, measured parallel to the plane of symmetry, deg
η	wing semispan station, $y/(b/2)$
η_c	spanwise extent of Coanda plate surface, $y/(b/2)$
η_f	flap system static turning efficiency, FR/Fg (average value)
$(\ )_u$	uncorrected

WIND TUNNEL INVESTIGATION OF A LARGE-SCALE UPPER SURFACE BLOWN-FLAP TRANSPORT MODEL HAVING TWO ENGINES

Kiyoshi Aoyagi, Michael D. Falarski and
David G. Koenig

Ames Research Center
and
U.S. Army Air Mobility R&D Laboratory
Moffett Field, Calif., 94035

SUMMARY

An investigation has been conducted to determine the aerodynamic characteristics of a large-scale subsonic jet transport model with an upper surface blowing flap system that would augment lift. The model had a 25° swept wing of aspect ratio 7.28 and two turbofan engines with the engine centerline located at 0.256 of the wing semispan. The lift of the flap system was augmented by turbofan exhaust impingement on the Coanda surface. Results were obtained for several flap deflections and engine nozzle configurations at jet momentum coefficients from 0 to 4.0.

Three-component longitudinal data are presented with two engines operating. Limited longitudinal and lateral data are presented with an engine out. In addition, limited exhaust and flap pressure data are presented.

A maximum $C_{L_{max}}$ value of 11.5 at a jet momentum coefficient of 4.0 was obtained with an engine exhaust nozzle that provided a maximum jet exhaust total pressure close to the wing and flap surfaces. A Coanda surface that extended from 0.11 to 0.43 of the wing semispan was determined to provide optimum lift values.

INTRODUCTION

The principle of augmenting lift by directing the jet exhaust over the wing upper surface and turning it over the deflected flap by the Coanda effect is currently being considered in some powered-lift transport designs. One reason for this consideration is the possibility of noise reduction due to wing shielding. Earlier investigations of the upper surface blowing concept have been reported in references 1 and 2 for aerodynamic characteristics and in reference 3 for noise characteristics. Since these investigations were based on small-scale models with simulated jet exhaust, additional investigations are required at higher Reynolds numbers with a realistic jet exhaust wake that corresponds to present-day turbofan engines.

To fill this need an investigation was undertaken in the Ames 40- by 80-foot Wind Tunnel with a large scale upper surface blown-flap model. The aerodynamic and noise characteristics of a large-scale 25° swept-wing transport were obtained with two turbofan engines mounted on top of the wing. Only the aerodynamic characteristics of the model will be presented in this report. The noise characteristic data will be reported separately. Results were obtained with several flap deflections and engine nozzle configurations at jet momentum coefficients from 0 to 3.0 in most cases. The data were obtained at Reynolds numbers from 1.8×10^6 to 3.0×10^6, based on a mean aerodynamic chord of 1.69 m (5.56 ft) and at dynamic pressures from 153 to 460 N/m^2 (3.2 to 9.6 psf), respectively.

MODEL AND APPARATUS

A photograph of the model in Ames 40- by 80-foot Wind Tunnel is shown in figure 1. Pertinent dimensions of the model are given in figure 2(a). The model was equipped with two JT15D-1 engines. This model is the same as that reported in reference 4 except for the trailing-edge flap system and the four engines located below the wing.

Wing

The wing had a quarter chord sweep of 25°, an aspect ratio of 7.28, and an incidence of 0°. The airfoil section had an NACA 63_2A214 thickness distribution at the root tapering linearly to an NACA 63_2A211 thickness distribution at the tip. The ordinates of these sections are given in table I. The upper surface of the wing was modified from η = 0.11 to 0.48 in order to provide a better fairing between the engine nozzle and the Coanda surface as shown in figure 2(b).

Leading-Edge Slats

Full span leading-edge slats were used to delay the wing leading-edge flow separation as shown in figure 2(c). A 0.19 c slat was deflected 48.5° from η = 0.08 to 0.19, and a 0.25 c slat was deflected 50° from η = 0.33 to 1.0 with respect to the wing chord plane. The slats were attached to the wing leading edge throughout the investigation.

Trailing-Edge Flap System

The basic flap system had two flap segments with fixed pivots as shown in figure 2(d). The flap system extended from η 0.11 to 0.75 and consisted of the first and second flap of a triple-slotted flap configuration used in reference 4. A detachable Coanda plate surface was installed over the double-slotted flap from η = 0.11 to 0.48 with breaks at η = 0.15, 0.34, 0.39 and 0.43. Separate Coanda plates were used to provide a jet flap deflection, δ_f, of 30°, 55°, and

75°. A .254 m (.834 ft) chord extension was added at the trailing edge of the Coanda plate used for δ_f = 75° to give δ_f = 90°.

A 0.10 c plain spoiler hinged at 0.725 c formed part of the shrouded trailing edge when undeflected and extended from η = 0.51 to 0.75. The spoiler was deflected 30° above the wing surface during the investigation.

Aileron

A slotted aileron extended from η = 0.75 to 1.0 and was deflected 20° parallel to the plane of symmetry throughout the investigation as shown in figure 2(d). The aileron is the same one reported in reference 4.

Propulsion

The JT15D-1 engines were housed in nacelles as shown in figure 2(b). The engines have a bypass ratio of 3 and a normal maximum gross thrust rating of 2200 pounds. The nacelle centerline was coincident with the engine centerline and was pitched up 1° with respect to the wing chord plane. The centerline was located at η = 0.256 which was the same as the inboard engine centerline location of reference 4.

The nacelle contours are defined in figure 2(e). The maximum frontal area was .67 m^2 (7.25 ft^2) with an overall length of 2.60 m (8.54).

The nozzle configurations investigated are shown in figure 2(f). The investigation was primarily concerned with nozzles B, B with deflector, and D. Nozzle A was tested wind off only. Nozzle C was similar to nozzle D but deflected with increasing thrust, and no data are presented for this configuration.

Fuselage

The fuselage had a constant 1.2 m (4.0 ft) diameter except at the nose and tail. The nose section had an elliptical outline with circular cross sections that decreased from 1.2 m to smaller diameters. The tail section tapered from a 1.2 m circular section to a small elliptical section.

Two fuselage fence configurations were investigated to prevent possible engine exhaust cross flow over or under the fuselage as shown in figure 2(g). The fence located behind the flap and close to the bottom of the fuselage is designated configuration 1. The fence located on top of the fuselage is designated configuration 2.

Tail

The geometry of the horizontal and vertical tails is described in figure 2(a). These tails are the same ones used in reference 4. The horizontal tail detail is shown in figure 2(h). The horizontal tail incidence and elevator deflection were set at 0° when the tail was on during the investigation. The vertical tail was on the model throughout the investigation.

CORRECTIONS

The data were corrected for wind tunnel effects. These corrections were determined by considering only the aerodynamic lift of the model (C_L') that resulted after the jet reaction components had been subtracted from the data as follows:

$$C_L' = C_L - \eta_f C_J[\sin(\delta_j + \alpha_u)]$$

$$\alpha = \alpha_u + .4175\ C_L'$$

$$C_D = C_{D_u} + .0073\ C_L'^2$$

$$C_m = C_{m_u} + .025\ C_L' \quad \text{(horizontal tail test only)}$$

The C_J values were based on the calibrations of the left hand engine static thrust variation with engine fan rotational speed with the engine alone as described in Appendix A. The right hand engine static thrust was assumed to be equivalent to that of the left engine alone thrust plus the difference between the static thrusts of the right and left engines measured when installed on the model. δ_j and η_f values used in the corrections are shown in figures 4(a) and 4(b). These values were obtained from wind off normal (F_N) and axial (F_A) force measurements with the engine installed on the model operating in the wind tunnel. The resultant thrusts (F_R) were divided by the engine alone static thrust values to compute η_f values.

The data that are presented in this report are not corrected for ram drag. In order to determine this, the variation of ram drag with C_J for the nozzles investigated are shown in figure 5.

TESTING AND PROCEDURE

In most cases, forces and moments were measured through an angle-of-attack range of -8° to 26°. Tests were conducted at Reynolds numbers of 1.8×10^6 to 3.0×10^6, based on a mean aerodynamic chord of 1.69 m (5.56 ft) and at dynamic pressures of 153 to 460 N/m^2 (3.2 to 9.6 psf), respectively. Force measurements to compute δ_j values were obtained in the wind tunnel with the wind off prior to the wind on tests. These measurements were recorded at two or three power settings with one engine operating in most cases before air re-circulation could be generated in the test section.

Tests With Constant C_J and Varying Angle of Attack

Two engines operating— A constant C_J was maintained as angle of attack was varied for each flap and nozzle configuration investigated. The nominal C_J values used in most cases during the investigation are as follows:

C_J (2 engine)	q, N/m^2	q, psf
0	230	4.8
.5	↓	↓
1.0		
2.0		
3.0		

The variables tested were nozzle configurations, spanwise extents of the Coanda surface, jet flap deflections, spoiler deflection, and fuselage fence configurations. Tests were conducted with and without the horizontal tail.

One engine operating— Tests were conducted with the left engine out with nozzle B and 0.15 m gap deflector. The data were obtained for one case with the Coanda surface removed behind the engine-out side. For the other case the Coanda surface was left on behind the engine-out side.

Tests With Constant C_J and Varying Angle of Sideslip

A constant C_J was maintained at $\alpha_u = 0°$ and $8°$ as sideslip, β was varied from $4°$ to $-19°$. Tests were conducted with nozzle D at $\delta_f = 75°$ and $90°$.

RESULTS AND DISCUSSION

The static turning efficiencies (η_f) and static turning angles (δ_j) for the nozzles investigated are shown in figure 4. Figure 5 shows the variation of $C_{D_{ram}}$ with C_J for the engine nozzles investigated. The jet exhaust total pressure distribution at the engine centerline behind the nozzle and at the flap trailing edge are shown in figure 6. The lateral total pressure distribution behind the engine exhaust nozzle is shown in figure 7. The basic aerodynamic data obtained from this investigation are presented in figures 8 through 25. An index to these data is given in table II. The flap chordwise surface pressures behind the engine centerline are shown in figure 26. Figures 27 through 30 are summary plots that show the variation of C_L with C_J at $\alpha = 0°$ and at $C_{L_{max}}$.

Static Turning

In most cases the δ_j and η_f values shown in figure 4 were obtained with only the left hand engine operating. The results obtained with the right hand engine aline were nearly the same as those obtained with the left engine alone.

With the addition of a deflector (0.15 m gap) behind nozzle B the δ_j value increased from 46.5° to 58° at δ_f = 75°. However, the η_f value decreased from 97% to approximately 90%. Similar results were obtained with nozzle D. The improvement in δ_j was coincident with the movement of the maximum jet exhaust total pressure toward the wing and flap surfaces (see figure 6). These measurements were obtained from pressure rakes located behind the left engine and at the flap trailing edge as shown in figure 2(b). A fairly uniform exhaust total pressure distribution across the nozzle span was obtained with nozzle D and with nozzle B and 0.15 m gap deflector as shown in figure 7. These measurements were obtained from the single engine test described in Appendix A.

A slightly higher δ_j value (66°) was obtained with two engines operating simultaneously at the same power setting compared to 62° with a single engine operating (see fig. 3(b)). As indicated from surface flow observation this probably resulted from the jet exhaust spreading over the top of the fuselage for one engine operation, whereas this spreading was limited to the model plane of symmetry for two engine operation.

Variation of Lift Coefficients with Jet Momentum Coefficient at α = 0° and $C_{L_{max}}$

The effect of the deflector behind nozzle B on the variation of C_L and C_J is shown in figure 27. The increase in C_L values was significant with the deflector at 0.15 m gap because of the higher δ_j value and the movement of the maximum jet exhaust total pressure toward the wing and flap surfaces (see fig. 6). Additional improvements in C_L and $C_{L_{max}}$ values (approximately 7% at C_J = 3.0) were obtained with nozzle D compared to the values obtained with nozzle B and 0.15 m gap deflector as shown in figure 28. A maximum $C_{L_{max}}$ value of 11.5 at C_J = 4.0 and δ_f = 75° was obtained with nozzle D.

The effect of the Coanda surface spanwise extents on the variation of C_L with C_J is shown in figure 29. A loss in C_L and $C_{L_{max}}$ (7% at α = 0°, 3.5% at $C_{L_{max}}$ for C_J = 3.0) values resulted when the spanwise extent of the Coanda surface was decreased from η_c = 0.11 to 0.39 to η_c = 0.15 to 0.39. Slightly higher C_L and $C_{L_{max}}$ values were obtained when the spanwise extent of the Coanda surface was increased from η_c = 0.11 to 0.39 to η_c = 0.11 to 0.43. The lift values were nearly the same when the spanwise extent of the Coanda surface was increased from η_c = 0.11 to 0.43 to η_c = 0.11 to 0.48.

The effect of the fuselage fence configurations that were investigated on the variation of C_L with C_J was small as shown in figures 30(a) and 30(b).

APPENDIX A

An accurate engine static thrust calibration could not be obtained with the engines installed on the model during the wind tunnel tests because the flaps could not be retracted. Therefore, static thrust and jet exhaust total pressure survey measurements of the engine alone were conducted at the Ames static test facility site after the wind tunnel tests were completed. The left engine and nacelle configuration was removed from the model and was installed on a platform that was attached to three load cells as shown in figures 3(a) and 3(b). The engine nozzle configurations and areas were duplicated by adding an extension plate under the nozzle exit. This plate was contoured to match the wing upper surface behind the engine nozzle of the model. The engine centerline was leveled and was located 3.14 m (10.30 ft) above the ground.

The thrust valves as a function of fan rotational speed were obtained for nozzle B, B and 0.15 m gap deflector, and D. In addition the jet exhaust total pressures were surveyed laterally for the latter two nozzle configurations. Some of these data are presented in figure 7.

The static engine thrust calibration for nozzle B and 0.18 m gap deflector was assumed to be equivalent to that of the engine alone with nozzle B plus the difference between the thrusts obtained with the two nozzles measured with the engines installed on the model.

REFERENCES

1. Turner, Thomas; Davenport, Edwin E.; and Riebe, John M.: Low-Speed Investigation of Blowing from Nacelles Mounted Inboard and on the Upper Surface of an Aspect-Ratio-7.0 35° Sweptwing with Fuselage and Various Tail Arrangements. NASA Memo 5-1-59L, 1959.

2. Phelps, Arthur E.; Letko, William; and Henderson, Robert L.: Low-Speed Wind-Tunnel Investigation of a Semispan STOL Jet Transport Wing-Body with an Upper-Surface Blown Jet Flap. NASA TN D-7183, May 1973.

3. Maglieri, Domenic J.; and Hubbard, Harvey H.: Preliminary Measurements of the Noise Characteristics of Some Jet-Augmented-Flap Configuration. NACA Memo 12-4-58L, 1959.

4. Aoyagi, Kiyoshi; Falarski, Michael D.; and Koenig, David G.: Wind-Tunnel Investigation of a Large-Scale 25° Swept-Wing Jet Transport Model with an External Blowing Triple-Slotted Flap. NASA TM X-62,197.

TABLE I. — WING SECTION CONTOURS OF ROOT AND TIP SECTIONS (other sections obtained using straight line elements between these sections)

x^*/c, % c	$^{**}y/c$, % c			
	Section at wing root (η = 0)		Section at wing tip (η = 1.0)	
	Upper	Lower	Upper	Lower
0	0	0	0	0
0.55	1.356	—	1.060	—
0.88	—	-1.275	—	-0.998
1.00	1.748	-1.358	1.379	-1.061
3.00	2.957	-2.324	2.363	-1.785
5.00	3.802	-2.962	3.055	-2.259
8.00	4.774	-3.662	3.852	-2.776
10.00	5.304	-4.032	4.288	-3.065
12.50	5.873	-4.419	4.757	-3.329
15.00	6.357	-4.741	5.157	-3.562
20.00	7.127	-5.232	5.796	-3.915
25.00	7.680	-5.558	6.258	-4.143
30.00	8.045	-5.740	6.566	-4.265
35.00	8.220	-5.772	6.721	-4.273
40.00	8.217	-5.662	6.730	-4.174
45.00	8.046	-5.422	6.604	-3.978
50.00	7.730	-5.071	6.358	-3.699
55.00	7.288	-4.633	6.010	-3.357
60.00	6.738	-4.137	5.572	-2.999
65.00	6.091	-3.643	5.053	-2.643
70.00	5.363	-3.149	4.465	-2.286
75.00	4.574	-2.655	3.824	-1.929
80.00	3.742	-2.161	3.138	-1.573
85.00	2.839	-1.667	2.382	-1.204
90.00	1.912	-1.173	1.605	-0.859
95.00	0.971	-0.679	0.814	-0.503
100.00	0	-0.185	0	-0.146

*Chordwise distance from wing leading edge parallel to model plane of symmetry.

**Distance above wing reference plane-positive up—perpendicular to wing reference plane.

TABLE II.– LIST OF BASIC DATA FIGURES

Figure	δ_f, deg	η_c	δ_{f_2}, deg	C_J	α_y, deg	Nozzle	Deflector gap, m	q, N/m^2	q, psf	β, deg	Tail	Fuselage fence config.	Remarks
8	75 ↓	.11-.48 ↓	44 ↓	0 1.04 2.14 3.27	-8 to 24 -8 to 26 ↓	B ↓	Off	229.8 ↓ 225.0 229.8 ↓	4.8 ↓ 4.7 4.8 ↓	0 ↓	Off ↓	None ↓	Effect of nozzle deflector with landing flap
9	↓	↓	↓	1.11 2.33 3.48	↓	↓	0.18 0.18 0.18	↓	↓	↓	↓	↓	
10	↓	↓	↓	0 1.20 2.51 3.83	-8 to 20 -8 to 26 ↓	↓	0.15 ↓	↓	↓	↓	↓	↓	
11(a)	↓	.11-.43 ↓	↓	0 1.12 2.39 3.68	-8 to 24 -8 to 26 ↓	↓	↓	↓ 225.0	↓ 4.7	↓	↓	↓	Effect of spanwise extent of Coanda surfaces
11(b)	↓	.11-.39 ↓	↓	0 1.13 2.39 3.68	-8 to 24 -8 to 26 ↓	↓	↓	234.6 ↓ 229.8 ↓	4.9 ↓ 4.8 ↓	↓	↓	↓	
11(c)	↓	.15-.39 ↓	↓	0 1.12 2.32 3.01	↓	↓	↓	234.6 229.8 234.6 ↓	4.9 4.8 4.9 ↓	↓	↓	↓	
12	↓	.11-.48 ↓	↓	0 2.49 3.19	-8 to 24 -8 to 26 -8 to 26	↓	↓	229.8 ↓	4.8 ↓	↓	↓	1 ↓	Effect of fuselage fence
13	30 ↓	.11-.39 ↓	↓	0 0.54 1.08 2.33 3.63	-8 to 24 -8 to 26 ↓	↓	↓	459.6 ↓ 225.0 ↓	9.6 ↓ 4.7 ↓	↓	↓	None ↓	Takeoff flap

TABLE II. — LIST OF BASIC DATA FIGURES — CONTINUED

Figure	δ_f, deg	η_c	δ_{f_2}, deg	C_J	α_y, deg	Nozzle	Deflector gap, m	q, N/m²	q, psf	β, deg	Tail	Fuselage fence config.	Remarks
14	55	.11-.43	27.5	0	-8 to 24	D	Off	229.8	4.8	0	Off	None	
				.95	-8 to 26								
				2.03									
				2.98									
15(a)	75		44	0	-8 to 27								
				0.48				225.0	4.7				R = 2.1×10^6
				.96				229.8	4.8				
				1.99									
				2.92				225.0	4.7				
				4.08				177.1	3.7				R = 1.8×10^6
15(b)				0.23				459.6	9.6				R = 3.0×10^6
				.47									
				1.00									
				1.58									
16(a)				0	-8 to 24			234.6	4.9		$i_t = 0°$		Tail on
				0.48	-8 to 27								
				.96									
				2.08				229.8	4.8				
				2.78									
16(b)				0	-8 to 24						$i_t = -10.5°$		
				1.00	-8 to 27								
				2.11									
				3.14									
17	90			0	-8 to 24			225.0	4.7		$i_t = 0°$		
				0.49	-8 to 27								
				1.02									
				2.17									
				3.03				229.8	4.8				
18(a)				0								1	
				0.91									
				1.97									
				3.07									

TABLE II. – LIST OF BASIC DATA FIGURES – CONTINUED

Figure	δ_f, deg	η_c	δ_{f_2}, deg	C_J	α_y, deg	Nozzle	Deflector gap, m	q, N/m²	q, psf	β, deg	Tail	Fuselage fence config.	Remarks
18(b)	90	.11-.43	44	0.89	-8 to 24	D	Off	234.6	4.9	0	$i_t=0°$	2	
	↓			1.98	-8 to 27			229.8	4.8				
19	75	↓		2.02	↓							Off	Spoiler effect δ_{sp} = 30°
	↓			3.20									
20	90	.11-.43		0.91									δ_f = 90° (η_c = .11 - .43)
	75	.43-.48		1.92	↓	↓	↓	↓	↓		↓		δ_f = 75° (η_c = .43 - .48)
21(a)	75	.11-.43		1.25	-8 to 26	B	0.15	225.0	4.7		Off		Longitudinal characteristics of the model with left hand engine out
				1.89				229.8	4.8				
21(b)				1.25				225.0	4.7				Lateral characteristics of the model with left hand engine out
		↓		1.89				229.8	4.8				
22(a)		.11-.43 Right hand side only		0				↓	↓				Longitudinal characteristics of the model with left hand Coanda surfaces removed and engine out
				0.58									
				1.23				225.0	4.7				
				1.91				↓	↓				
22(b)				0				229.8	4.8				Lateral characteristics of the model with left hand Coanda surfaces removed and engine out
				0.58				↓	↓				
				1.23				225.0	4.7				
	↓	↓	↓	1.91	↓	↓	↓	↓	↓	↓	↓	↓	
Variation of side force, yawing-moment, and rolling-moment coefficients with sideslip													
23(a)	90	.11-.43	44	0	0	D	Off	234.6	4.9	4 to -19	$i_t=0°$	Off	
				0.92				229.8	4.8				
				1.95				↓	↓				
				3.01	↓			215.5	4.5				
23(b)				0	8			229.8	4.8				
				0.91									
				1.95				↓	↓				
	↓	↓	↓	2.92	↓	↓	↓	158.0	3.3	↓	↓	↓	

TABLE II. — LIST OF BASIC DATA FIGURES — CONCLUDED

Figure	δ_f, deg	η_c	δ_{f_2}, deg	C_J	α_y, deg	Nozzle	Deflector gap, m	q, N/m^2	q, psf	β, deg	Tail	Fuselage fence config.	Remarks
24(a)	90	.11-.43	44	0.92	0	D	Off	229.8	4.8	4 to -19	$i_t = 0°$	1	
				1.96									
				2.93				153.2	3.2				
24(b)				0.91	8			229.8	4.8				
				1.95									
				3.02				148.4	3.1				
25	75			2.01	0			229.8	4.8			Off	
				2.96				225.0	4.7				
				2.02	8								
				2.99									

Figure 1.— Photograph of the model as mounted in the the Ames 40- by 80-Foot Wind Tunnel.

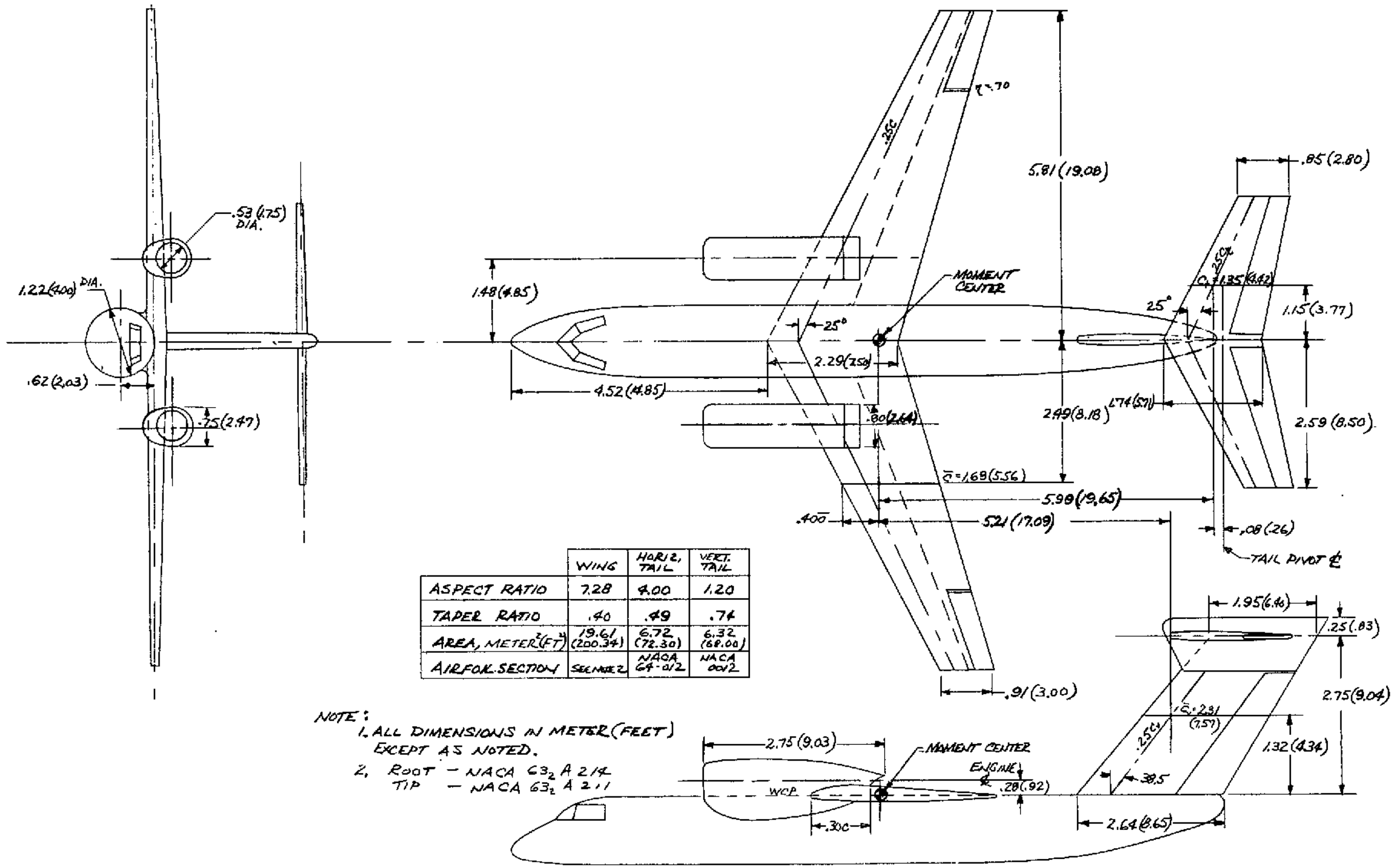

	WING	HORIZ. TAIL	VERT. TAIL
ASPECT RATIO	7.28	4.00	1.20
TAPER RATIO	.40	.49	.74
AREA, METER^2 (FT^2)	19.61 (200.34)	6.72 (72.30)	6.32 (68.00)
AIRFOIL SECTION	SEE NOTE 2	NACA 64-012	NACA 0012

NOTE:
1. ALL DIMENSIONS IN METER (FEET) EXCEPT AS NOTED.
2. ROOT – NACA 63_2 A 214
   TIP – NACA 63_2 A 211

(a) GENERAL ARRANGEMENT OF THE MODEL

FIGURE 2.– GEOMETRIC DETAILS OF THE MODEL.

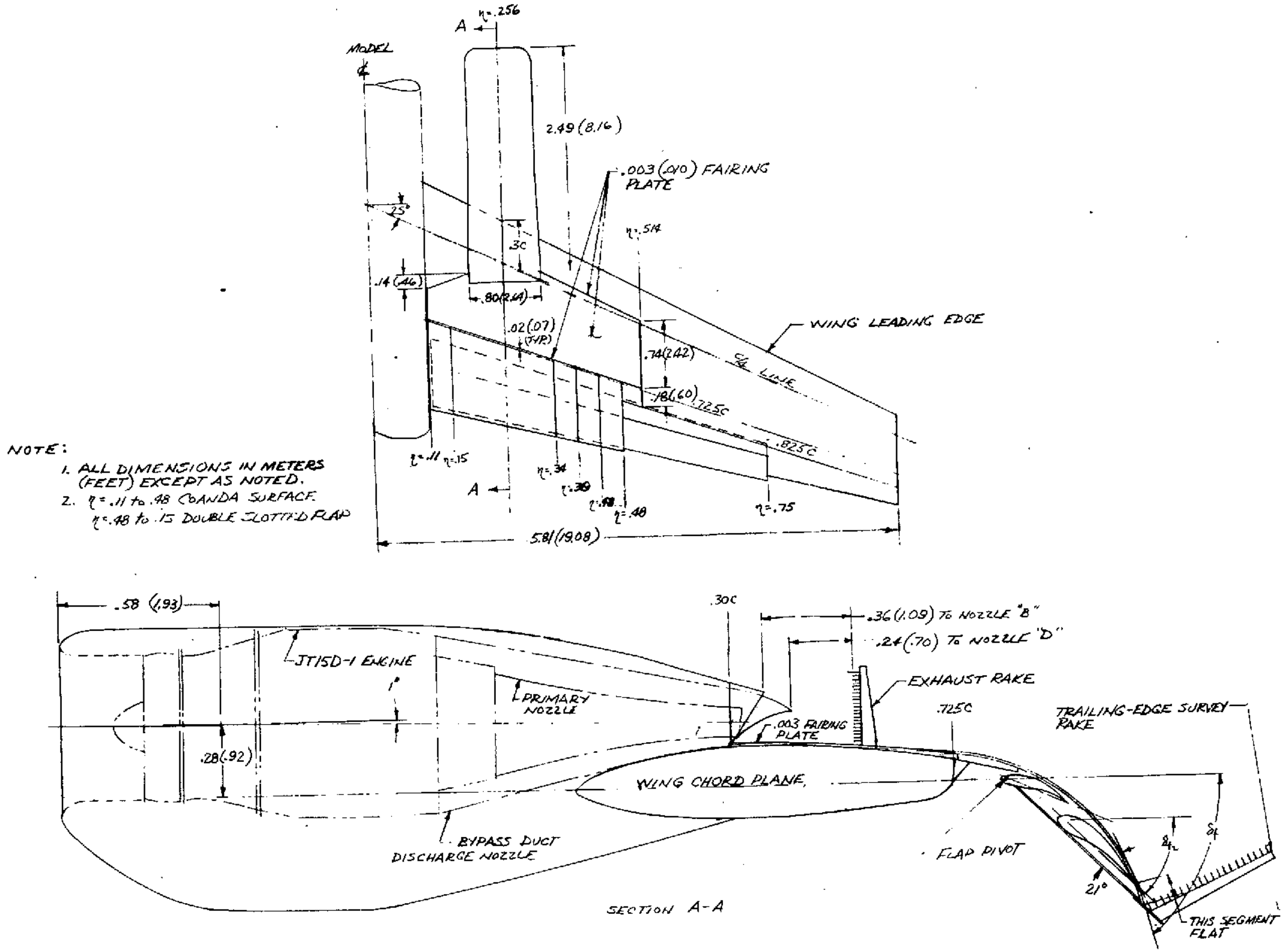

(b) UPPER SURFACE BLOWING FLAP AND NOZZLE ARRANGEMENT

FIGURE 2 – CONTINUED.

SEC. A-A ORDINATES			SEC. B-B ORDINATES		
x, %c	Y_U, %c	Y_L, %c	x, %c	Y_U, %c	Y_L, %c
0	.38	—	0	0	0
.23	1.41	—	.31	.95	-.54
.47	1.86	—	.62	1.30	-.74
.70	2.30	—	1.25	1.82	-.99
.94	2.47	—	1.87	2.22	-1.06
1.41	2.93	—	2.50	2.50	-1.13
1.88	3.29	—	3.75	2.96	-1.04
2.35	3.55	—	5.00	3.28	-.97
2.82	3.78	—	6.25	3.50	-.79
3.76	4.01	.49	7.50	3.67	-.47
4.70	4.31	1.38	10.00	1.24	.10
5.64	4.38	1.95	12.50	3.43	.59
6.58	4.37	2.34	15.00	2.93	.68
7.52	4.30	2.58	17.50	2.26	.55
9.40	3.92	2.71	20.00	1.59	.35
11.29	3.37	2.53	22.50	.87	1.11
13.18	2.67	2.12	23.75	.42	-.04
15.05	1.86	1.52	25.00	0	-.16
16.94	1.01	.75			
18.80	.07	-.07			
LER 1.80; SLOPE .2					

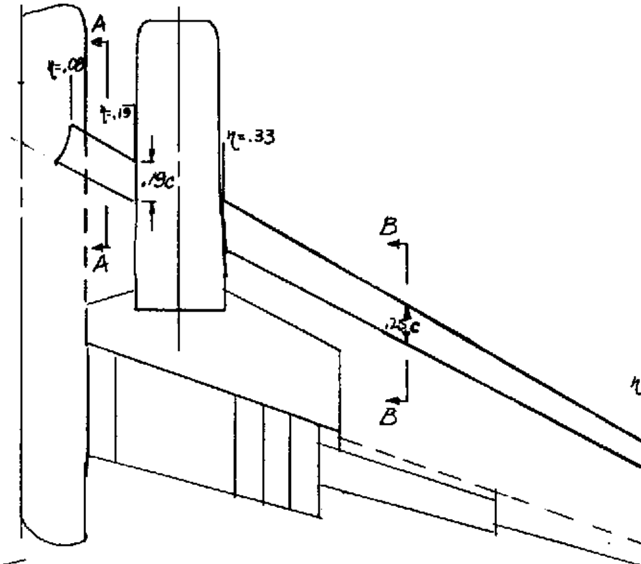

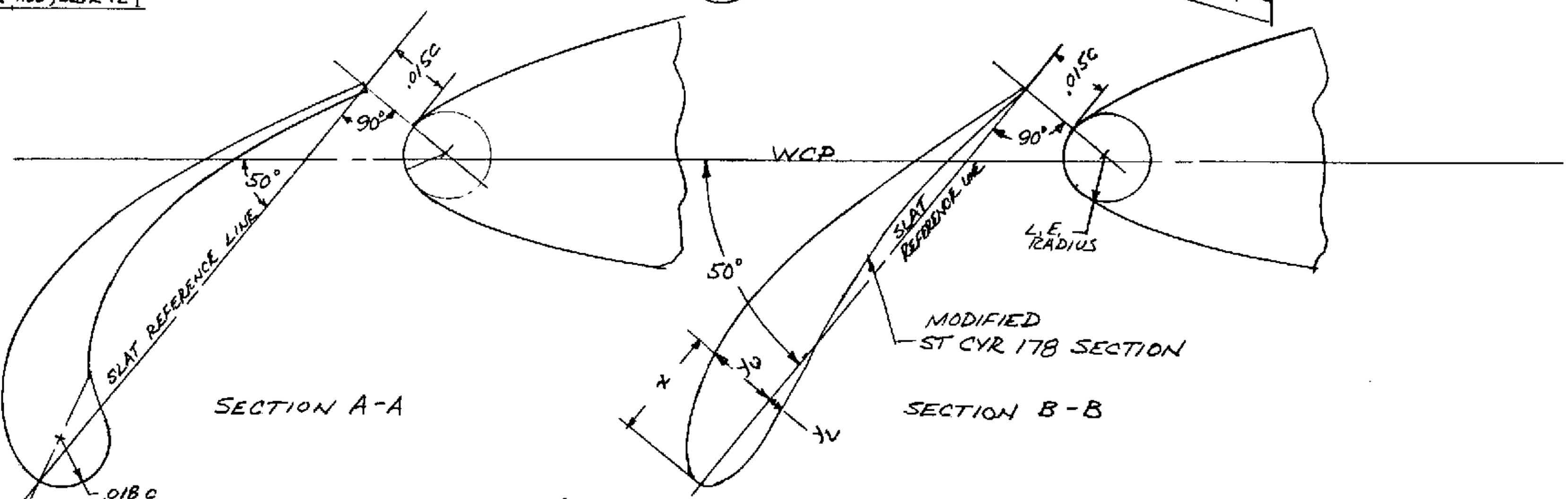

(c) LEADING-EDGE SLAT ARRANGEMENT

FIGURE 2. — CONTINUED.

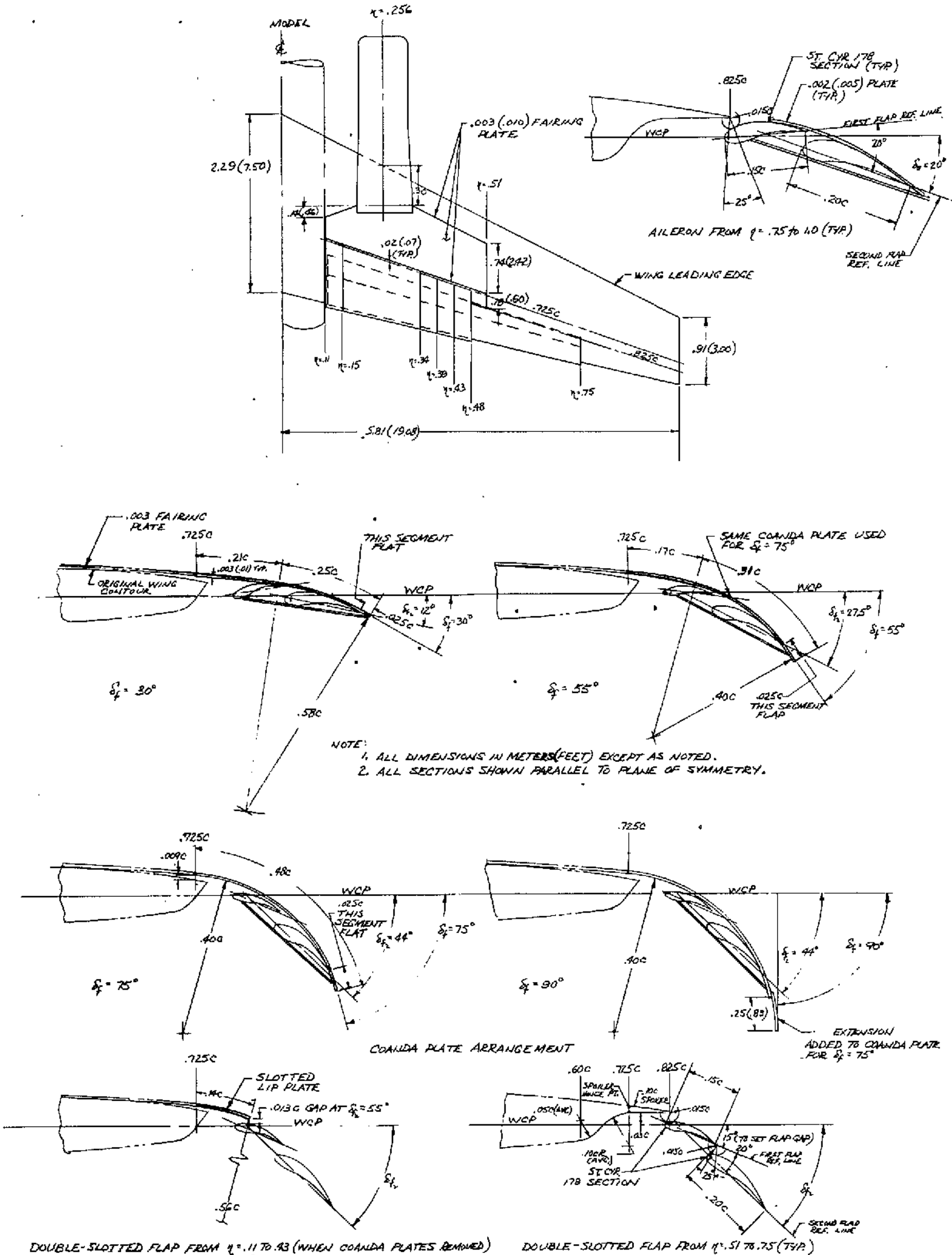

(d) TRAILING-EDGE FLAP AND AILERON ARRANGEMENT

FIGURE 2 — CONTINUED.

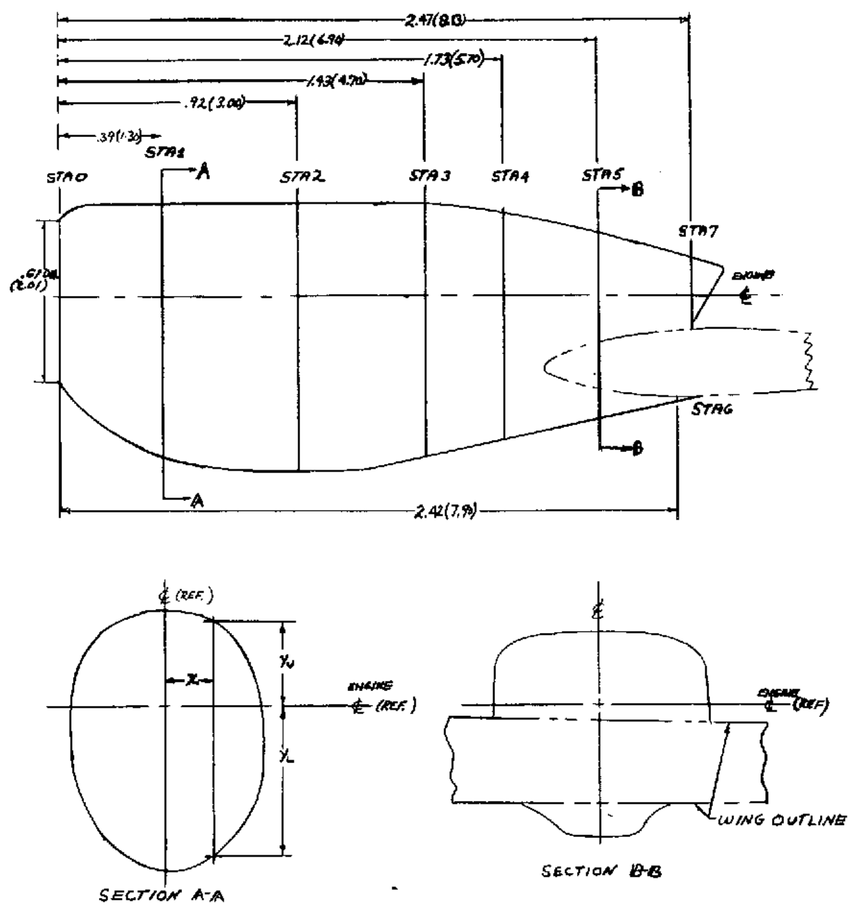

STA #1

x	Y_U (AVG)	Y_L (AVG)
0	.38	.64
.05	.38	.64
.10	.37	.62
.15	.35	.60
.20	.32	.56
.25	.28	.51
.30	.22	.43
.36	.12	.31
.38	0	0

STA #2

x	Y_U (AVG)	Y_L (AVG)
0	.37	.73
.05	.37	.73
.10	.36	.72
.15	.34	.68
.20	.31	.63
.25	.27	.56
.30	.21	.48
.36	.12	.37
.38	0	0

STA #3

x	Y_U (AVG)	Y_L (AVG)
0	.38	.66
.05	.38	.66
.10	.37	.66
.15	.35	.61
.20	.32	.53
.25	.28	.48
.30	.23	.43
.36	.14	.36
.39	0	0

STA #4

x	Y_U (AVG)	Y_L (AVG)
0	.36	.60
.05	.36	.60
.10	.35	.59
.12	—	.58
.15	.34	.56
.20	.33	.49
.25	.30	.45
.30	.26	.41
.36	.21	.35
.39	—	.25
.43	0	0

STA #5

x	Y_U (AVG)	Y_L (AVG)
0	.29	.51
.05	.29	.51
.10	.28	.51
.12	—	.51
.15	.28	.49
.20	.28	.44
.25	.27	.40
.30	.26	.38
.36	.24	.35
.41	.16	.32
.42	0	0

x	STA #7 Y_U (AVG)	STA #6 Y_L (AVG)
0	.19	.45
.05	.19	.45
.10	.19	.45
.12	—	.44
.15	.19	.42
.20	.19	.39
.25	.19	—
.30	.19	—
.36	.19	—
.41	.17	—
.42	0	0

NOTE:
1. ALL DIMENSIONS IN METERS(FEET).

(c) NACELLE CONTOUR.
FIGURE 2.- CONTINUED.

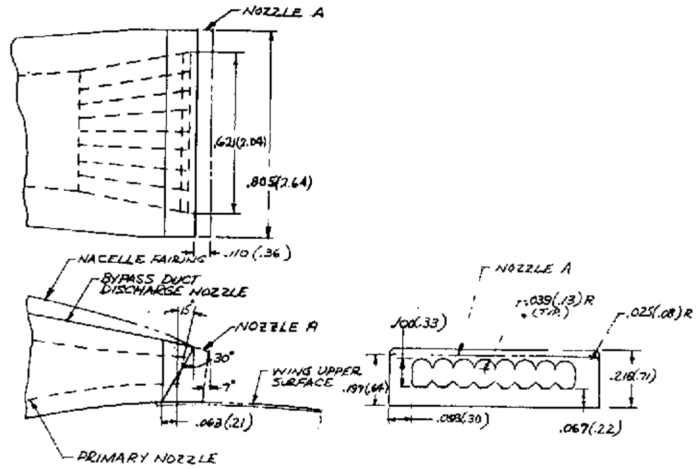

NOZZLE A & B

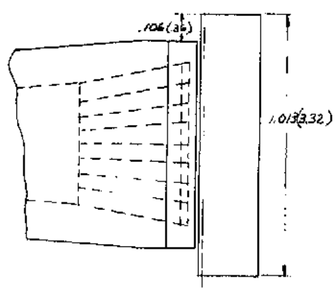

NOTE:
1. ALL DIMENSIONS IN METERS (FEET) EXCEPT AS NOTED.
2. NOZZLE C SIMILAR TO D BUT DEFORMED WHEN LOADED.

NOMINAL GAP	a	b	c
.15	.162(.53)	.149(49)	.143(.47)
.18	.187(.61)	.175(.57)	.164(.54)

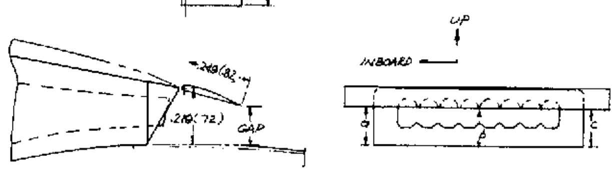

NOZZLE B WITH DEFLECTOR

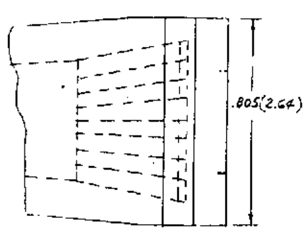

NOMINAL GAP	a	b	c
.15	.152(.50)	.155(.51)	.160(.53)

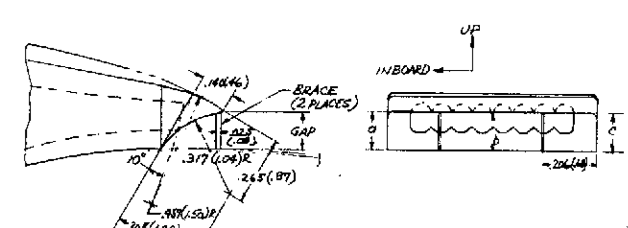

NOZZLE D

(f) ENGINE NOZZLE ARRANGEMENT
FIGURE 2.- CONTINUED.

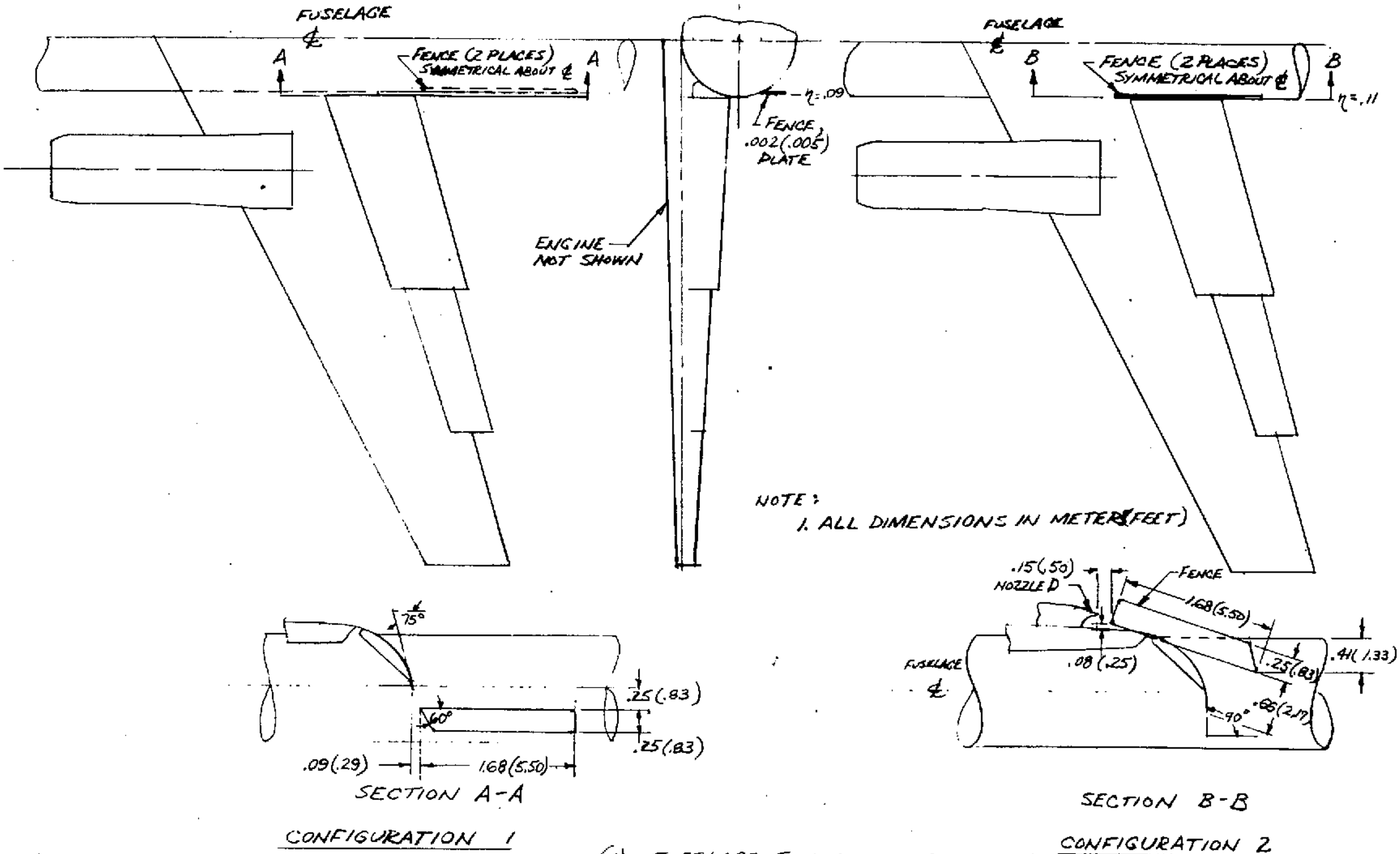

(g). FUSELAGE FENCE CONFIGURATIONS

FIGURE 2.– CONTINUED.

SHROUD COORDINATES			ELEVATOR COORDINATES		
X, %c_t	Y_U, %c_t	Y_L, %c_t	X, %c_t	Y_U, %c_t	Y_L, %c_t
62.00	3.98	-4.28	0	0	0
64.00	2.75	-4.06	.44	.57	-.98
65.00	1.93	-3.95	.87	.78	-1.36
66.00	1.22	-3.84	1.75	.98	-1.89
68.00	.14	-3.61	2.63	.97	-2.20
70.00	-.67	-3.39	3.50	.95	-2.63
72.00	-1.28	-3.17	5.26	.90	-3.16
74.00	-1.68	-2.95	7.00	.85	-3.52
75.00	-1.84	-2.84	8.75	.80	-3.77
76.00	-1.98	-2.73	10.50	.75	-3.90
78.00	-2.14	-2.50	14.00	.65	-3.92
80.00	-2.19	-2.28	17.50	.55	-3.40
			21.00	.45	-2.90
			24.50	.35	-2.20
			18,00	.25	-1.50
			31.50	.15	-.80
			33.00	.10	-.50
			35.00	.05	-.05
			LER = .89%c_t		

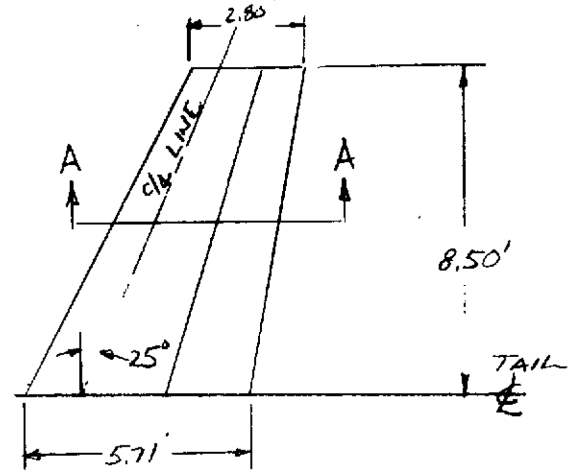

PLANFORM

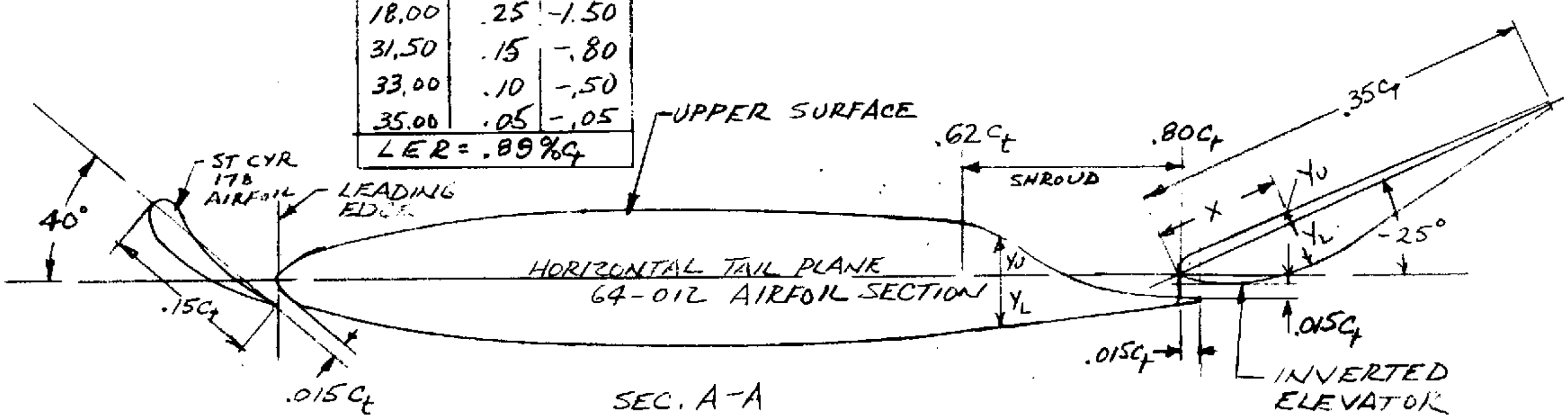

SEC. A-A

(h) HORIZONTAL TAIL DETAIL

FIGURE 2.- CONCLUDED.

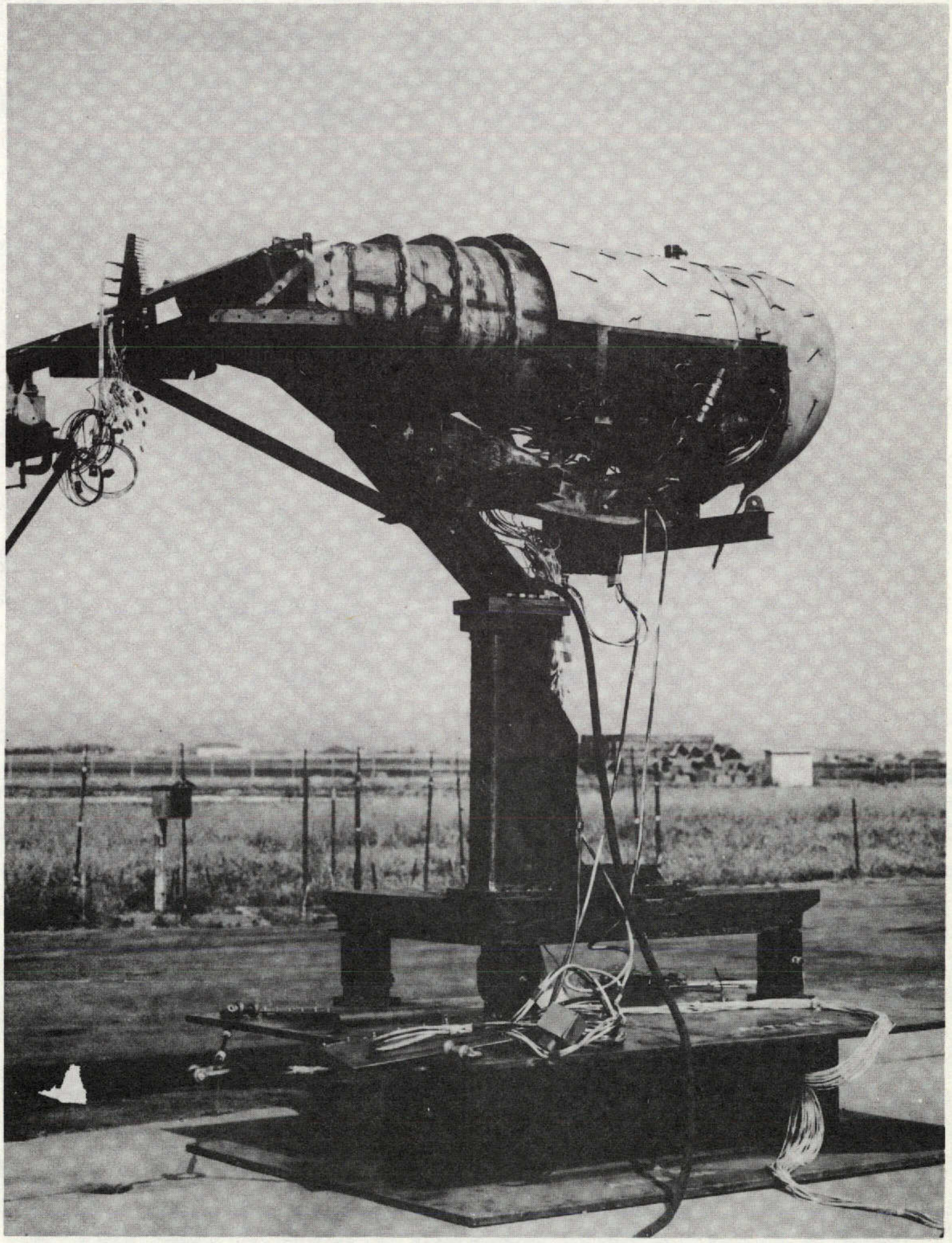

(a) Photograph of the JT15D-1 engine at the
Ames static test facility site

Figure 3.— Single JT15D-1 engine static thrust stand installation.

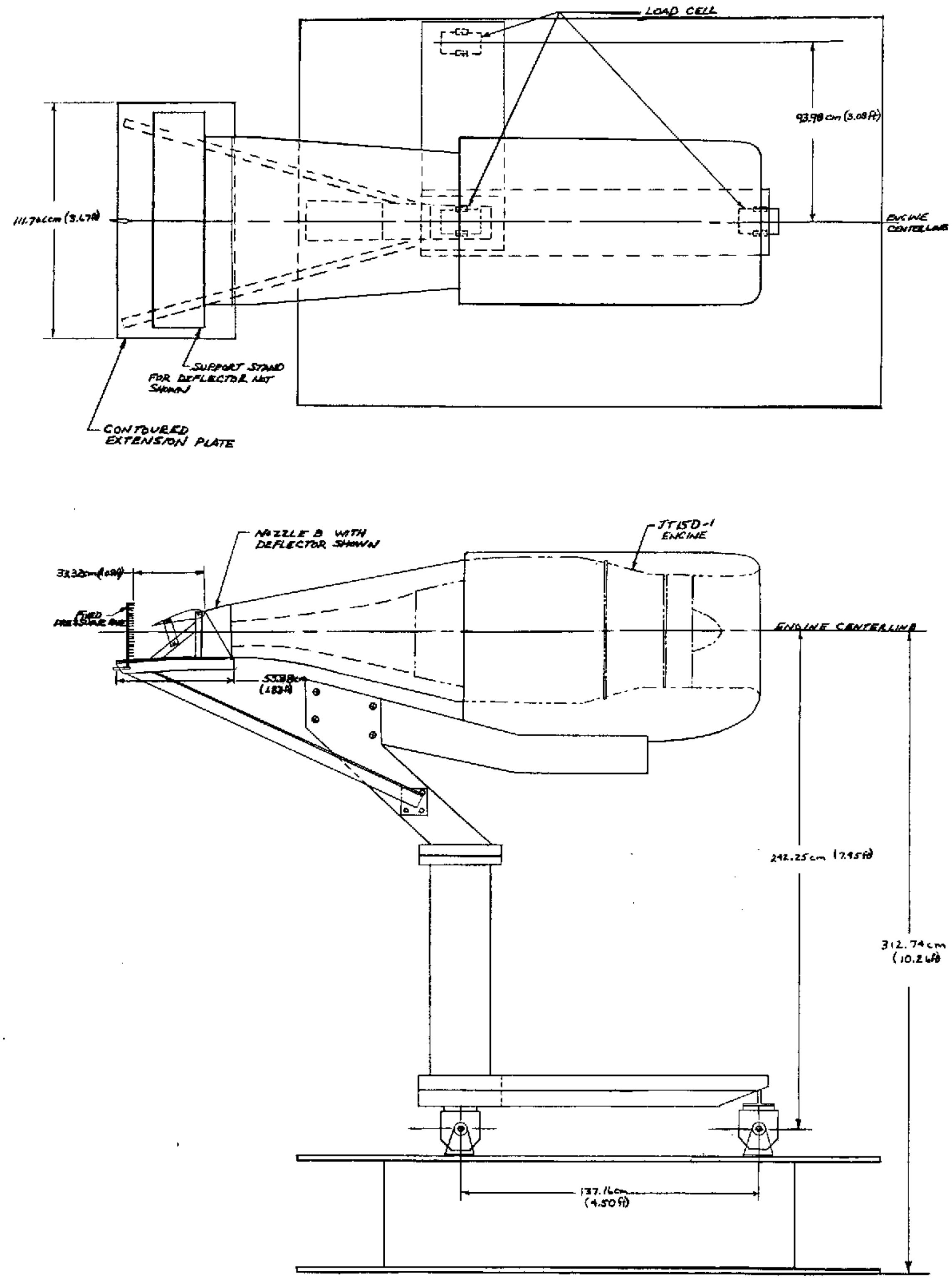

(b) JT15D-1 Engine Static Test Stand.

Figure 3.– Concluded.

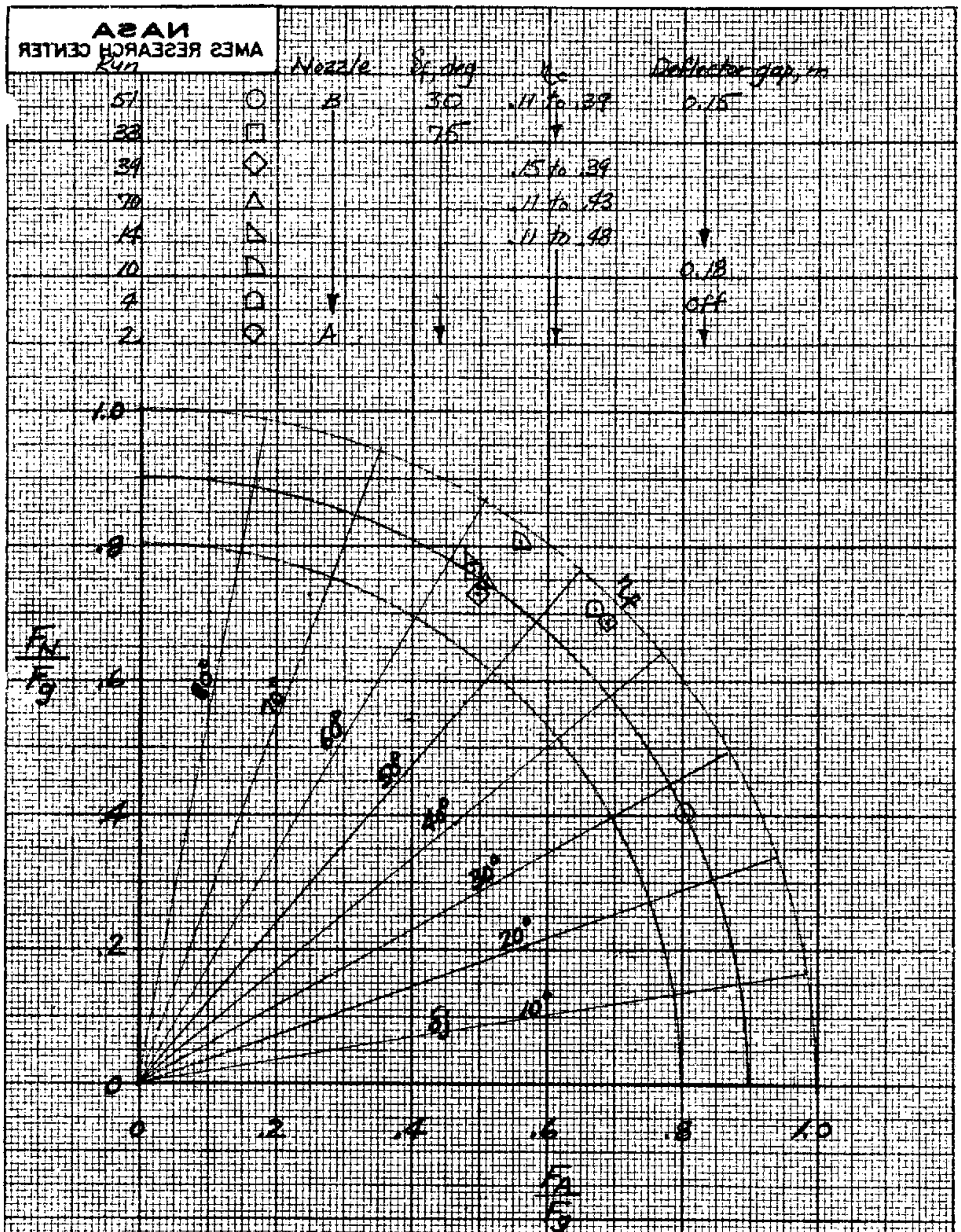

(b) Nozzle B with and without deflector; Nozzle A

Figure 4.— Flap static turning efficiency and turning angle.

Run		δ_{f_z}, deg	η_o	Engine operating
64	○	55	.11 to .43	Left
73	□	75	↓	↓
96	◇	90	↓	↓
124	△	90	↓	Left and Right

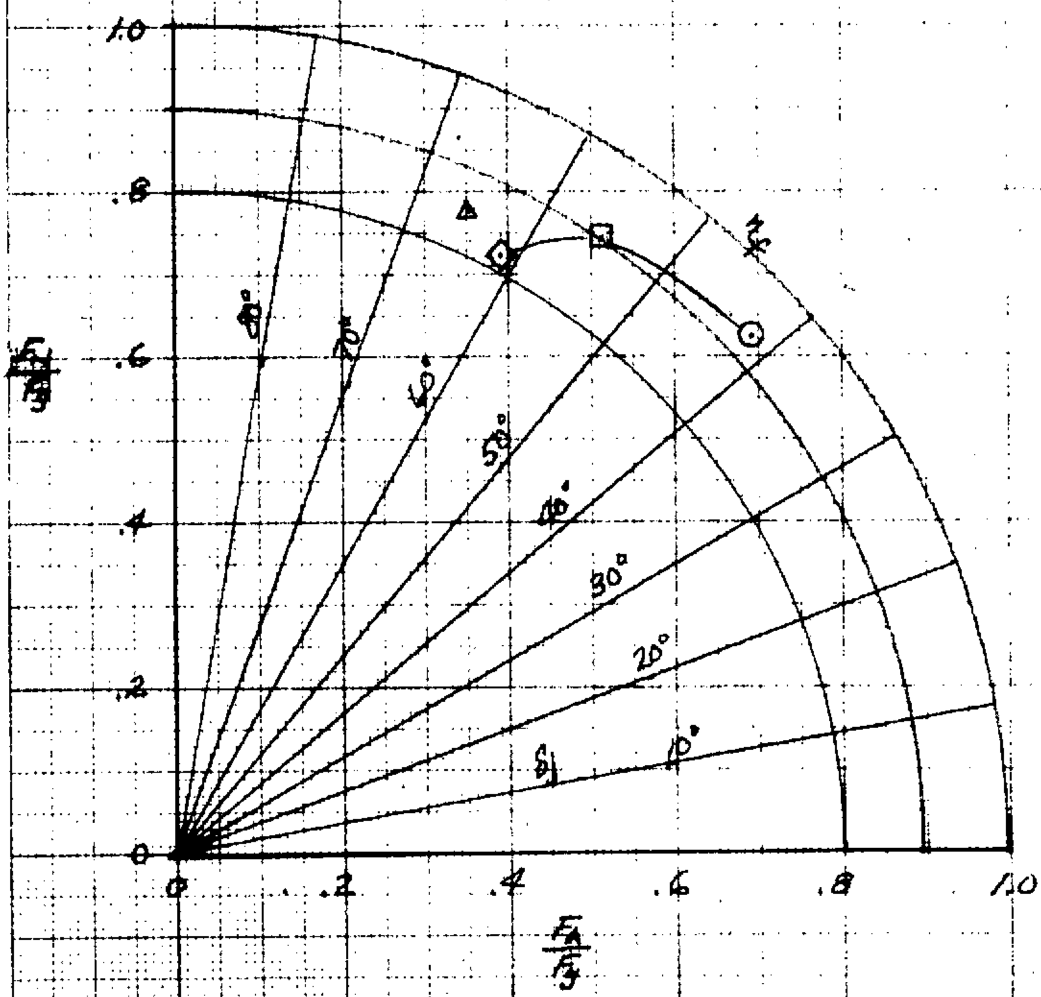

(b) Nozzle D

Figure 4.— Concluded.

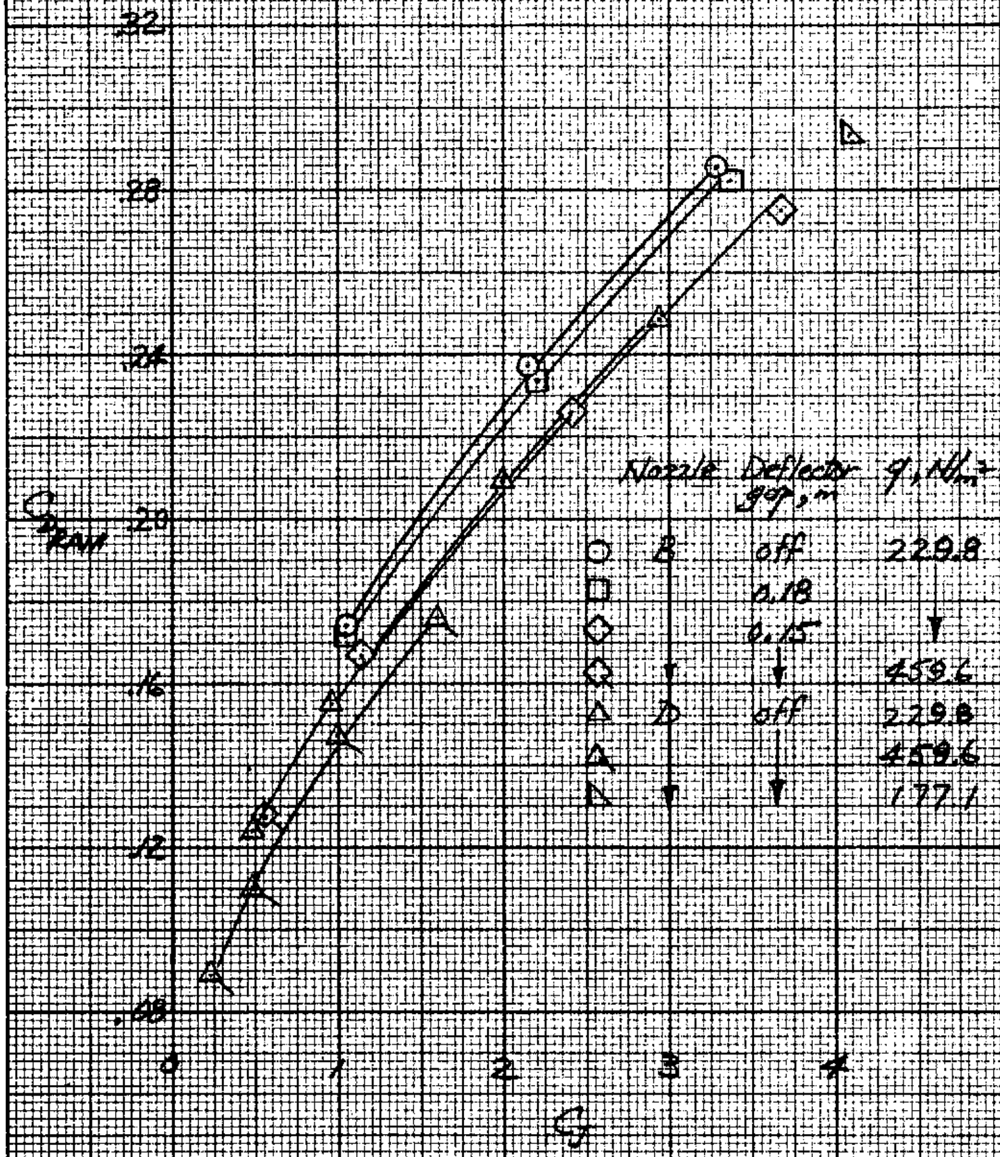

Figure 5 – Variation of $C_{D_{RAM}}$ with C_J for the exhaust nozzles investigated.

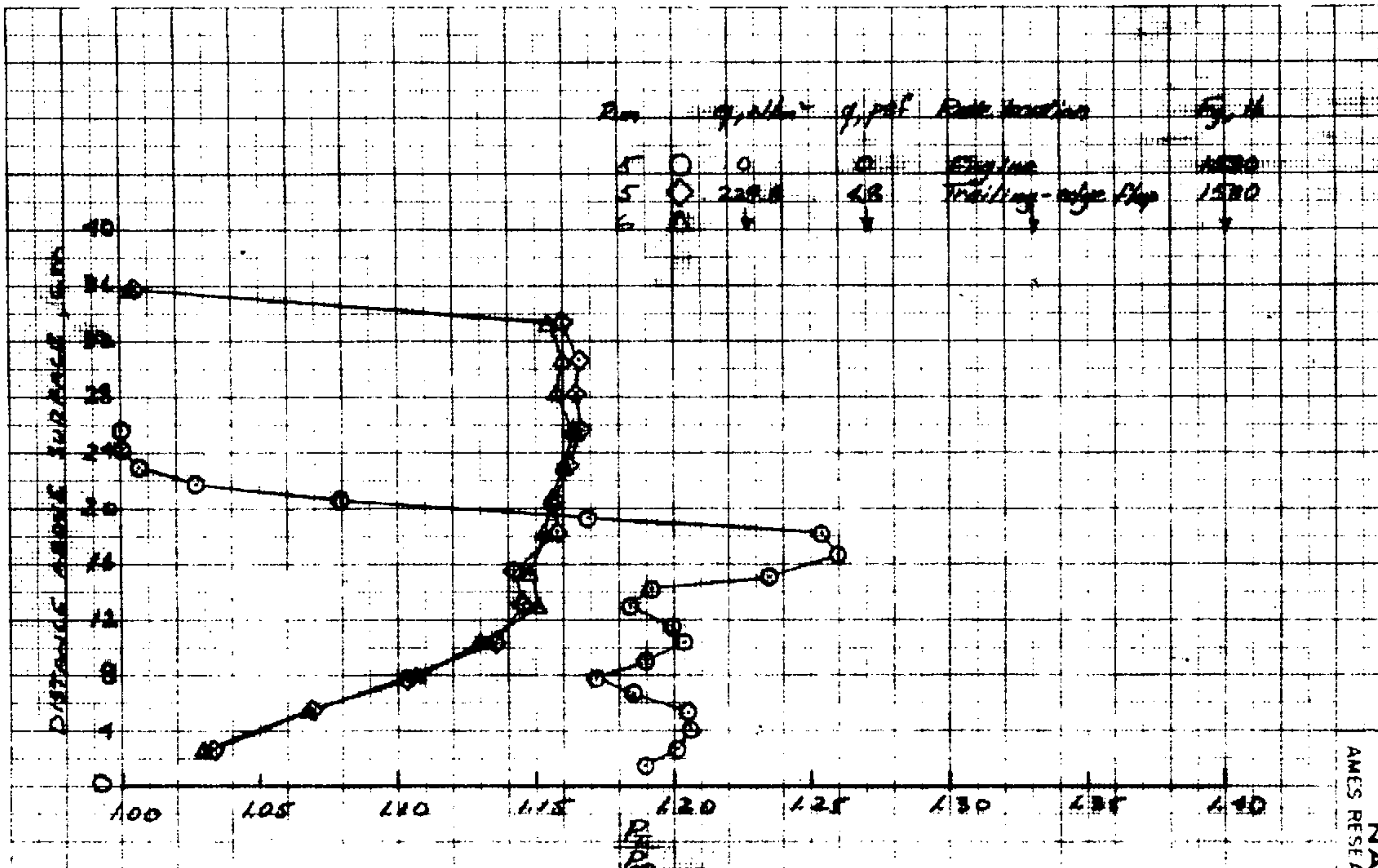

(a) Nozzle B; $\delta_f = 75°$ (η_c = .11 to .48).

Figure 6.- Jet exhaust pressure ratio at the left hand engine centerline behind the nozzle and flap trailing-edge, $\alpha_u = 0°$.

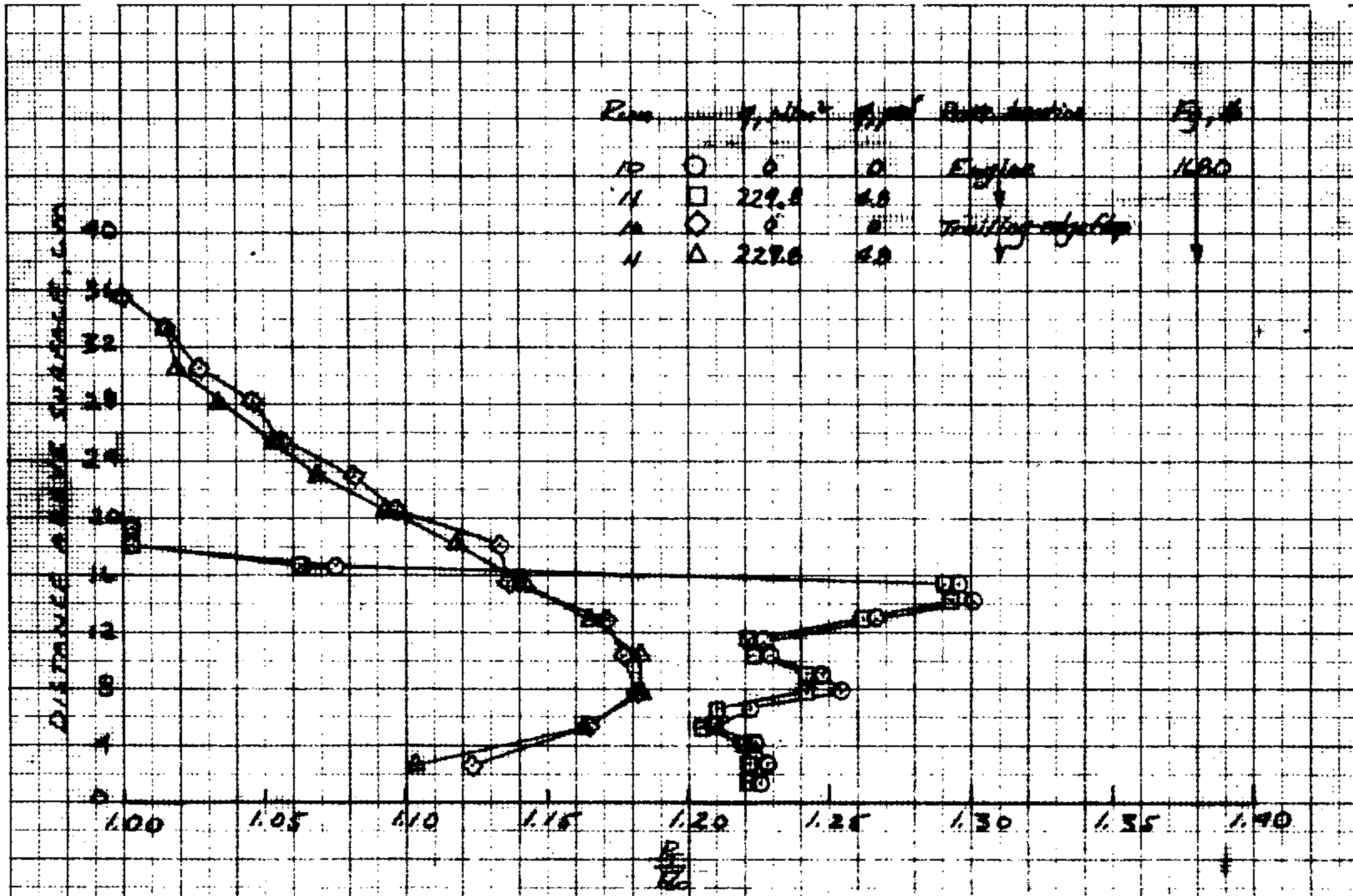

(b) Nozzle B with 0.10 in gap deflector; $\delta_f = 75°$ (η_c = .11 to .48).

Figure 6.– Continued.

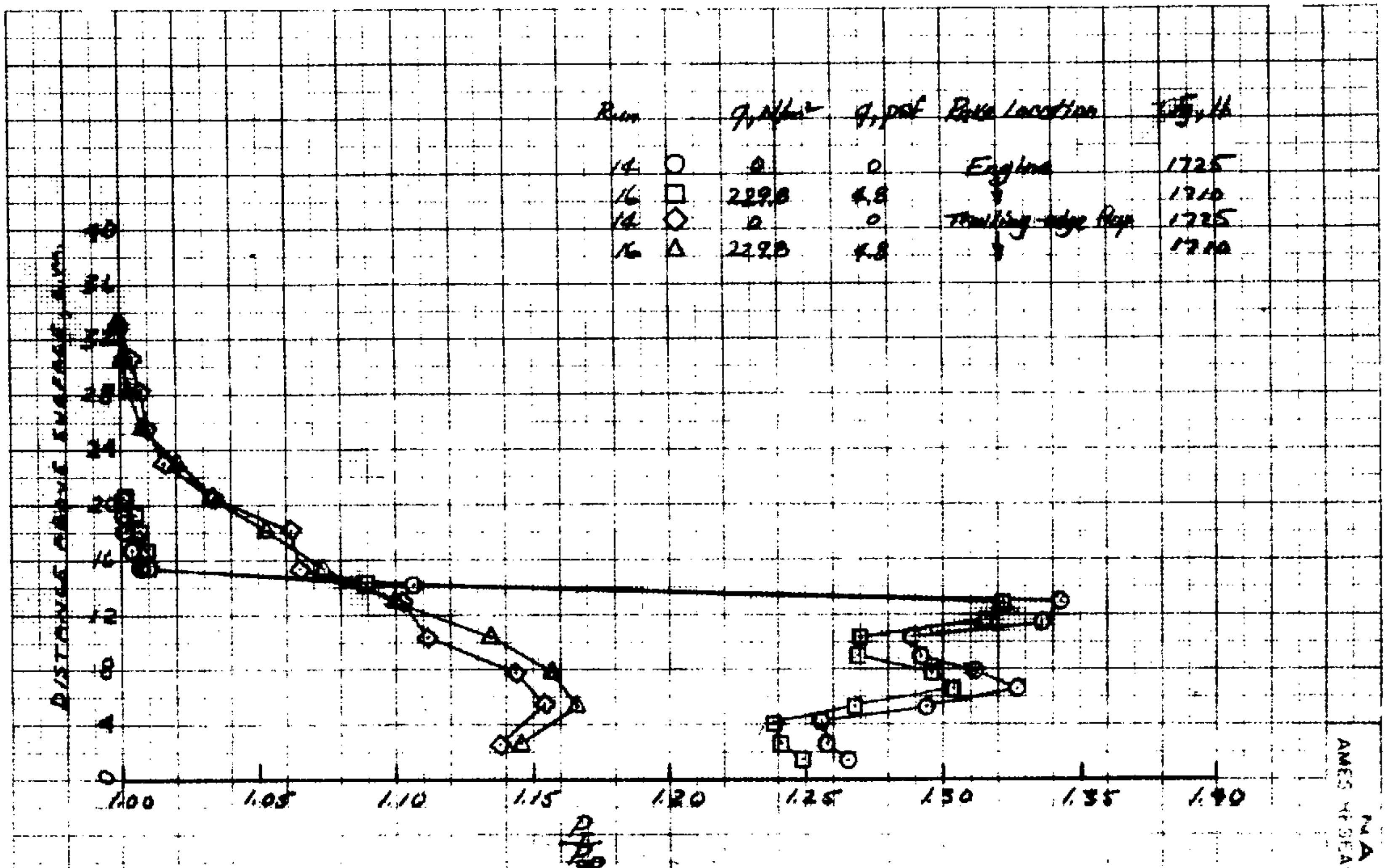

(c) Nozzle B with 0.15m deflector; $\delta_f = 75°$ (η_c = .11 to .48)

Figure 6. — Continued.

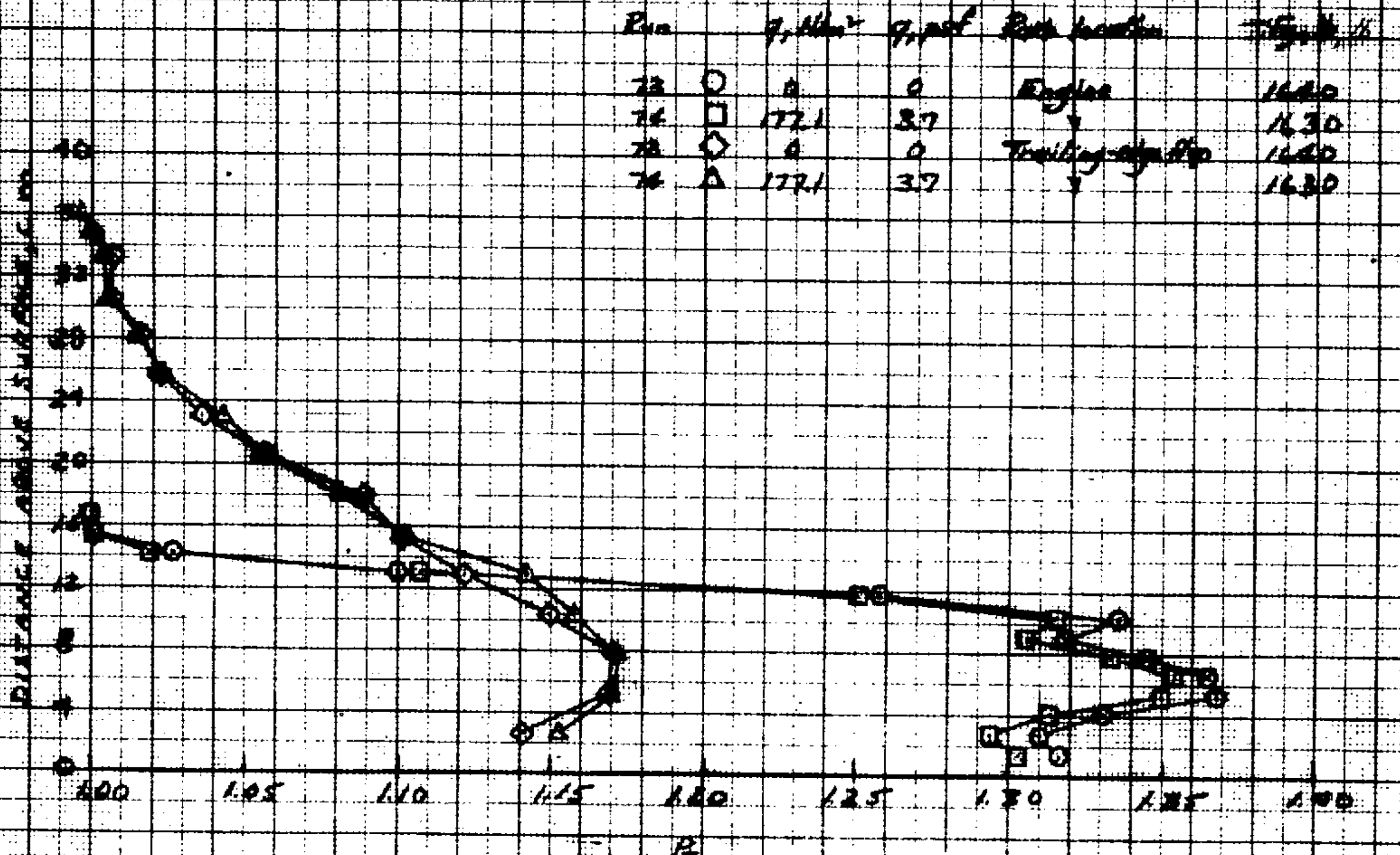

(d) Nozzle D; $\delta_f = 75°$ (η_c = .11 to .43).

Figure 6. – Concluded.

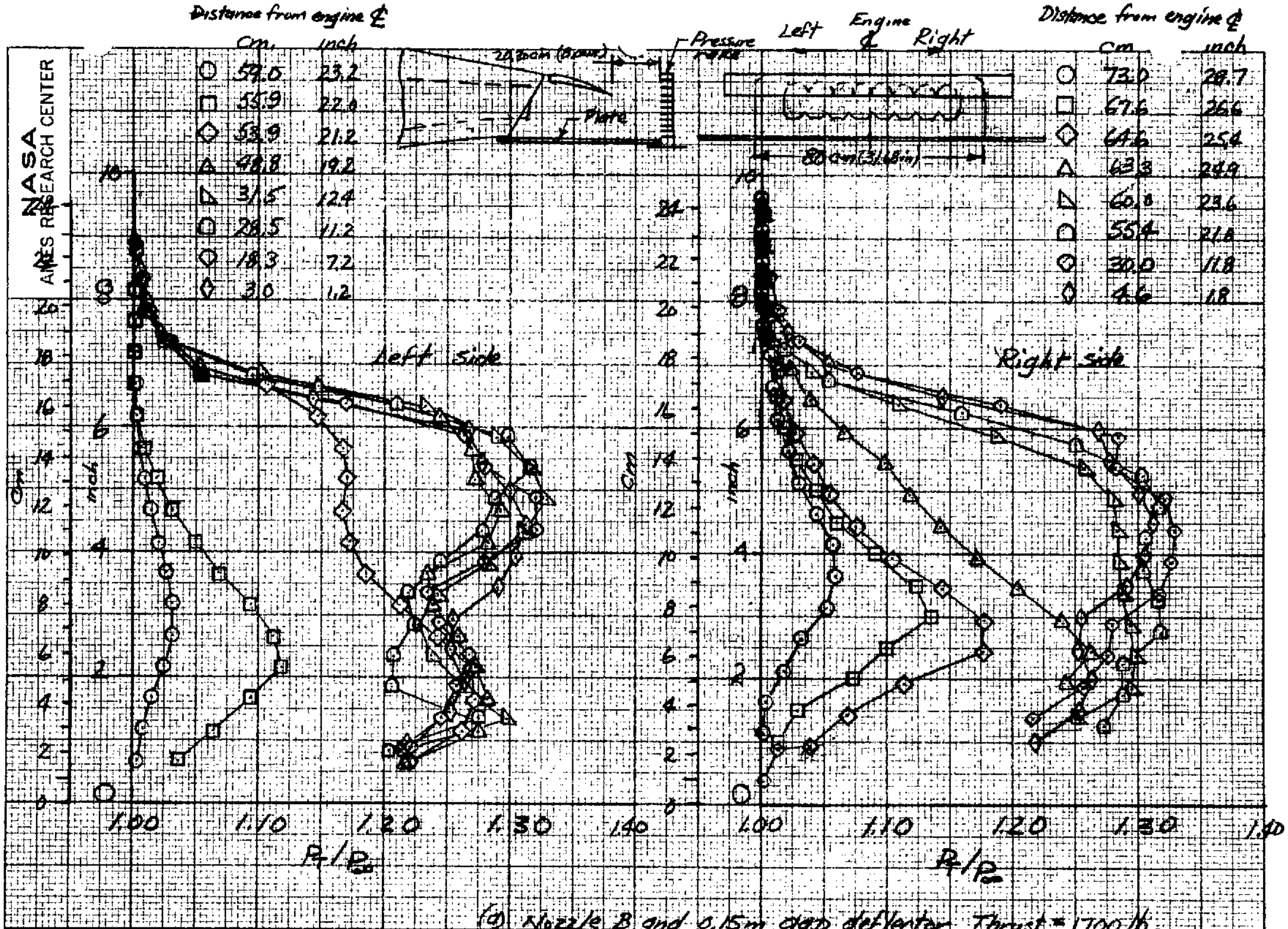

Figure 7.- Lateral total pressure distribution behind engine exhaust nozzle; q = 0 N/m²

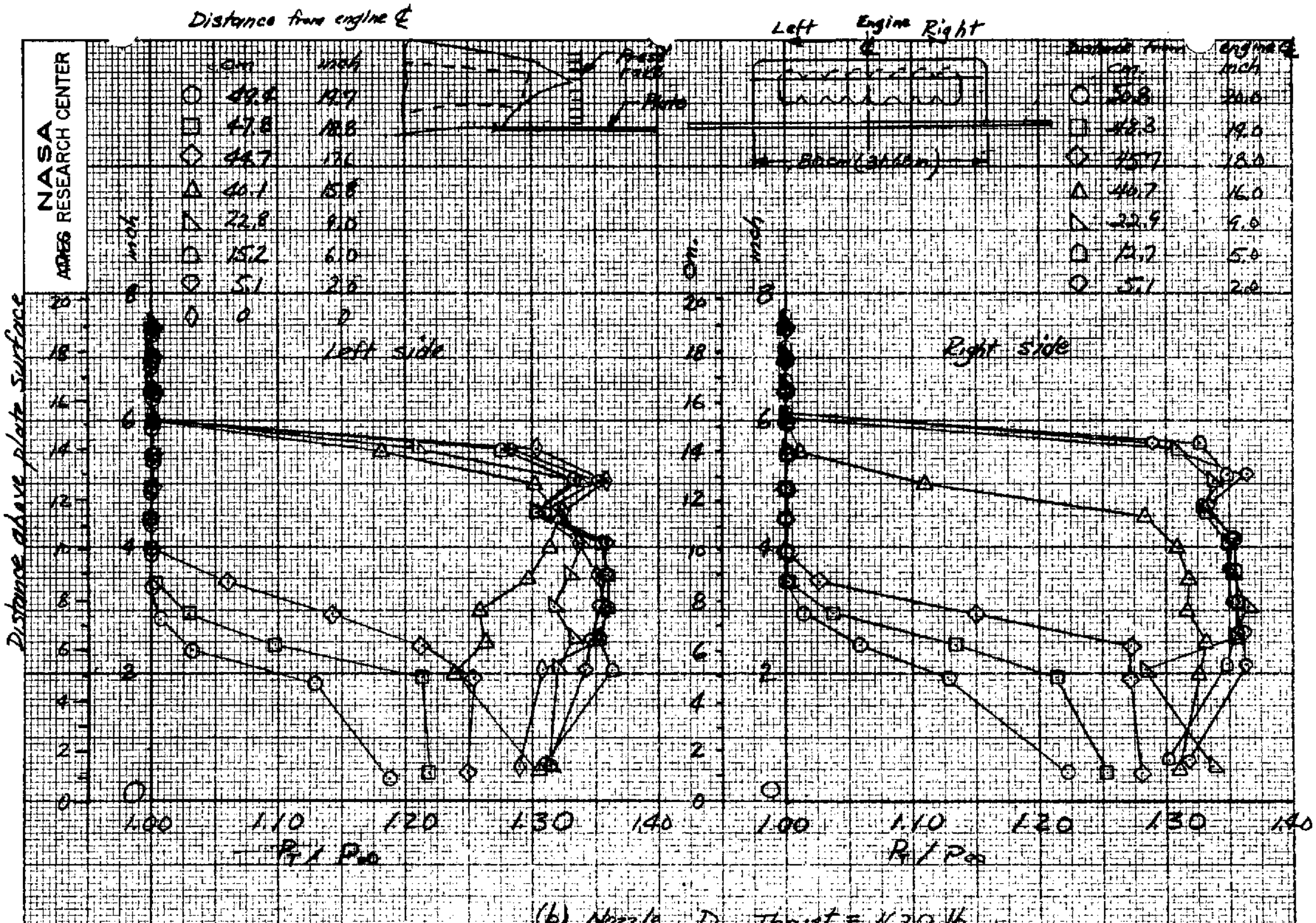

(b) Nozzle D, Thrust = 1620 lb.

Figure 7 .- Concluded

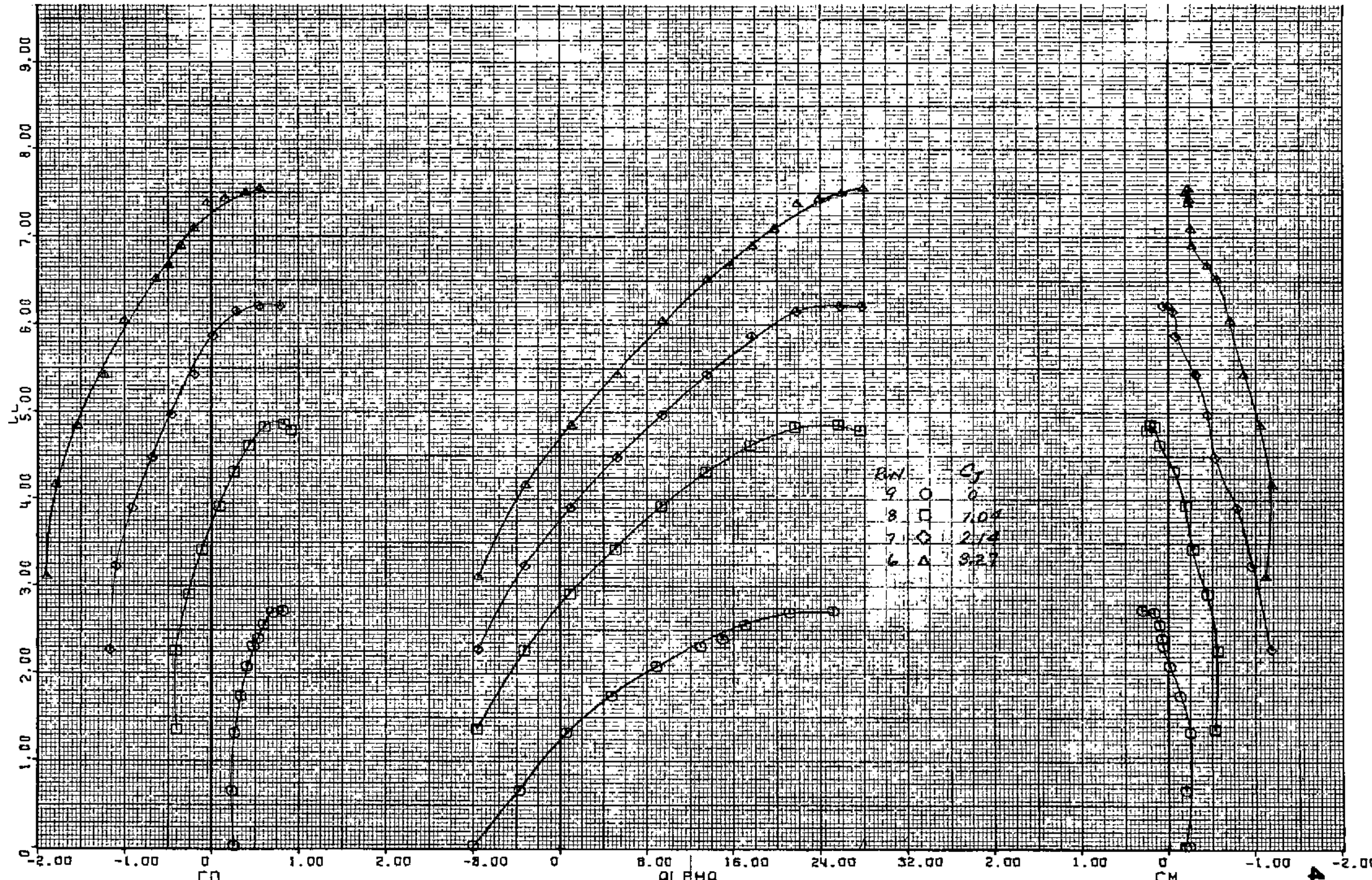

Figure 8 .- Longitudinal characteristics of the model with nozzle B; $\delta_f = 75°$ (t_c = .11 to .48), δ_{f_2} = 44°, tail off.

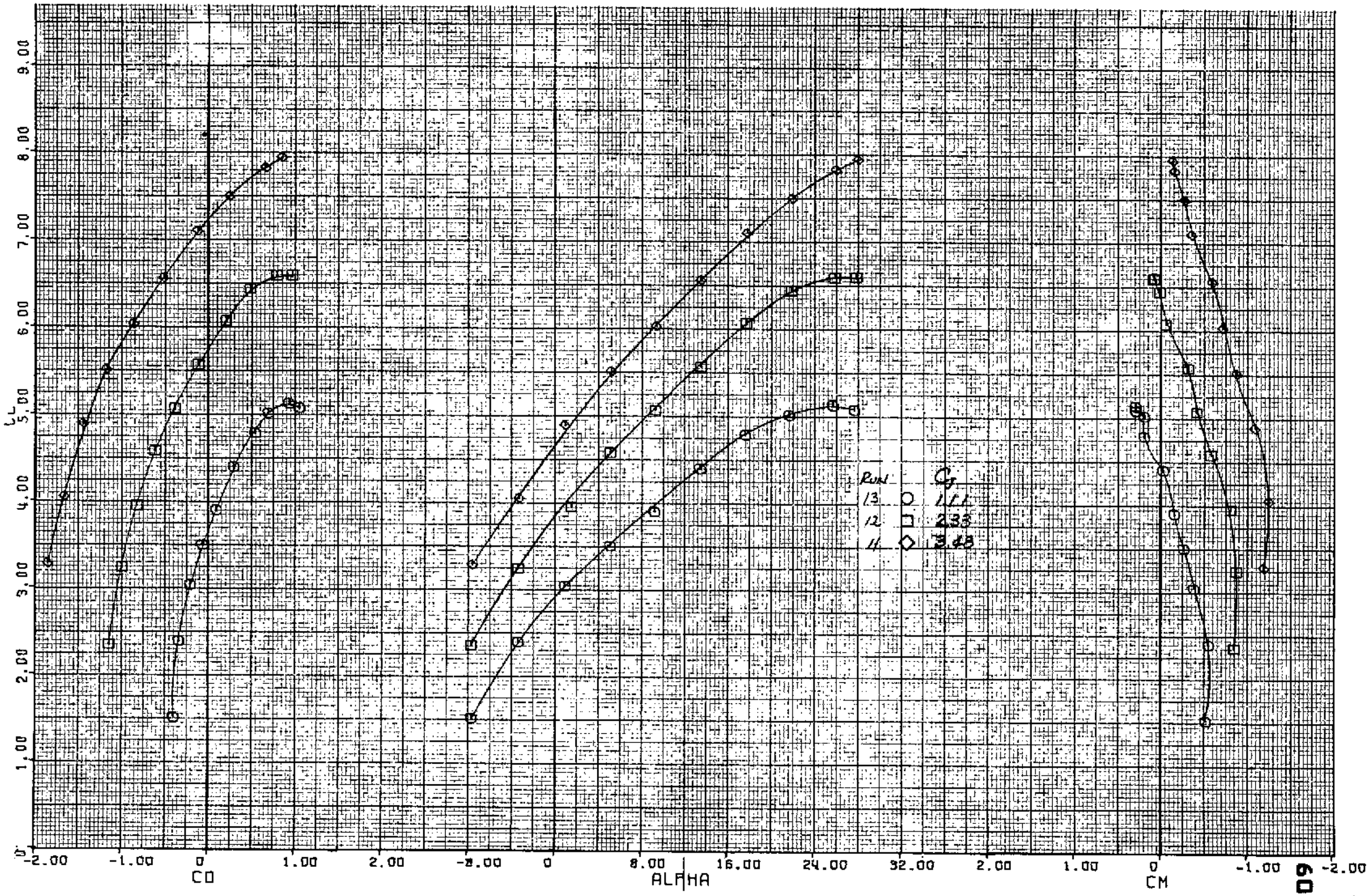

Figure 9. – Longitudinal characteristics of the model with nozzle B and 0.18 m gap deflector; $\delta_f = 75°$ (η_c = .11 to .48), $\delta_h = 44°$; tail off.

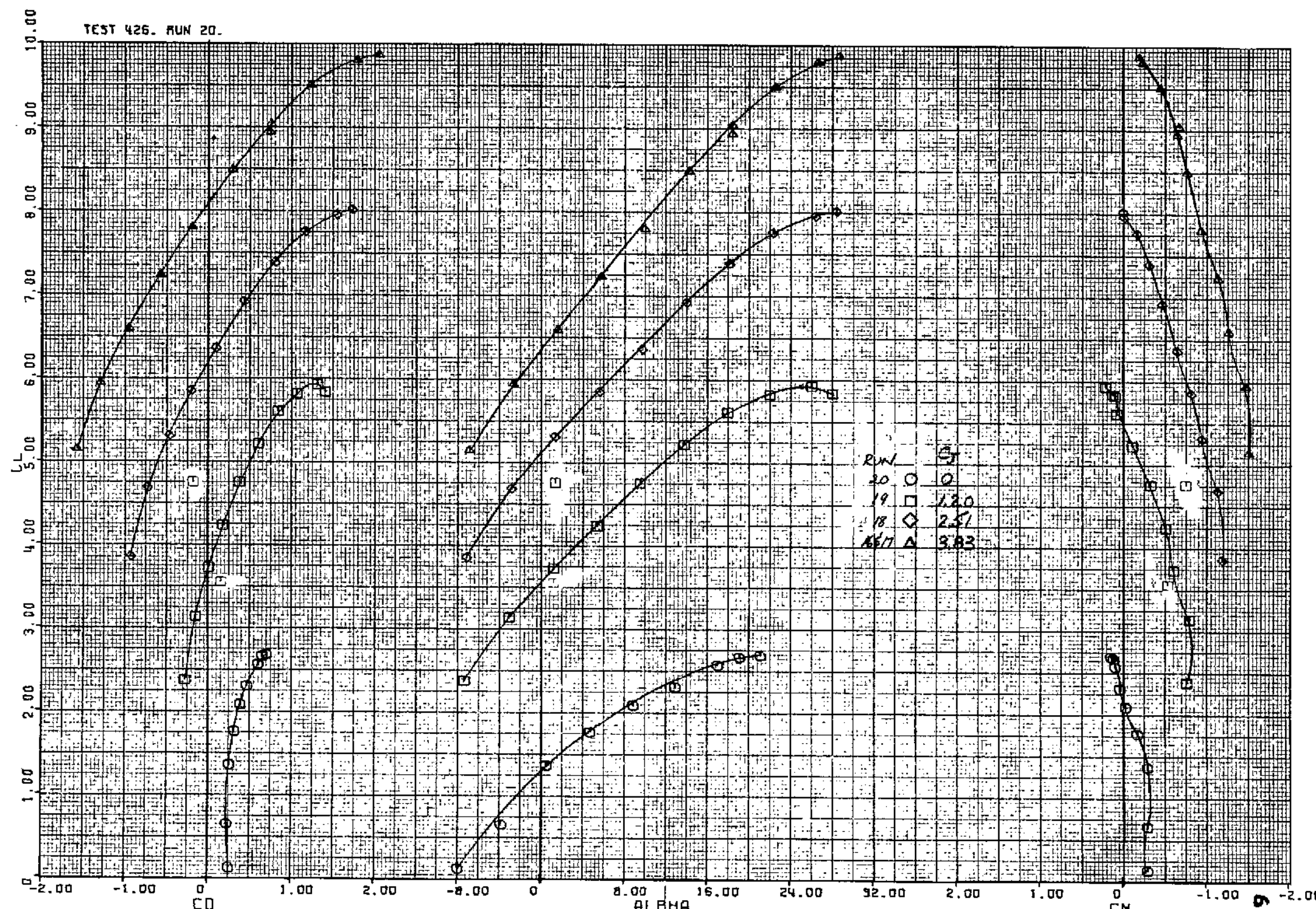

Figure 10 .– Longitudinal characteristics of the model with nozzle B and 0.15m gap deflector; $\delta_f = 75°$ ($\eta_c = .11$ to $.48$), $\delta_h = 44°$, tail off.

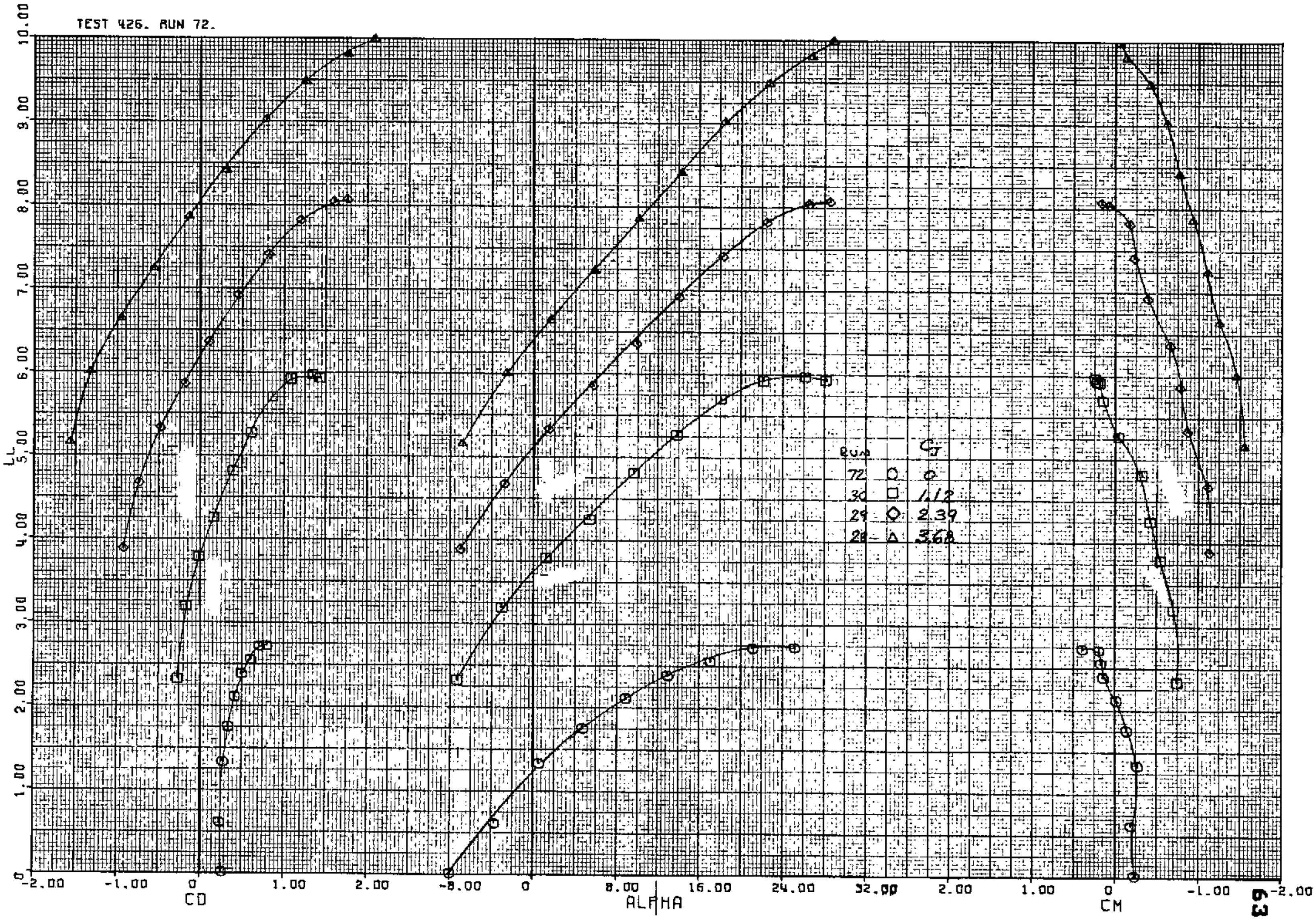

(a) η_c = .11 to .43.

Figure 11 .- Longitudinal characteristics of the model with nozzle B and 0.15m gap deflector at several spanwise extent of Coanda surfaces; δ_f = 75°, δ_2 = 44°, tail off.

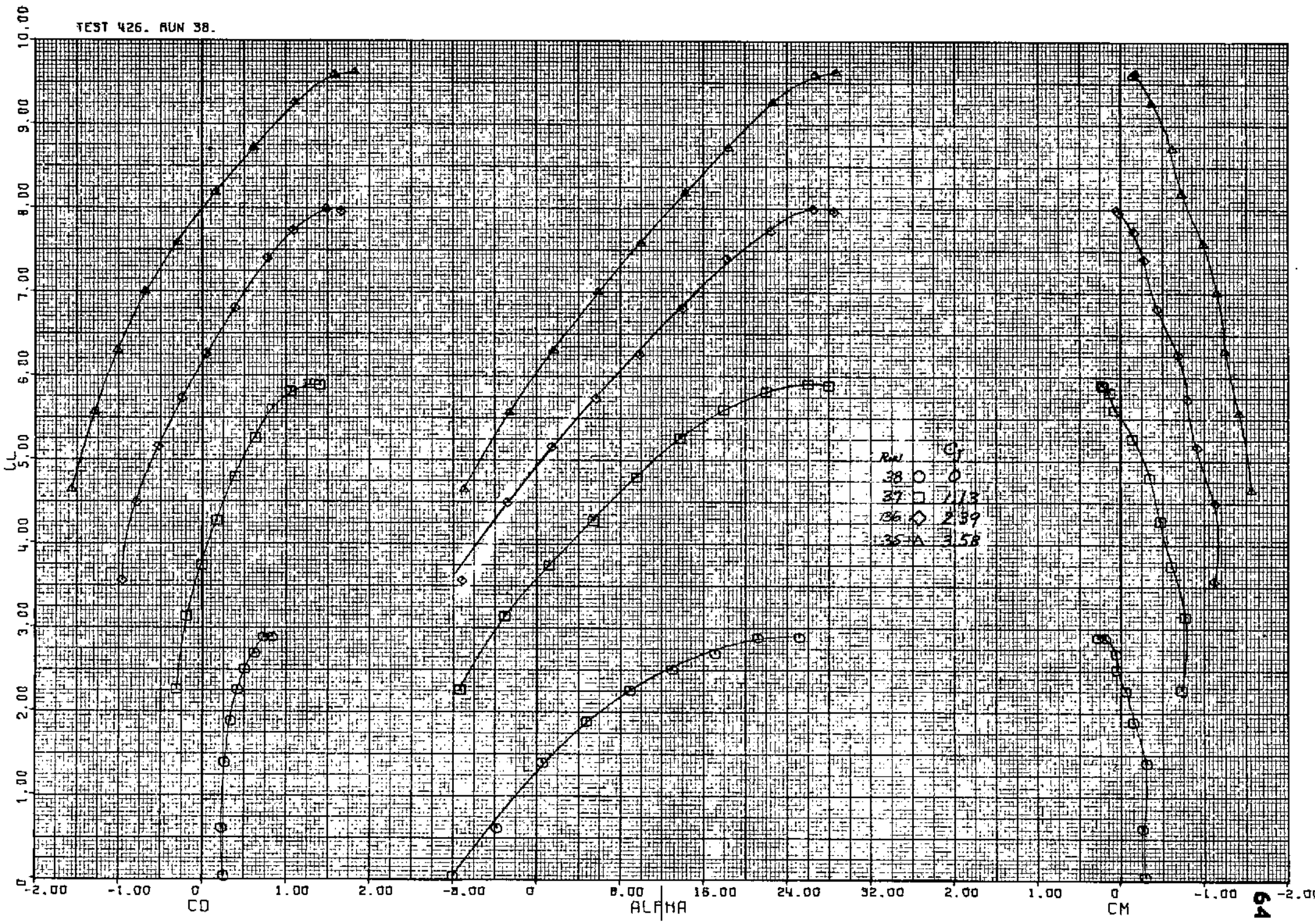

(b) η_c = .11 to .39.

Figure 11 .- Continued.

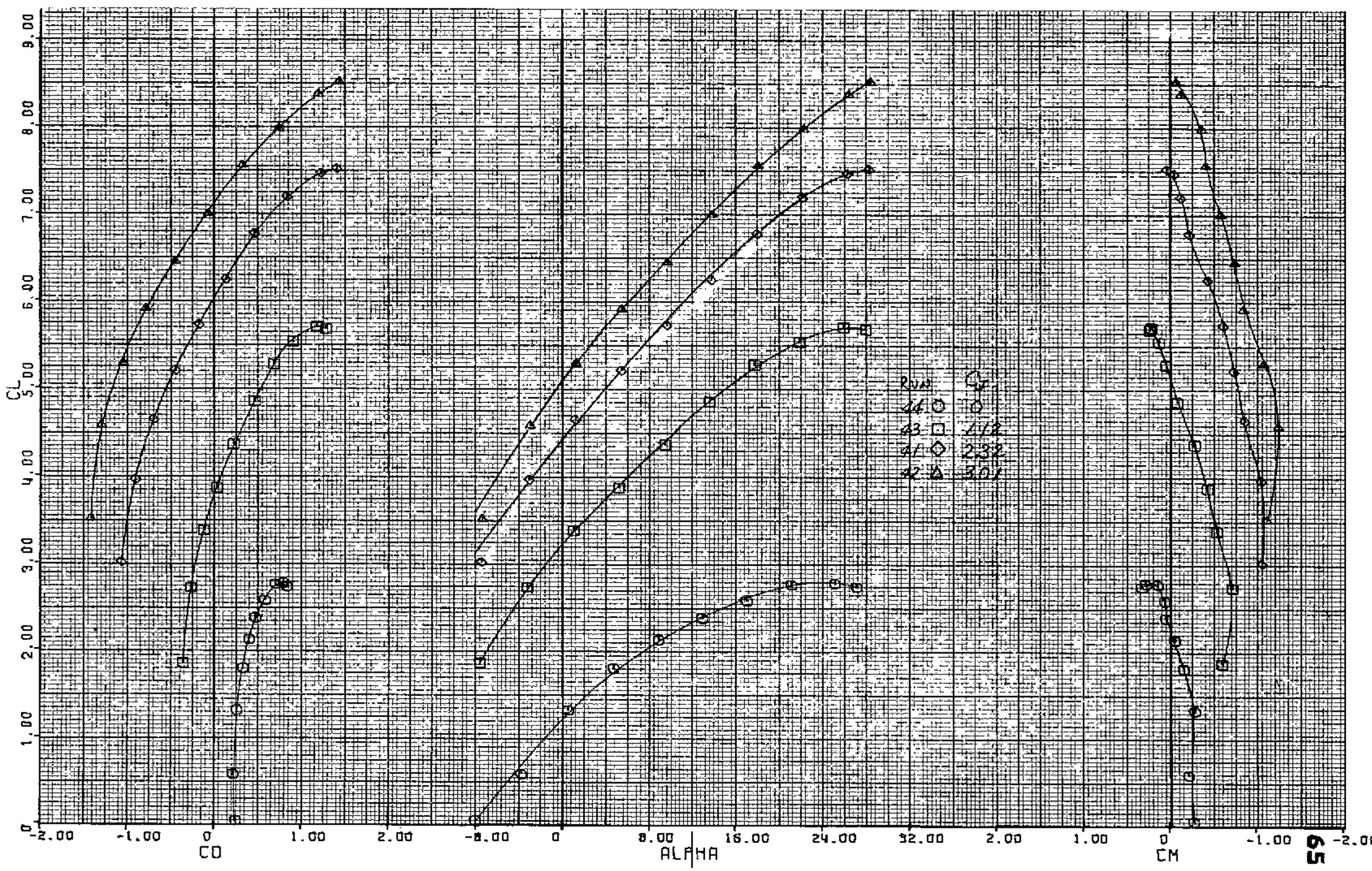

(c) η_c = .15 to .39.

Figure 11. - Concluded.

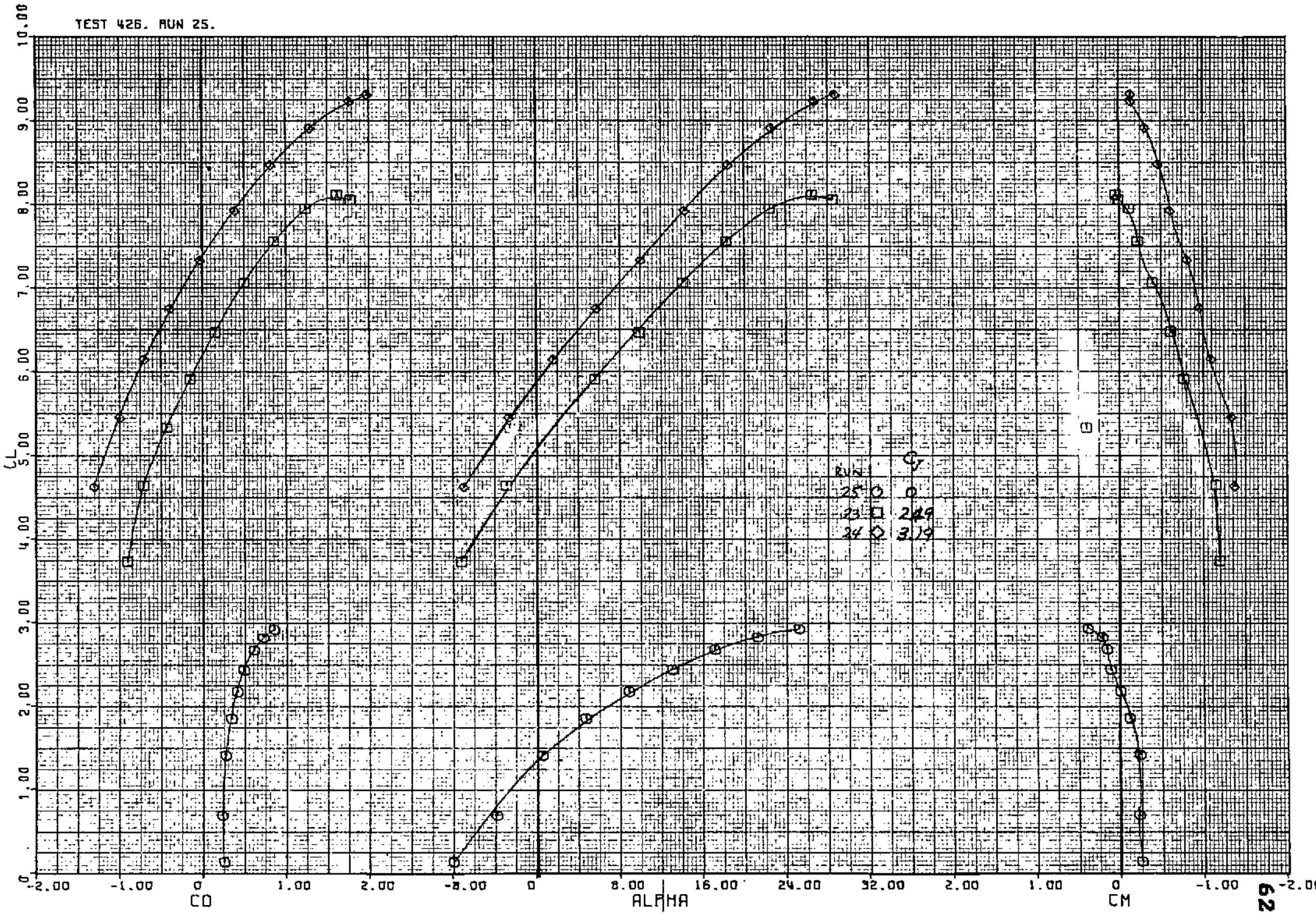

Figure 12 .— Longitudinal characteristics of the model with fuselage fence configuration 1; nozzle B with 0.15 m gap deflector, $\delta_f = 75°$ (η_c = .11 to .48), $\delta_{f_2} = 44°$, tail off.

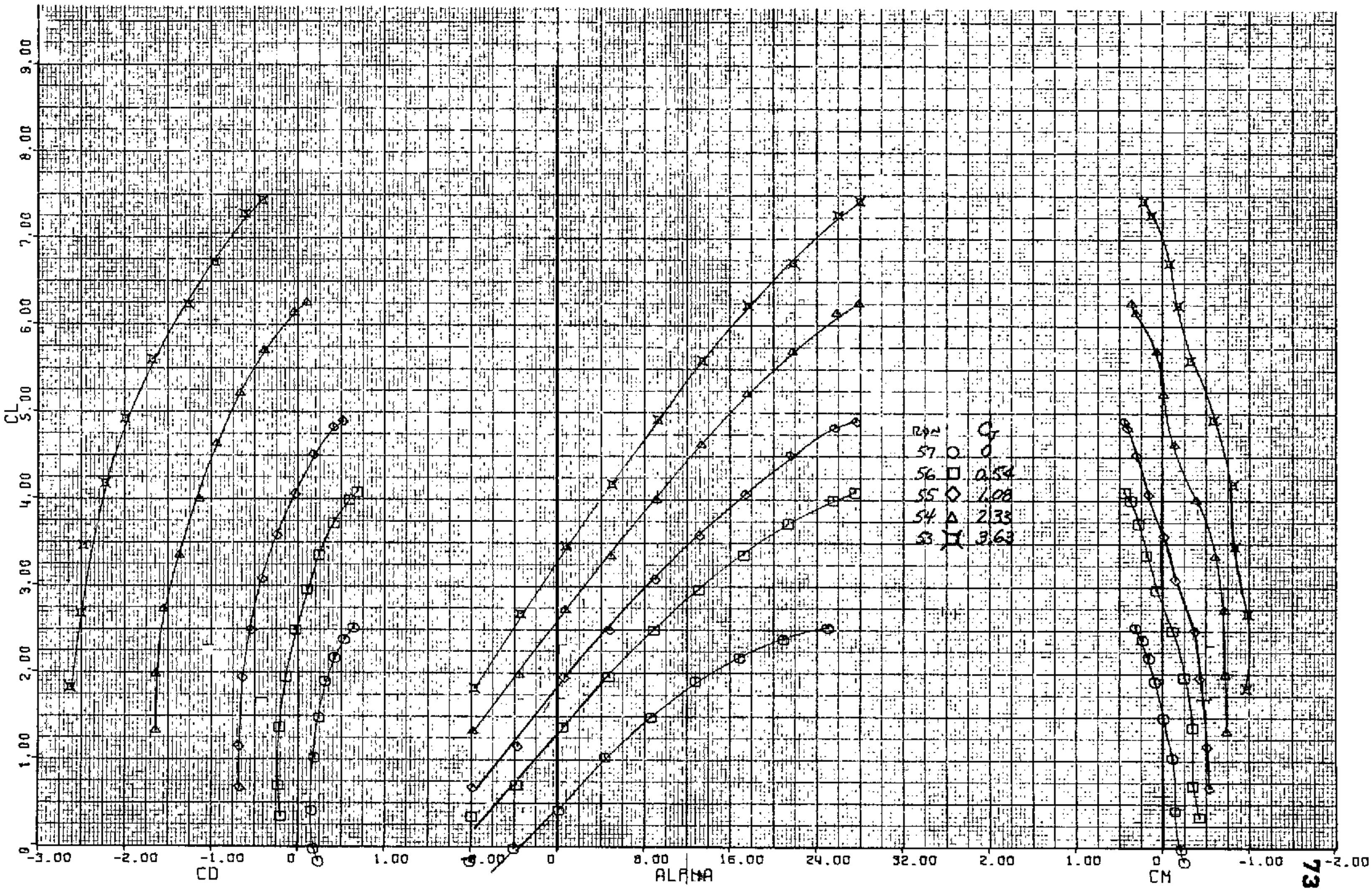

Figure 13.- Longitudinal characteristics of the model with nozzle B and 0.15m gap deflector; $\delta_f = 30^\circ (\eta_c = .11 \text{ to } .38)$, $\delta_t = 12^\circ$, tail off.

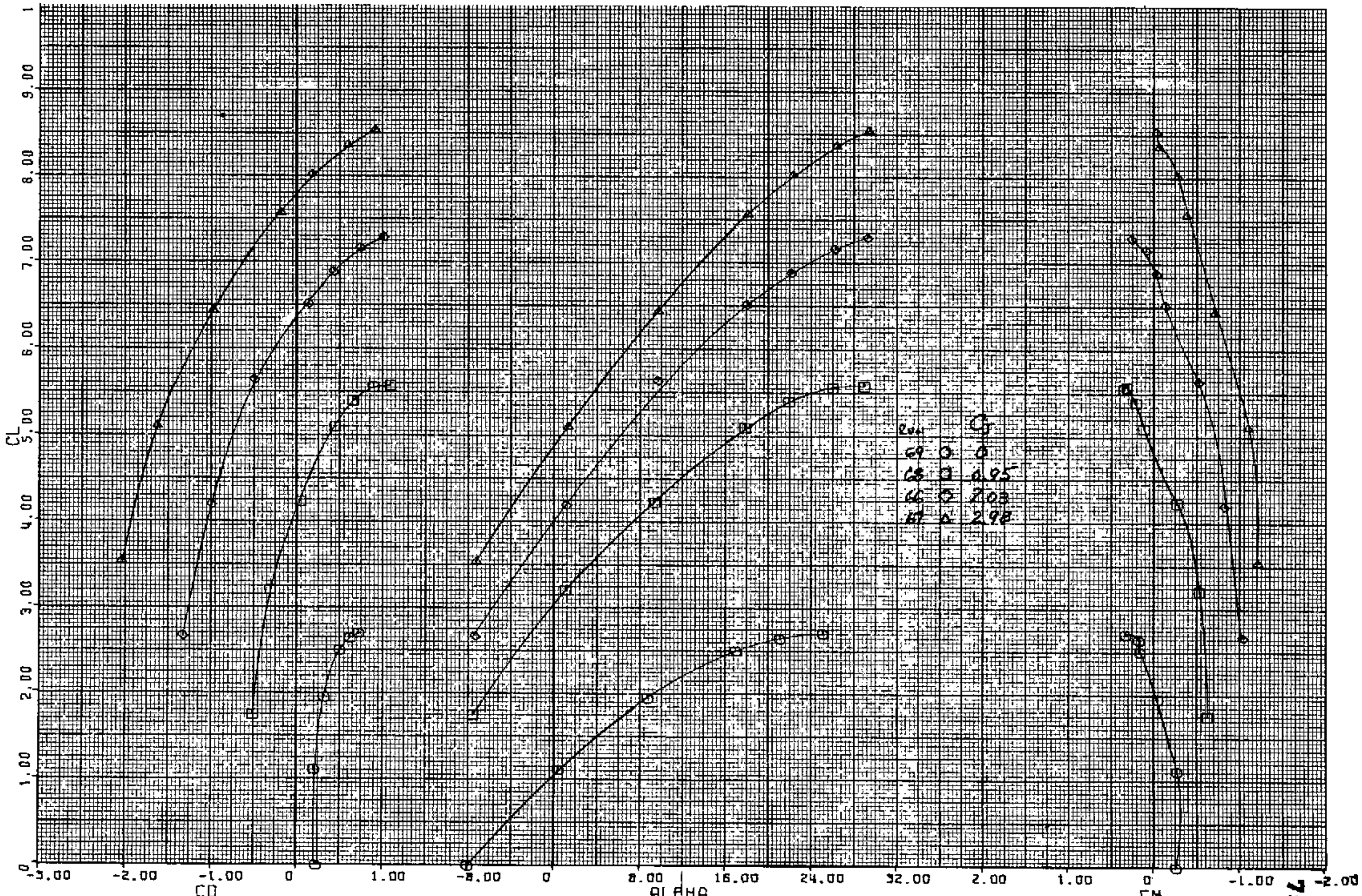

Figure 14.- Longitudinal characteristics of the model with nozzle D_J; $\delta_f = 55°$ ($\eta_c = .11$ to $.43$), $\delta_{f_2} = 27.5°$, tail off.

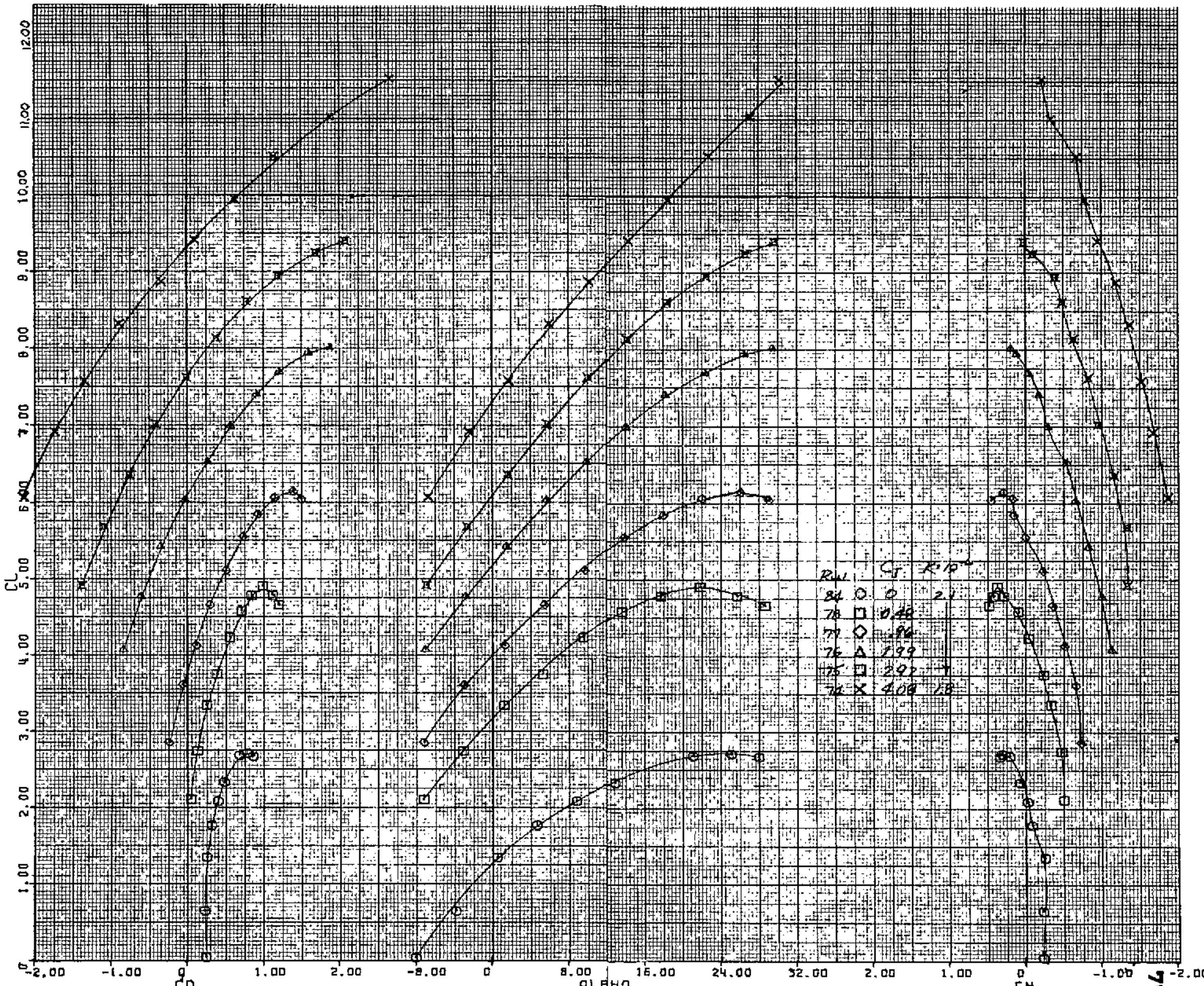

(a) $R = 2.1 \times 10^6$ (Except at $C_J = 4.08$)

Figure 15.- Longitudinal characteristics of the model with nozzle D; $\delta_f = 75°$ ($\tau_c = .11$ to $.48$), $\delta_h = 44°$, tail off.

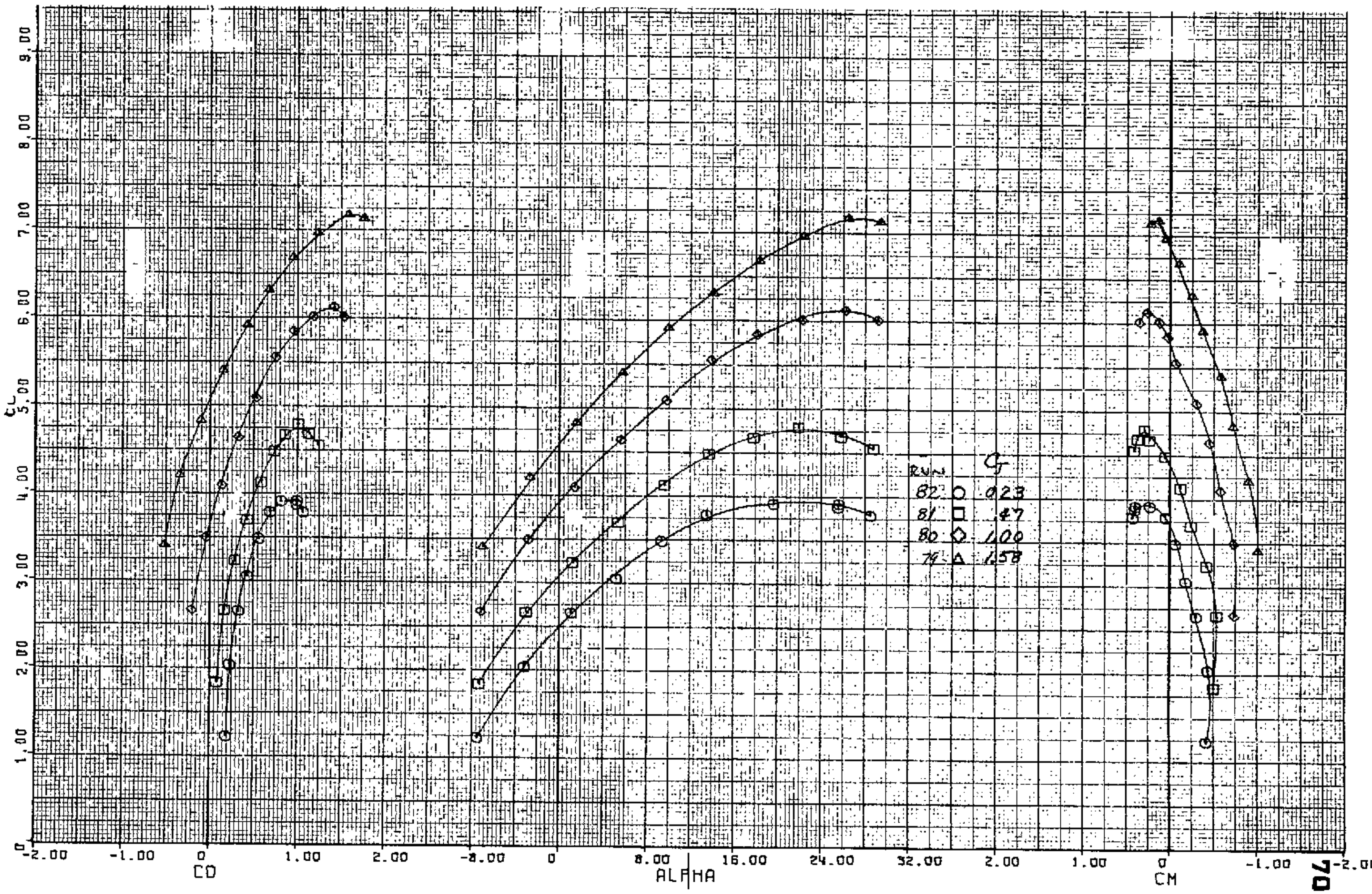

(b) $R = 3.0 \times 10^6$

Figure 15.- Concluded.

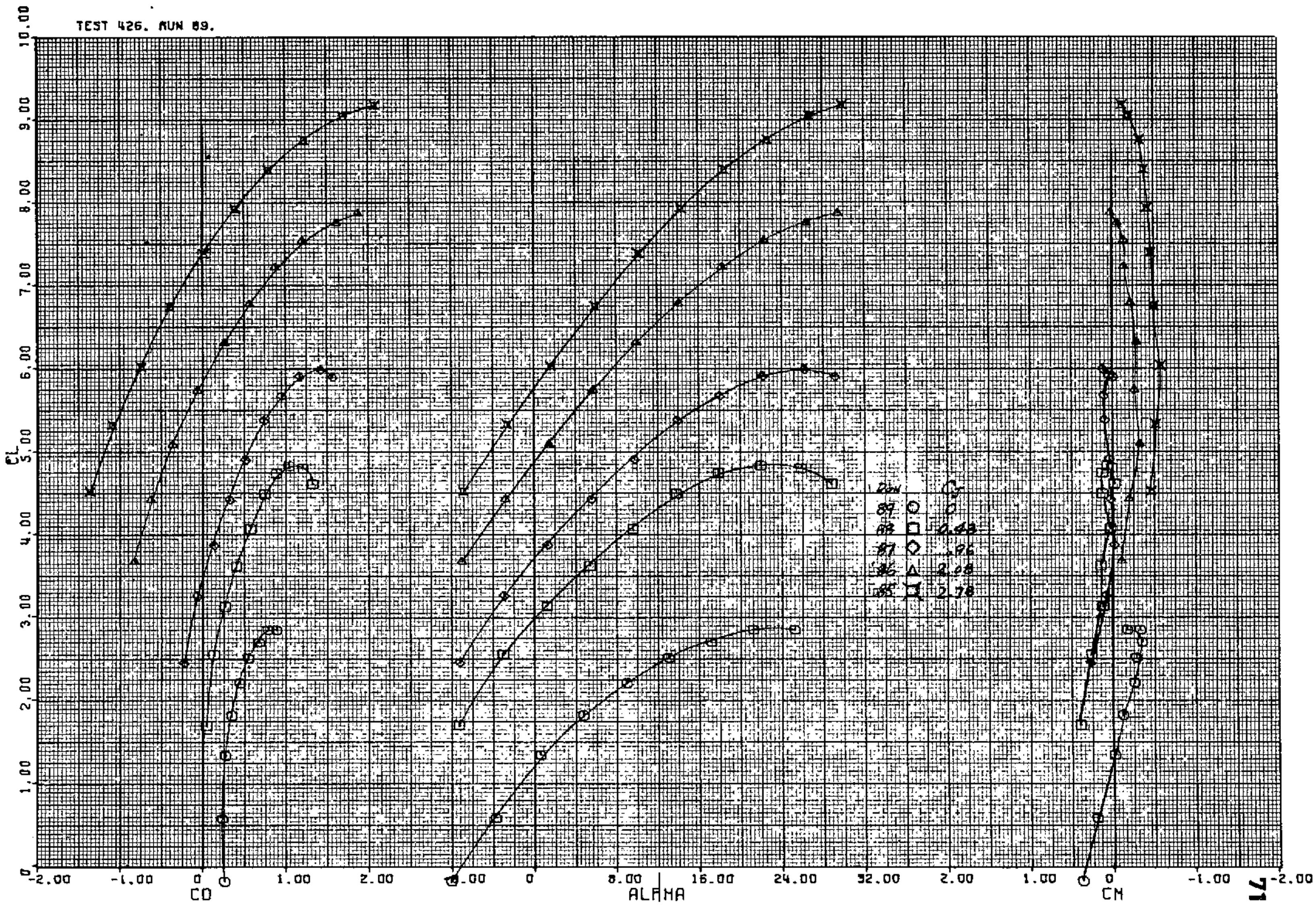

(a) $i_t = 0°$.

Figure 16.- Longitudinal characteristics of the model at several tail incidences; nozzle D, $\delta_f = 75°$ (η_c = .11 to .43), $\delta_{f_2} = 44°$.

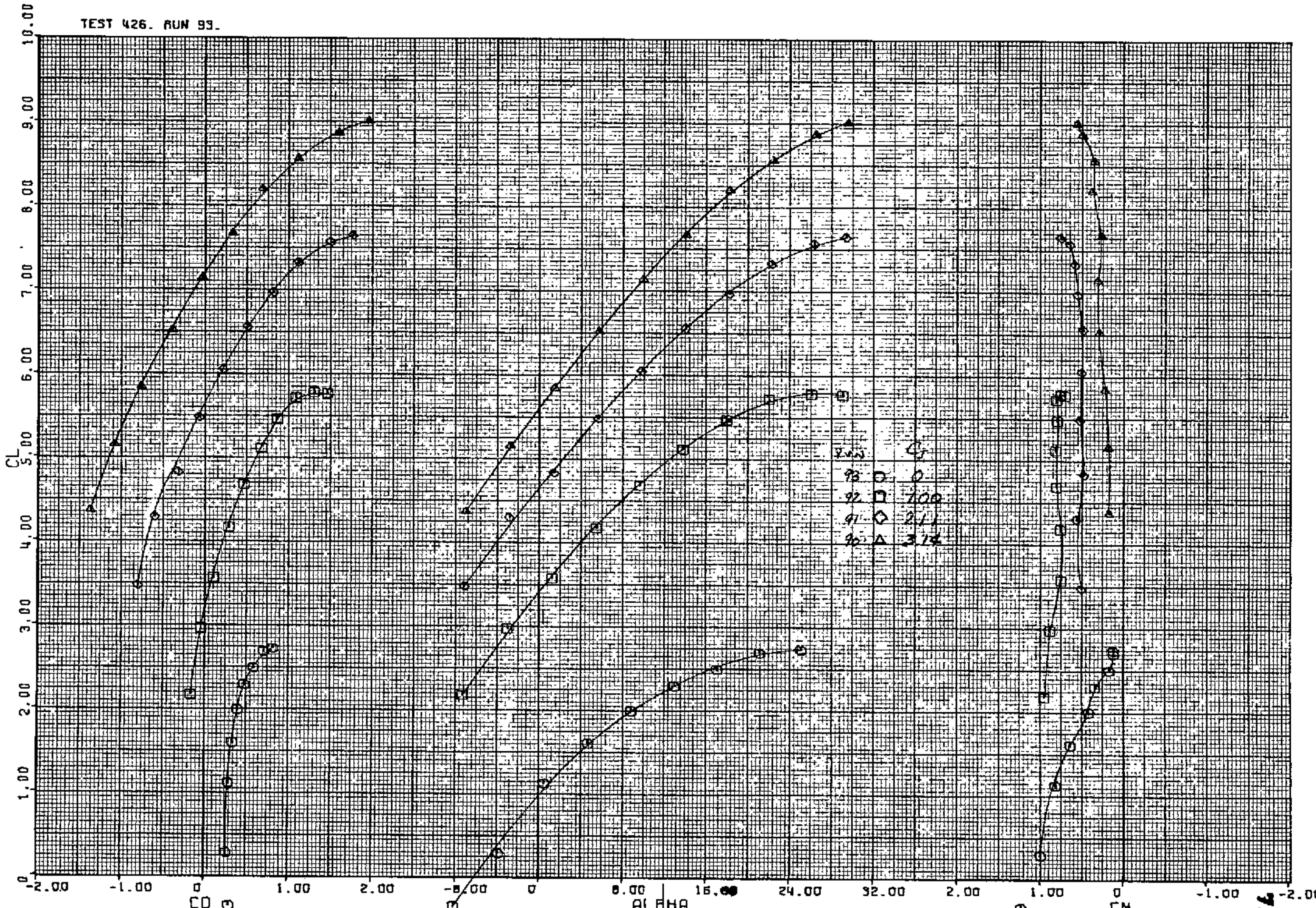

(b) $i_t = -10.5°$.

Figure 16.- Concluded.

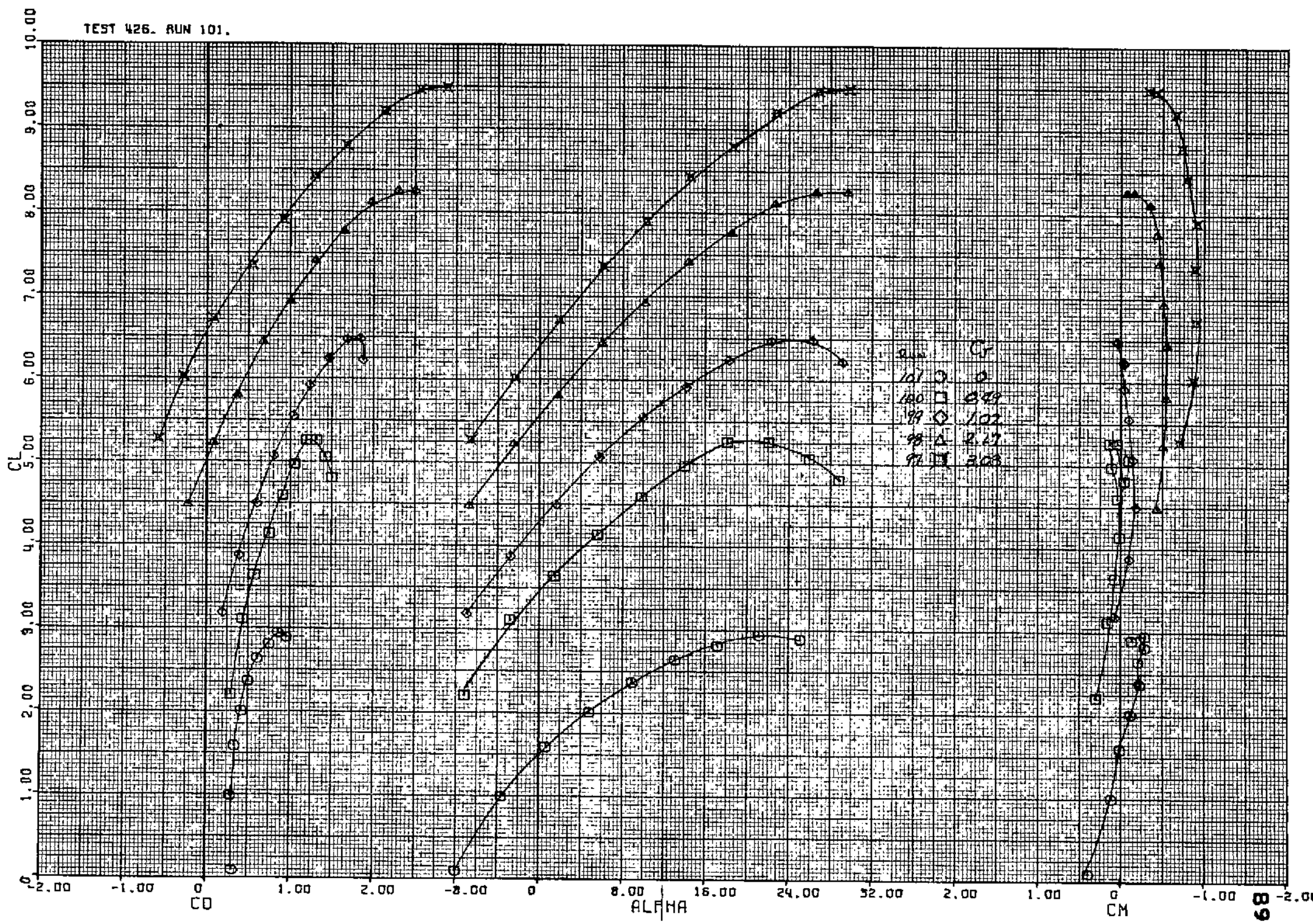

Figure 17. - Longitudinal characteristics of the model with nozzle D; $\delta_f = 90°$ (t_c = .11 to .43), $\delta_{f_2} = 44°$; i_t – 0°.

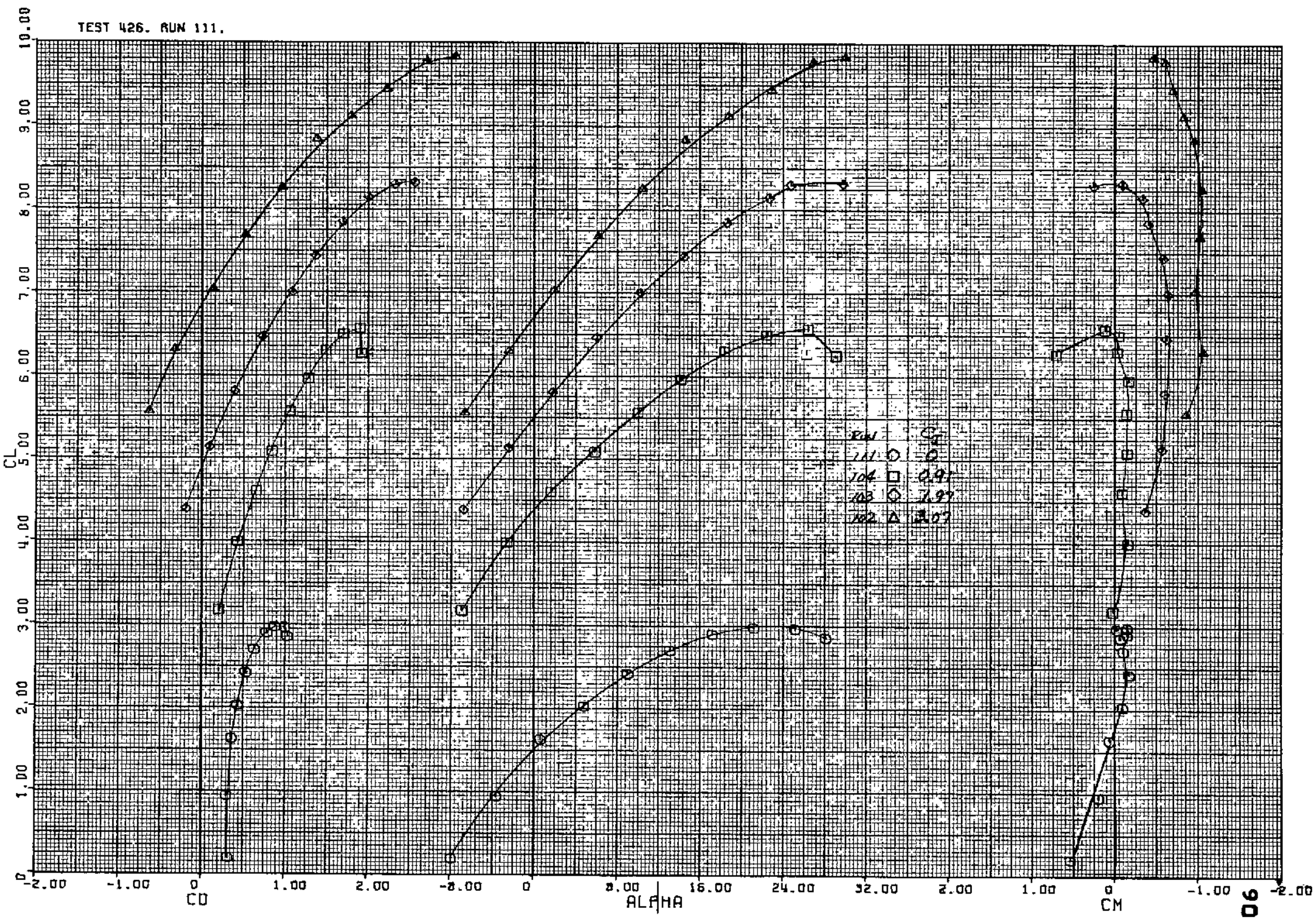

(a) Fuselage fence configuration 1.

Figure 18.- Longitudinal characteristics of the model with fuselage fence; nozzle D, $\delta_f = 90°$ (η_o = .11 to .43), $\delta_h = 44°$, $i_t = 0°$.

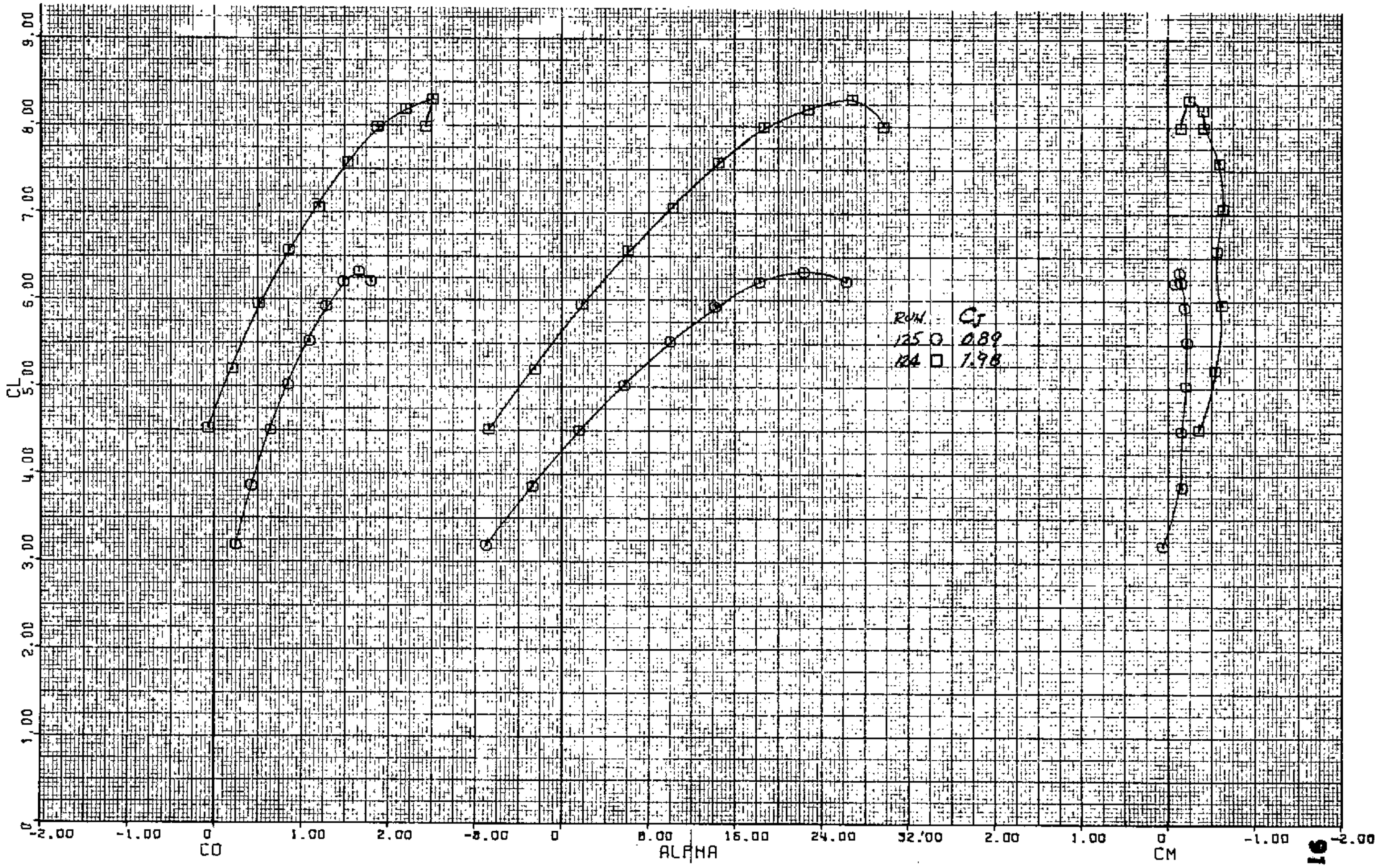

(b) Fuselage fence configuration 2.

Figure 18. – Concluded.

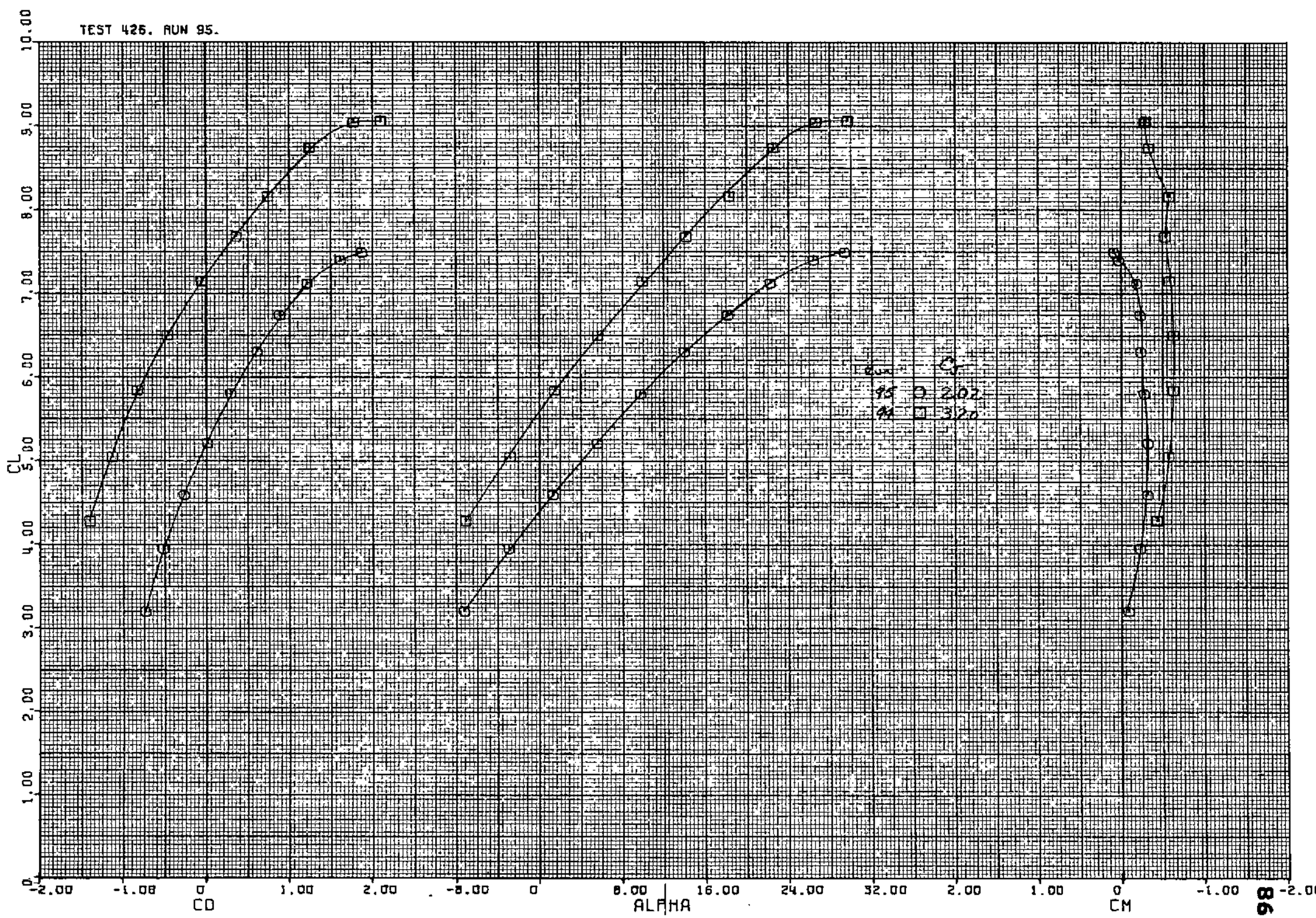

Figure 17.– Longitudinal characteristics of the model with spoilers deflected; nozzle D, $\delta_f = 75°$ ($\eta_c = .11$ to $.43$), $\delta_{s_i} = 44°$; $i_t = 0°$; $\delta_{sp} = 30°$.

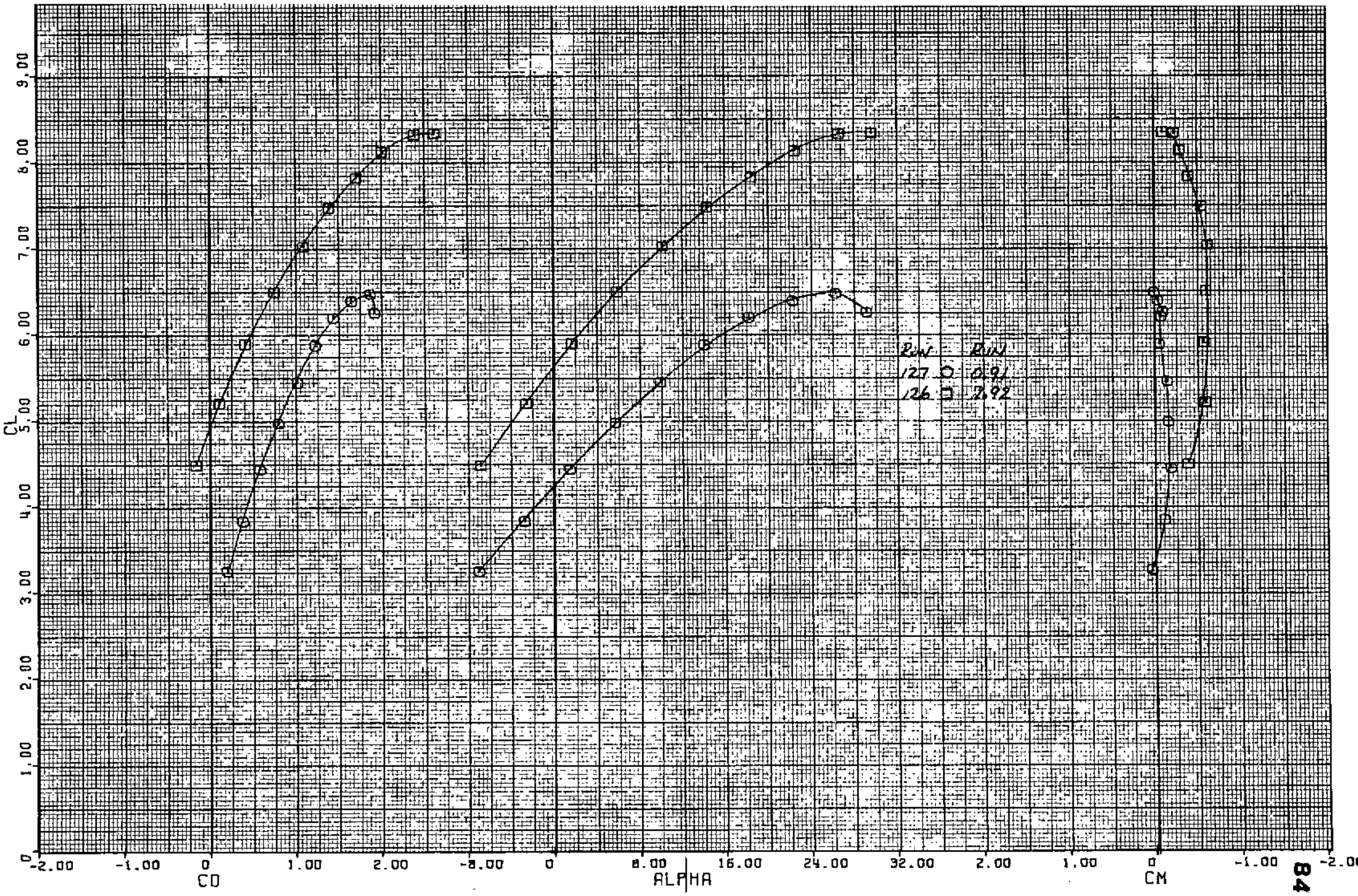

Figure 20.- Longitudinal characteristics of the model with nozzle D; $\delta_f = 90°(\eta_c = .11$ to $.43)$, $\delta_f = 75°(\eta_c = .43$ to $.48)$, $\delta_f = 44°$, $i_t = 0°$.

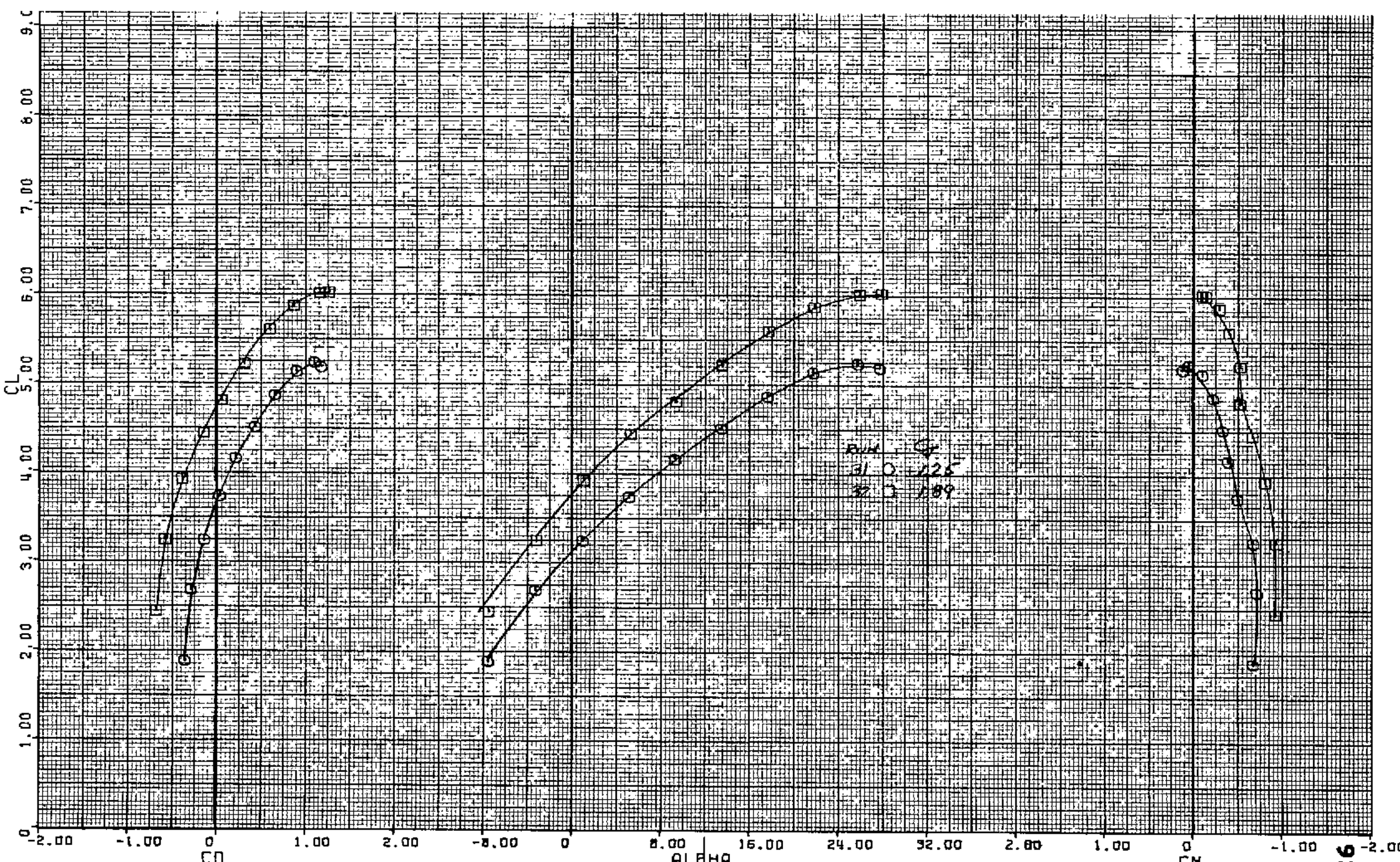

(a) Longitudinal characteristics of the model.

Figure 21.- Aerodynamic characteristics of the model with left hand engine out; nozzle B with 0.15 m gap deflector, $\delta_{f_1} = 75°$ (η_c = .11 to .43), $\delta_{f_2} = 44°$, tail off.

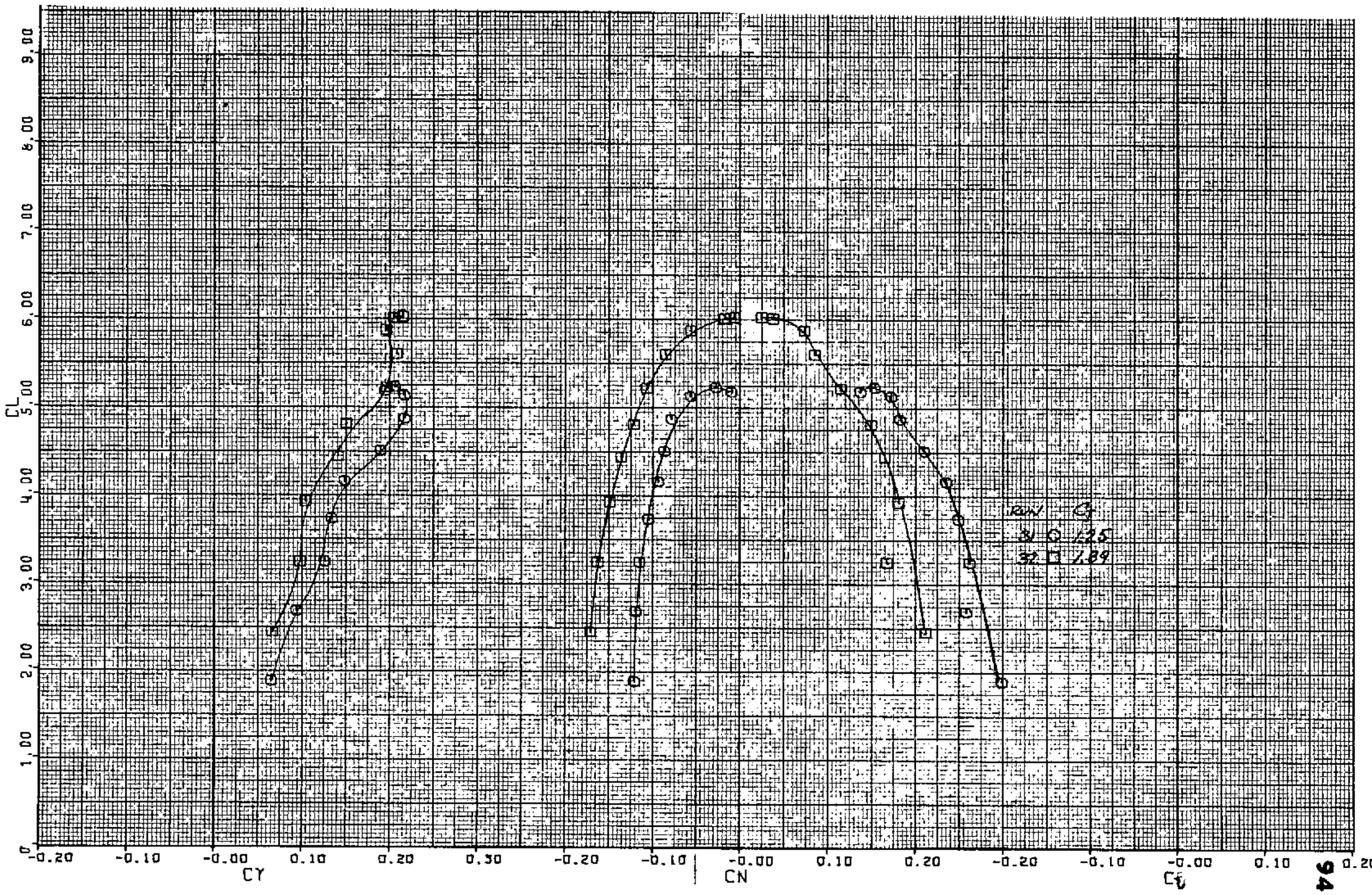

(b) *Lateral characteristics of the model.*

Figure 21.— Concluded.

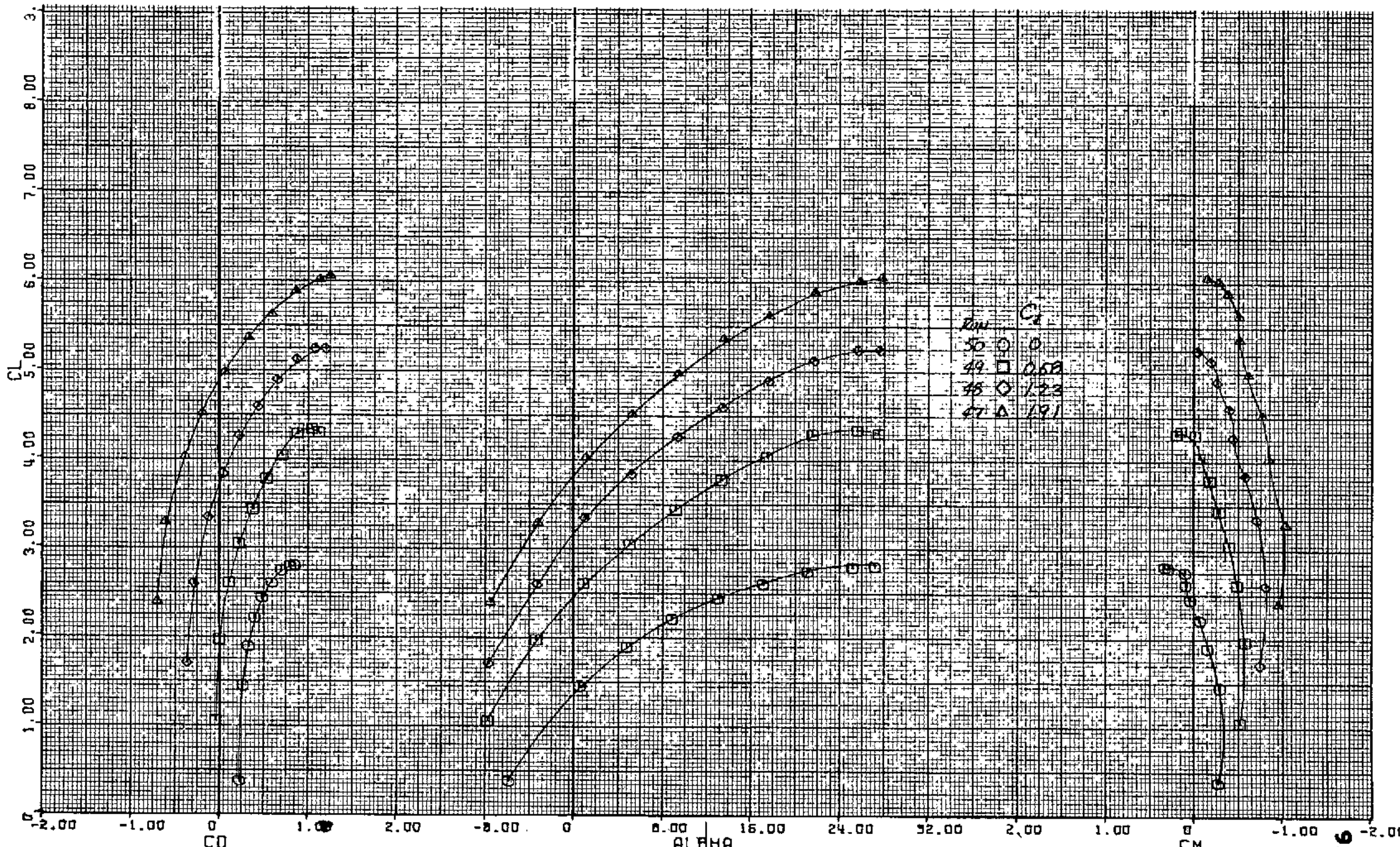

(a) Longitudinal characteristics of the model.

Figure 22.- Aerodynamic characteristics of the model with left hand Coanda surfaces removed and engine out; nozzle B with 0.15 cm deflector, $\delta_f = 75°$ (C_μ = all to .43, right hand side only), $\delta_c = 44°$, tail off.

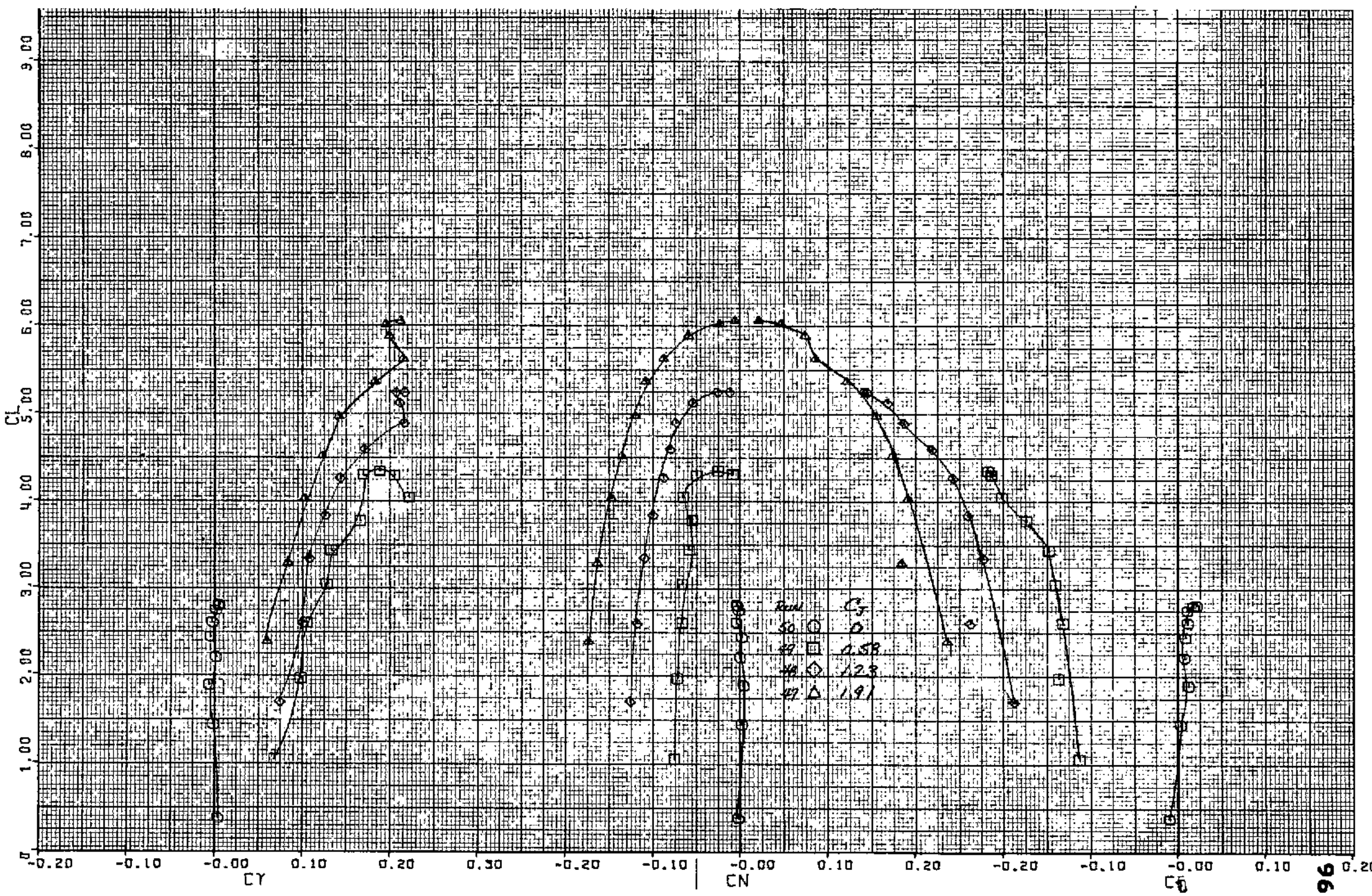

(b) Lateral characteristics of the model.

Figure 22. – Concluded.

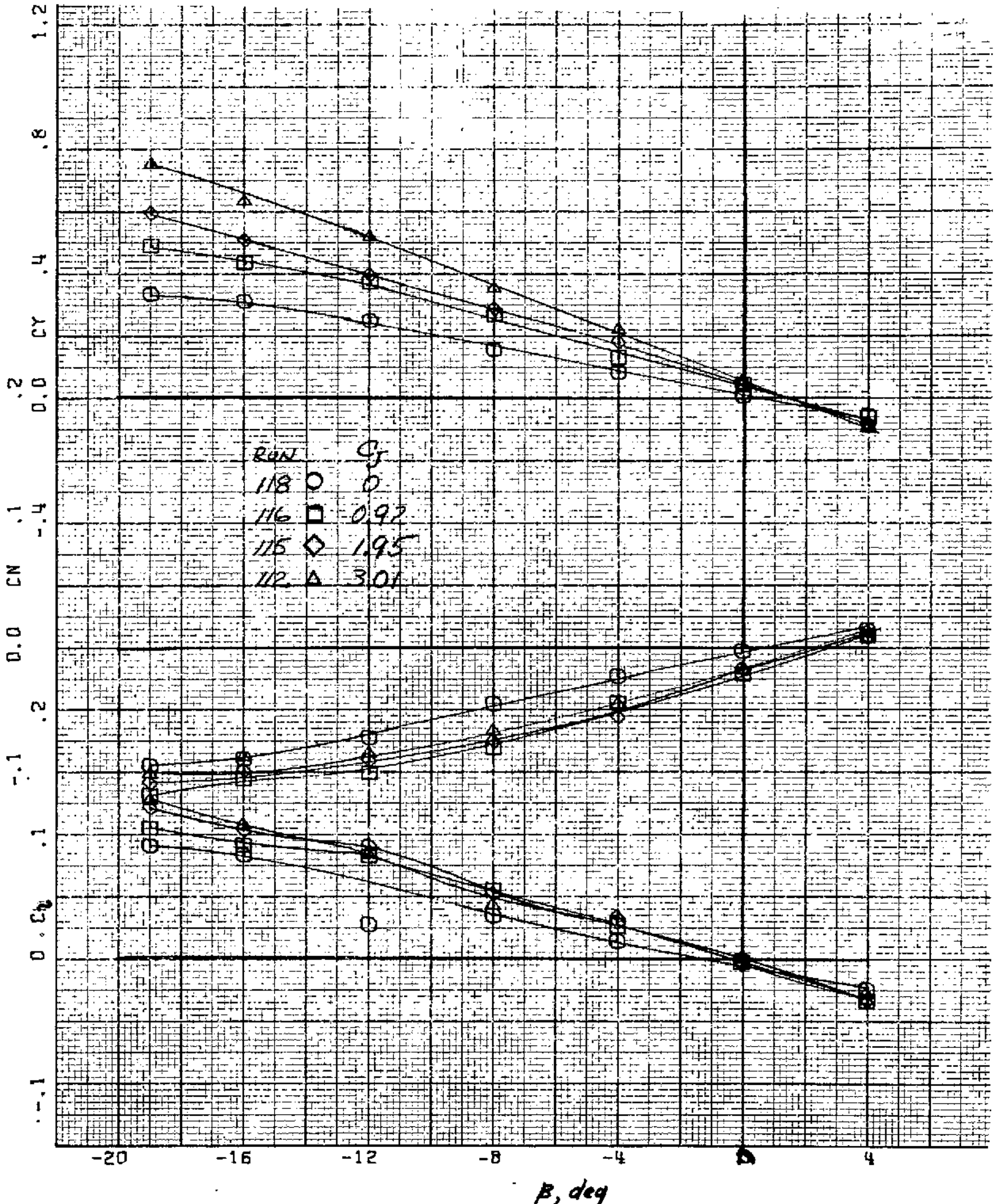

(a) $\alpha_v = 0°$

Figure 23 - Variation of side force, yawing-moment, and rolling-moment coefficients with sideslip; nozzle D, $\delta_f = 90°$ ($\eta_c = .11$ to $.43$), $\delta_{f_2} = 44°$, $\psi = 0°$,

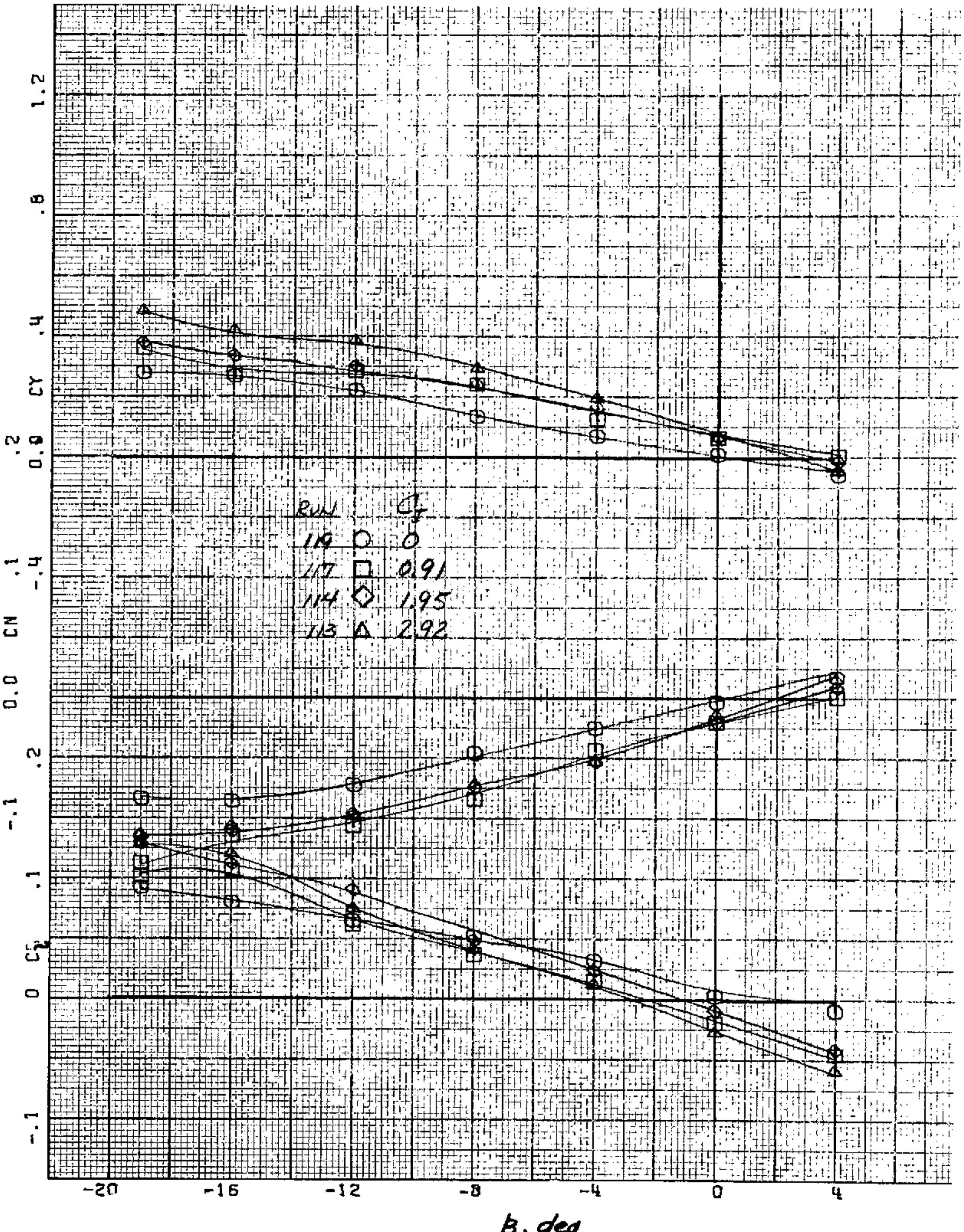

(b) $\alpha_y = 8°$

Figure 23.- Concluded.

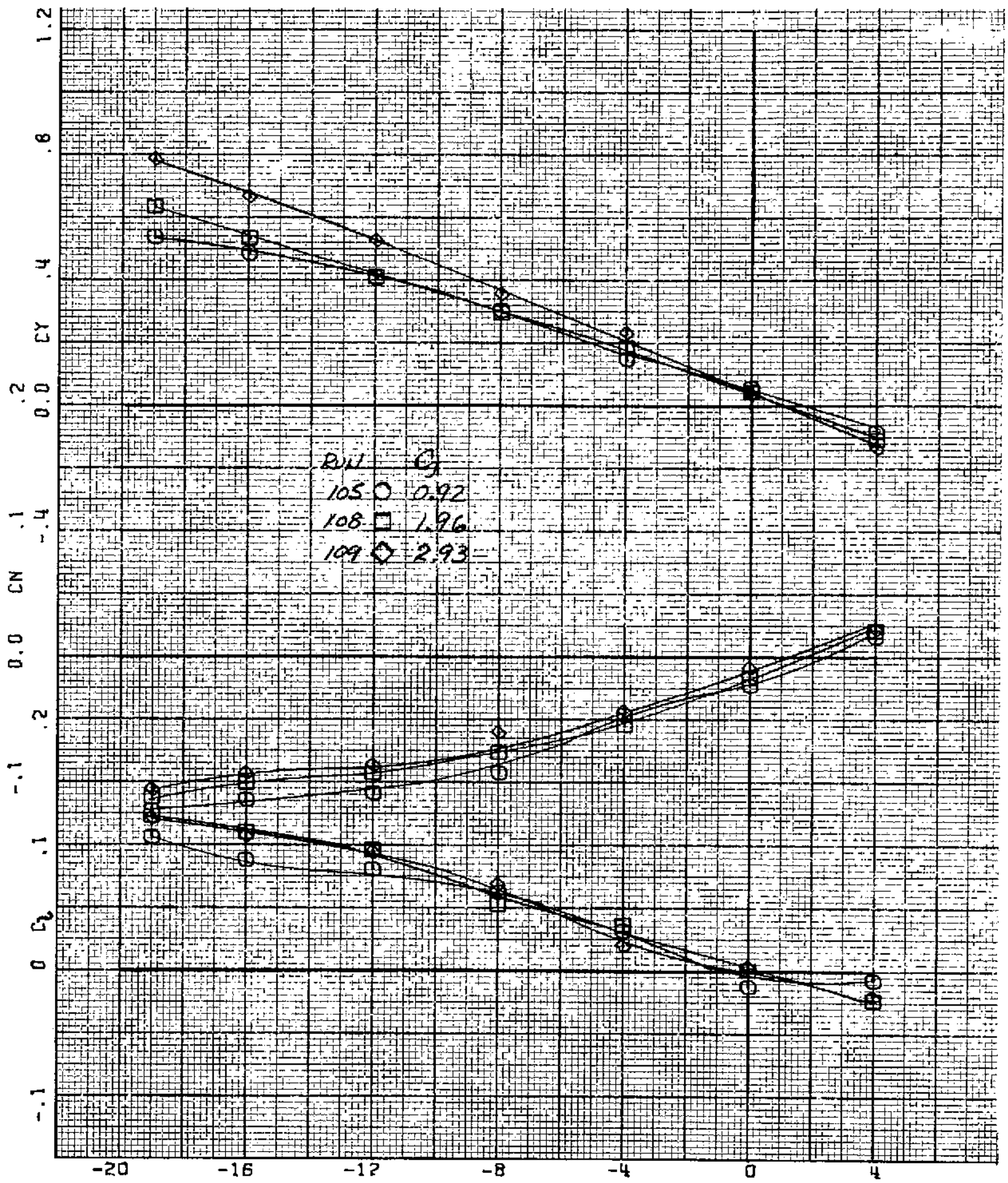

(a) $\alpha_u = 0°$.

Figure 24. - Variation of side force, yawing-moment, and rolling-moment coefficients with sideslip; nozzle D, $\delta_f = 90°$ (η_c = .11 to .43), $\delta_{f_2} = 44°$; $i_t = 0°$, fuselage fence configuration 1.

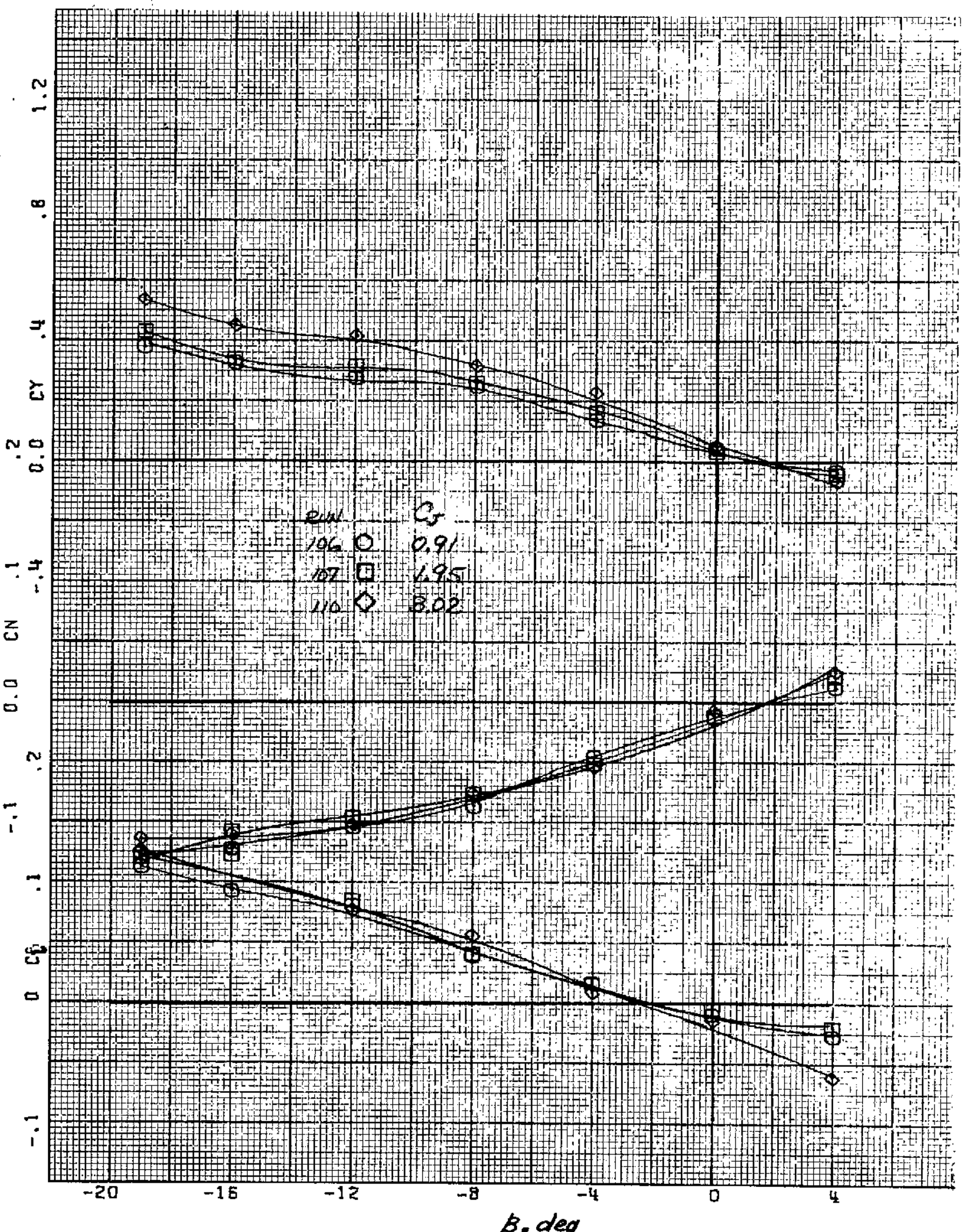

(b) $\alpha_u = 8°$.

Figure 24.- Concluded.

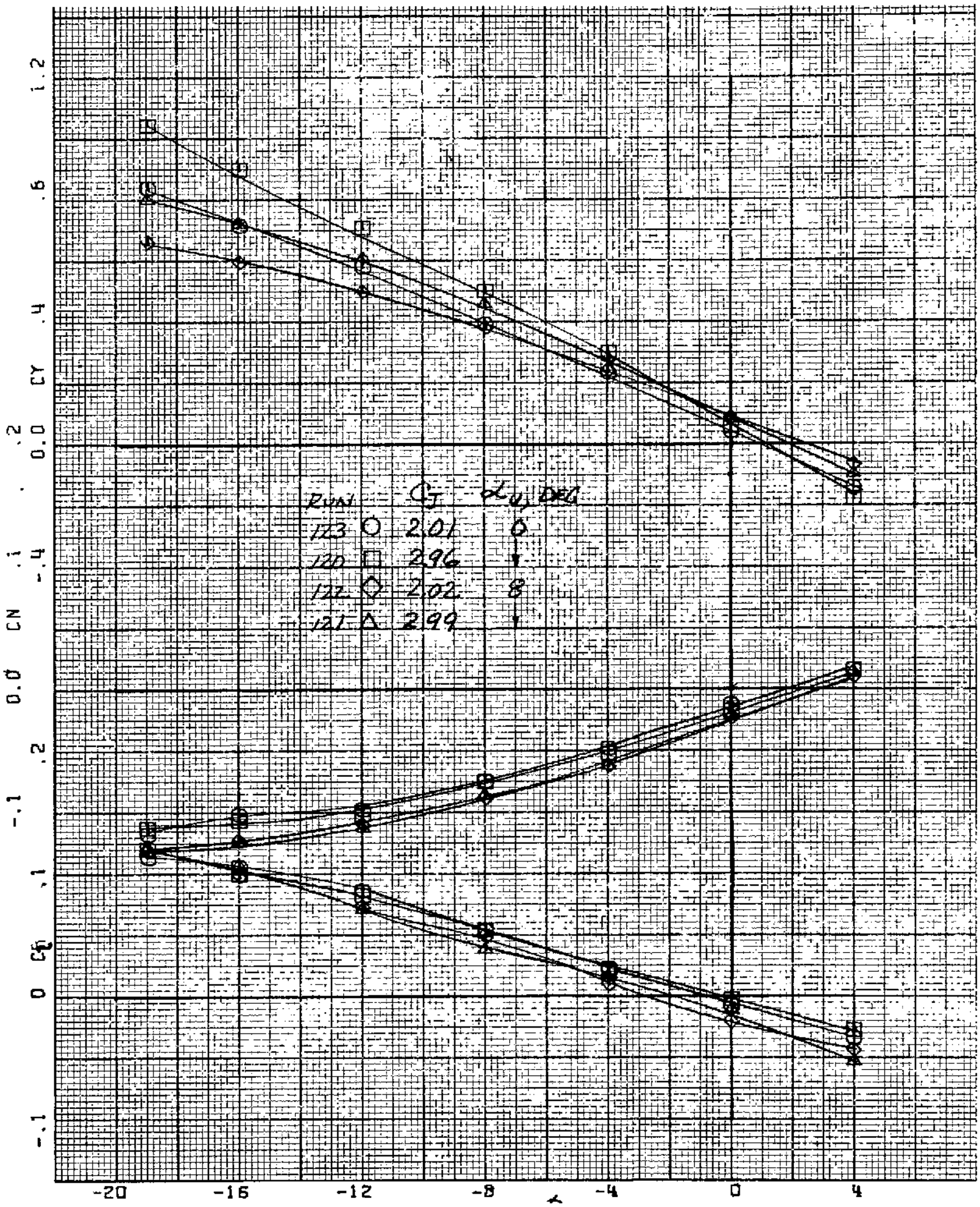

Figure 25.- Variation of side force, yawing-moment, and rolling-moment coefficients with sideslip; nozzle D, $\delta_f = 75°$ (η_c = .11 to .43), $\delta_{f_2} = 44°$, $i_t = 0°$.

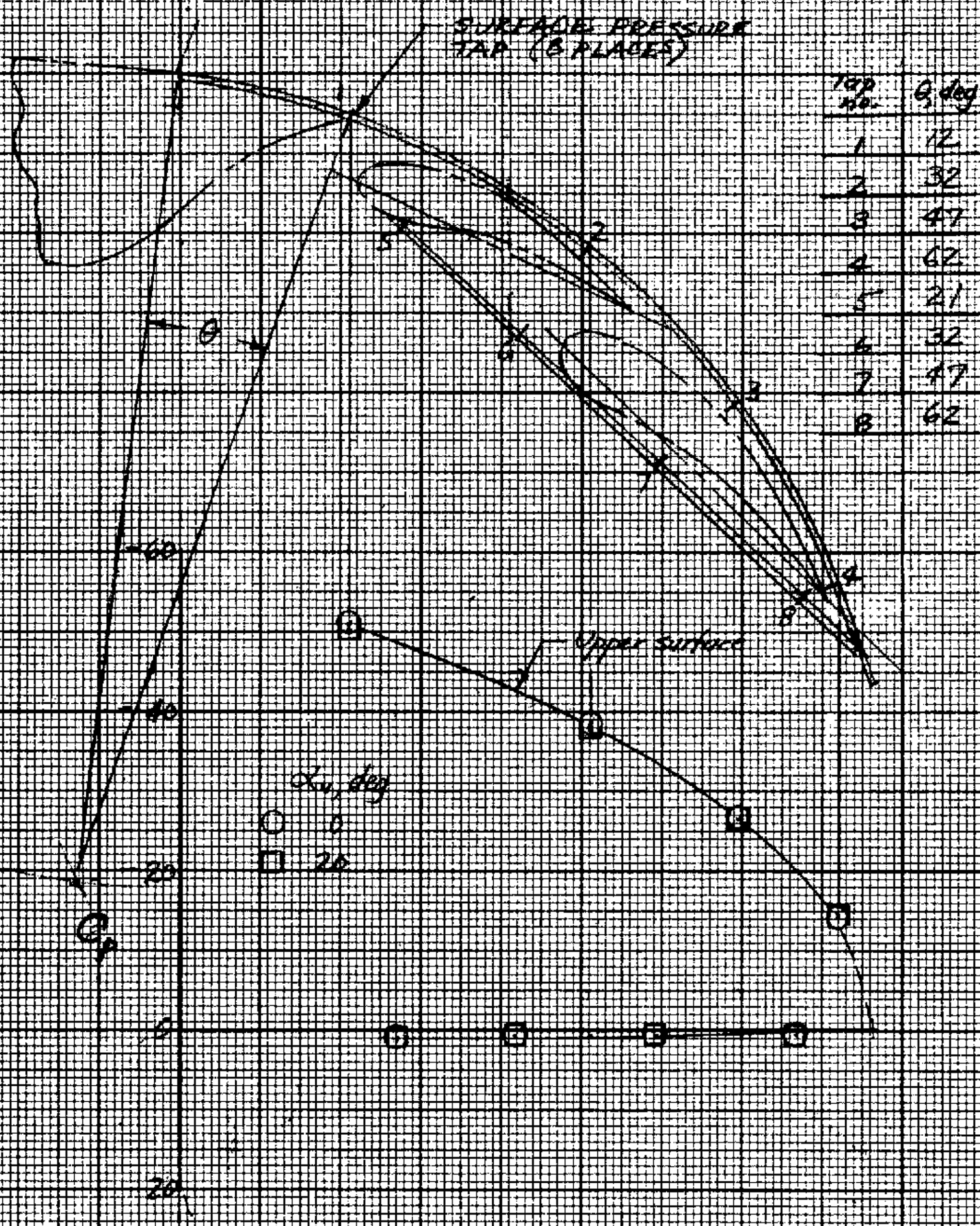

Figure 26 – Flap surface pressures behind engine centerline (η = .256) with nozzle B and 0.15 m gap deflector; δ_f = 75° (x/c = .41 to .48), δ_{f_2} = 44°, C_J = 3.83, q = 229.8 N/m²

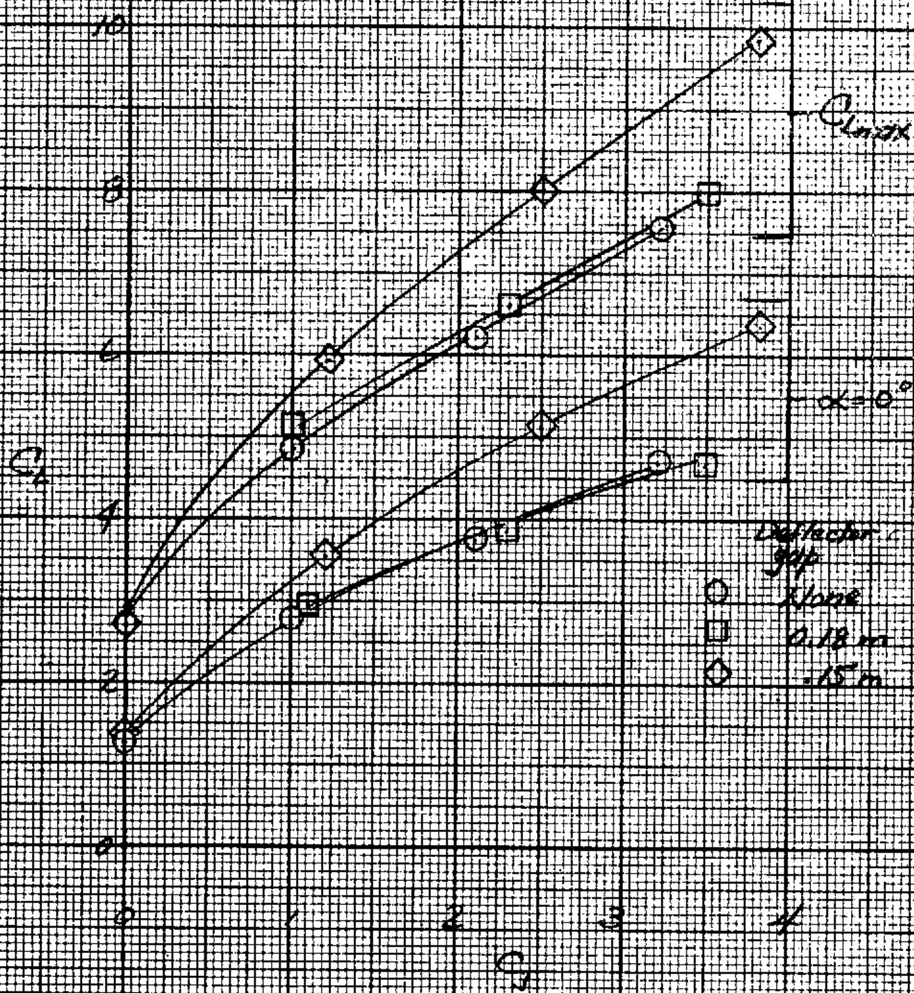

Figure 27. — Effect of deflector gap on the variation of C_L with C_J with nozzle B; $\delta_j = 25°$ (δ_c = [illegible]), $\delta_f = 40°$, tail off

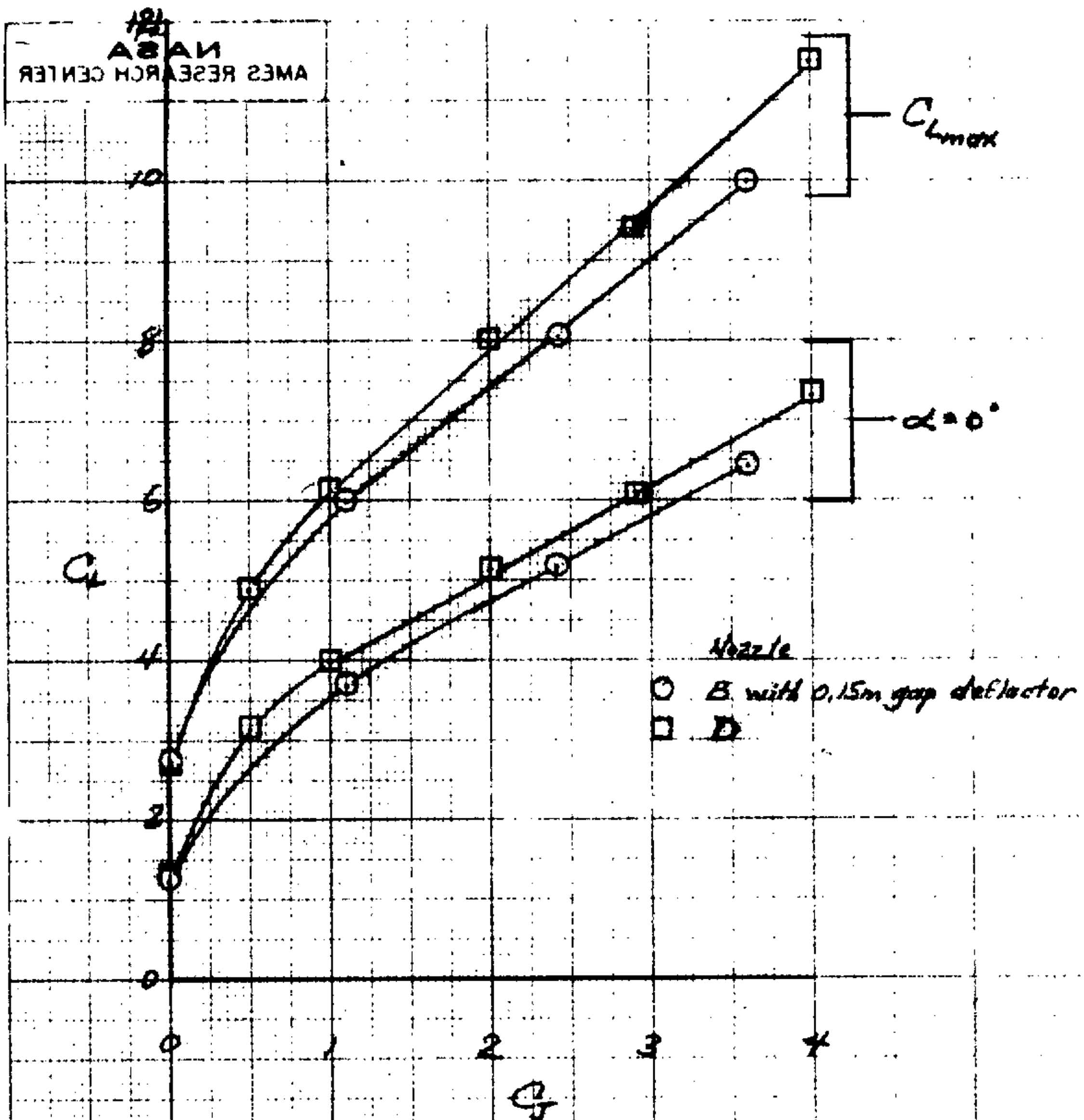

Figure 38.— Effect of nozzle on the variation of C_L with C_J; $\delta_f = 75°$ (η_c = .11 to .43), $\delta_{f_2} = 44°$, tail off

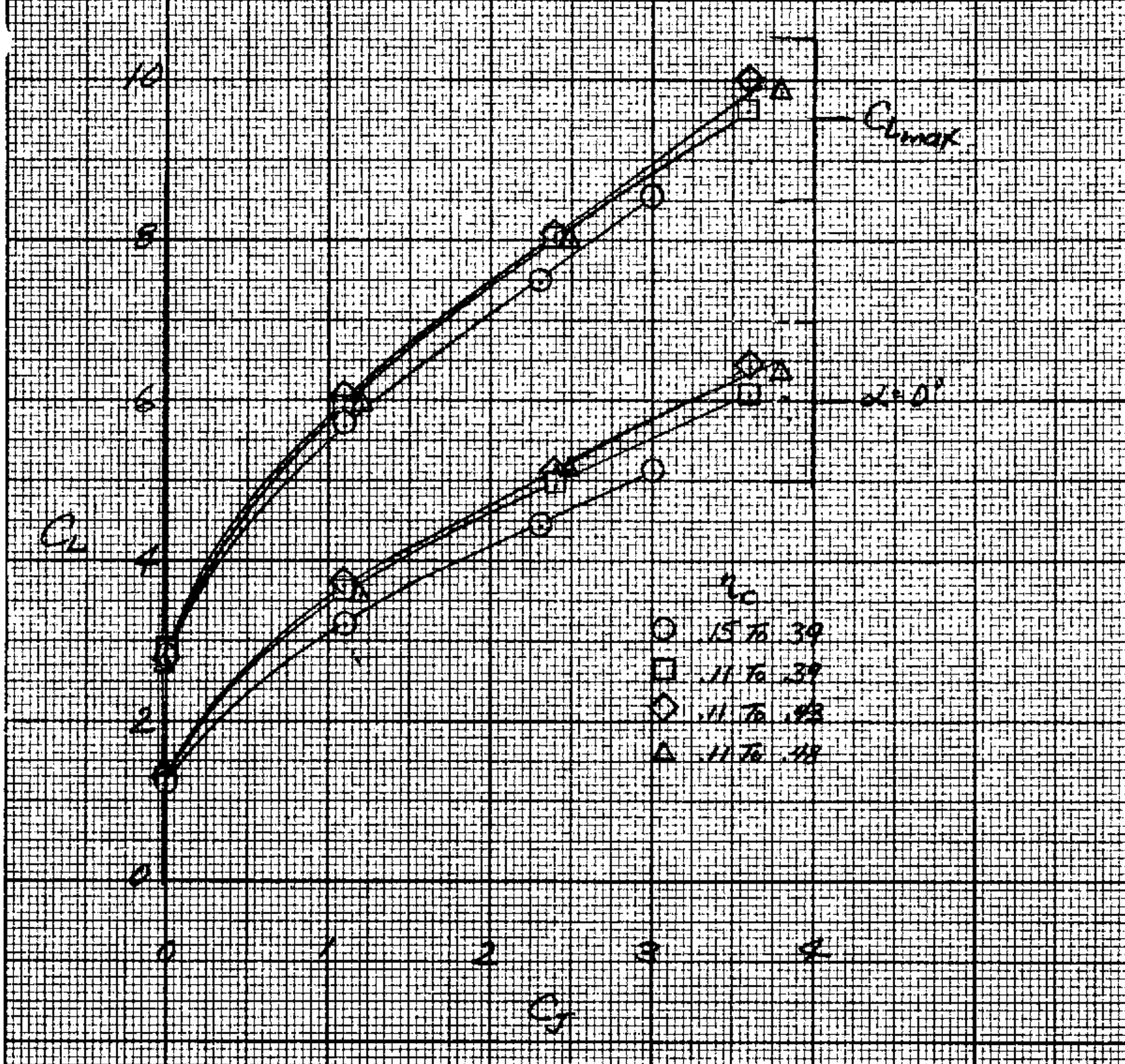

Figure 29. — Effect of Coanda surface spanwise extent on the variation of C_L with C_J with nozzle B and 0.15 in gap deflector; $\delta_J = 75°$, $\delta_{f_2} = 48$, tail off.

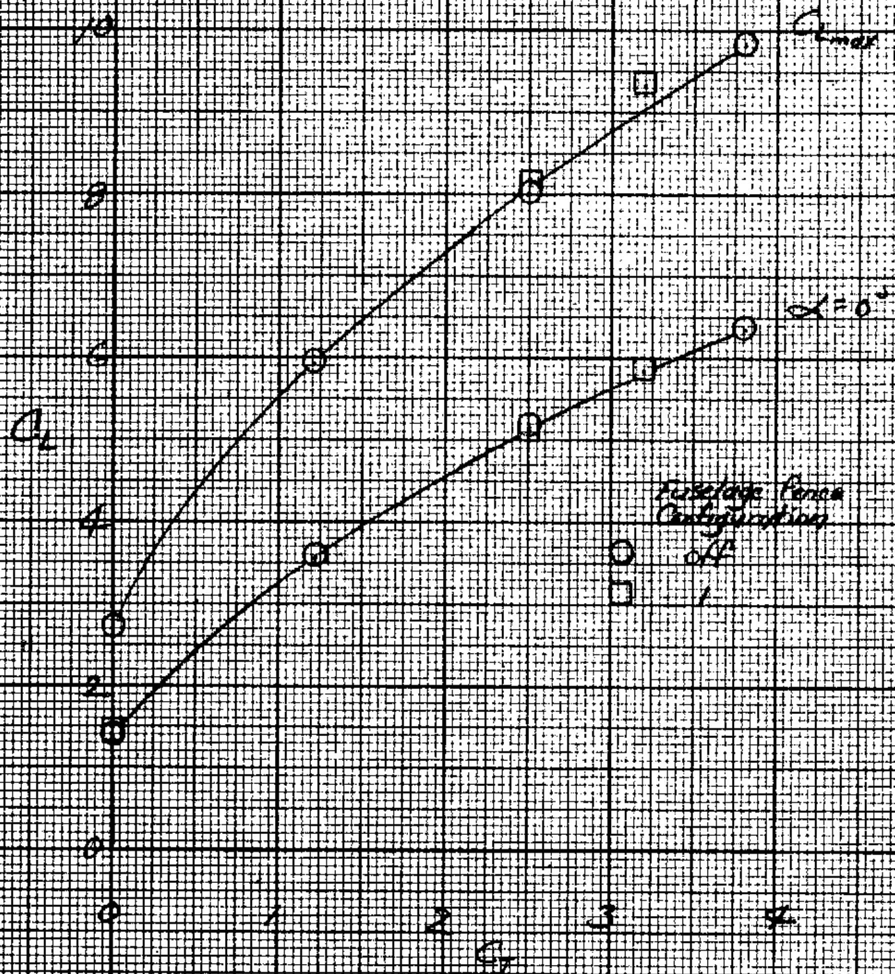

(a) Nozzle B and 0.15-in gap deflector, $\delta_j = 25°$ (δ_t = 11 to 48)
tail off

Figure 20.- Effect of fuselage fence on the variation of C_L with C_J

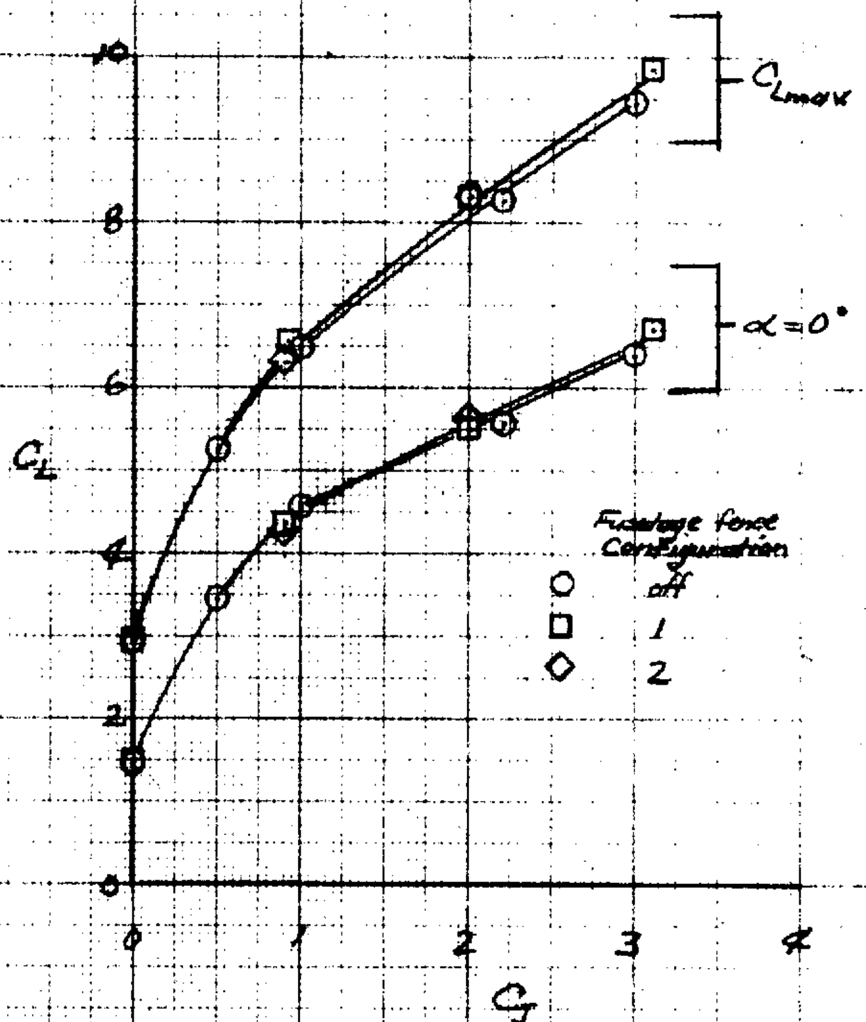

(b) Nozzle D, $\delta_f = 90°$ (η_c = .11 to .43), $\psi_f = 0°$.

Figure 30. – Concluded